

CATALYTIC APPLICATIONS OF CuO LOADED MESOPOROUS CeO<sub>2</sub> AND  
CuO LOADED MESOPOROUS CeO<sub>2</sub>-ZrO<sub>2</sub> CATALYST

Sureerat Jampa

A Dissertation Submitted in Partial Fulfilment of the Requirements  
for the Degree of Doctor of Philosophy

The Petroleum and Petrochemical College, Chulalongkorn University

in Academic Partnership with

The University of Michigan, The University of Oklahoma,  
and Case Western Reserve University

2018

บทคัดย่อและแฟ้มข้อมูลฉบับเต็มของวิทยานิพนธ์ตั้งแต่ปีการศึกษา 2554 ที่ให้บริการในคลังปัญญาจุฬาฯ (CUIR)  
เป็นแฟ้มข้อมูลของนิสิตเจ้าของวิทยานิพนธ์ที่ส่งผ่านทางบัณฑิตวิทยาลัย

The abstract and full text of theses from the academic year 2011 in Chulalongkorn University Intellectual Repository (CUIR)  
are the thesis authors' files submitted through the Graduate School.

**Thesis Title:** Catalytic Applications of CuO Loaded Mesoporous CeO<sub>2</sub> and CuO Loaded Mesoporous CeO<sub>2</sub>-ZrO<sub>2</sub> Catalyst  
**By:** Sureerat Jampa  
**Program:** Polymer Science  
**Thesis Advisors:** Prof. Sujitra Wongkasemjit  
Prof. Apanee Luengnaruemitchai  
Assoc. Prof. Thanyalak Chaisuwan

---

Accepted by The Petroleum and Petrochemical College, Chulalongkorn University, in partial fulfilment of the requirements for the Degree of Doctor of Philosophy.

..... College Dean  
(Prof. Suwabun Chirachanchai)

**Thesis Committee:**

..... (Assoc. Prof. Apirat Laobuthee)	..... (Prof. Sujitra Wongkasemjit)
..... (Prof. Apanee Luengnaruemitchai)	..... (Assoc. Prof. Thanyalak Chaisuwan)
..... (Asst. Prof. Manit Nithitanaku)	..... (Asst. Prof. Bussarin Ksapabutr)

**ABSTRACT**

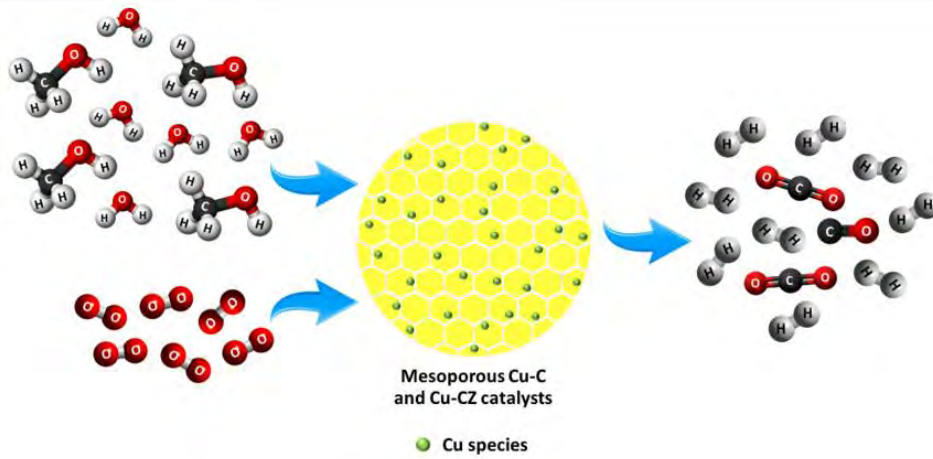
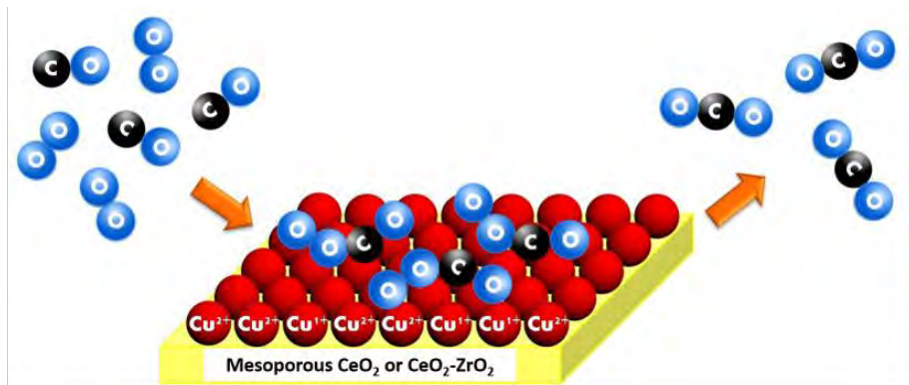
5792004063: Polymer Science Program

Sureerat Jampa: Catalytic Applications of CuO Loaded Mesoporous CeO<sub>2</sub> and CuO Loaded Mesoporous CeO<sub>2</sub>-ZrO<sub>2</sub> Catalyst.

Thesis Advisors: Prof. Sujitra Wongkasemjit, Prof. Apanee Luengnaruemitchai, and Assoc. Prof. Thanyalak Chaisuwan 150 pp.

Keywords: Mesoporous CeO<sub>2</sub>/ Mesoporous CeO<sub>2</sub>-ZrO<sub>2</sub>/ Cu-CeO<sub>2</sub>/ Cu-CeO<sub>2</sub>-ZrO<sub>2</sub>/ Nanocasting process/ Deposition-precipitation method/ Preferential oxidation of CO (CO-PROX)/ Autothermal steam reforming of methanol (ASRM)

Copper oxide (CuO) loaded mesoporous ceria (CeO<sub>2</sub>) and Copper oxide (CuO) loaded mesoporous ceria-zirconia (CeO<sub>2</sub>-ZrO<sub>2</sub>) catalysts are successfully synthesized for preferential oxidation of CO (CO-PROX) and autothermal steam reforming of methanol (ASRM). Mesoporous CeO<sub>2</sub> and mesoporous CeO<sub>2</sub>-ZrO<sub>2</sub> as catalyst supports with high specific surface area and ordered structure are prepared via a nanocasting process by using MCM-48 as template. Deposition-precipitation technique is chosen to load various Cu contents (1 to 9 wt.%) on the synthesized mesoporous supports. The synthesized CuO loaded mesoporous CeO<sub>2</sub> (Cu-C) and CuO loaded mesoporous CeO<sub>2</sub>-ZrO<sub>2</sub> (Cu-CZ) catalysts are characterized by N<sub>2</sub> adsorption-desorption, X-ray diffraction, transmission electron microscopy, atomic absorption spectroscopy, X-ray photoelectron spectroscopy, and temperature-programmed reduction by H<sub>2</sub>. The catalytic performance of Cu-C and Cu-CZ catalysts for the CO-PROX reaction in presence of excess hydrogen and autothermal steam reforming of methanol (ASRM) reaction are investigated. The Cu-C and Cu-CZ catalysts illustrate an excellent efficiency for these reactions.



## บทคัดย่อ

สุรรัตน์ จำปา : การประยุกต์ใช้ในเชิงการเร่งปฏิกิริยาต่างๆของตัวเร่งปฏิกิริยาคอปเปอร์ออกไซด์บนตัวรองรับซีเรียและคอปเปอร์ออกไซด์บนตัวรองรับซีเรีย-เซอร์โคเนียที่มีขนาดรูพรุนในช่วงมีโซพอร์ (Catalytic applications of CuO loaded mesoporous CeO<sub>2</sub> and CuO loaded mesoporous CeO<sub>2</sub>-ZrO<sub>2</sub> catalyst) อ. ที่ปรึกษา : ศาสตราจารย์ ดร.สุจิตรา วงศ์เกษมจิตต์, ศาสตราจารย์ ดร. อาภาณี เหลืองนฤมิตชัย และรองศาสตราจารย์ ดร. รัญญลักษณ์ ฉายสุวรรณ 150 หน้า

ตัวเร่งปฏิกิริยาคอปเปอร์ออกไซด์บนตัวรองรับซีเรียและคอปเปอร์ออกไซด์บนตัวรองรับซีเรีย-เซอร์โคเนียที่มีขนาดรูพรุนในช่วงมีโซพอร์ถูกสังเคราะห์ขึ้นมา เพื่อนำมาใช้สำหรับการเร่งปฏิกิริยาออกซิเดชันของคาร์บอนมอนอกไซด์และปฏิกิริยาอโตเทอร์มอลสตรีมรีฟอร์มมิงของเมทานอล ซีเรียและซีเรีย-เซอร์โคเนียที่มีขนาดรูพรุนในช่วงมีโซพอร์, มีค่าพื้นที่ผิวจำเพาะสูง และมีโครงสร้างที่เป็นระเบียบ ถูกสังเคราะห์ด้วยกระบวนการนาโนแคสติงโดยใช้ MCM-48 เป็นตัวแม่แบบ เพื่อนำมาใช้เป็นวัสดุรองรับสำหรับตัวเร่งปฏิกิริยา ตัวเร่งปฏิกิริยาคอปเปอร์ในปริมาณที่แตกต่างกัน (1-9 เปอร์เซ็นต์ โดยน้ำหนัก) ถูกเติมบนวัสดุรองรับซีเรียและซีเรีย-เซอร์โคเนียด้วยวิธี Deposition-precipitation ตัวเร่งปฏิกิริยาคอปเปอร์ออกไซด์บนตัวรองรับซีเรียและคอปเปอร์ออกไซด์บนตัวรองรับซีเรีย-เซอร์โคเนียที่สังเคราะห์ได้ถูกนำไปพิสูจน์เอกลักษณ์ด้วยเทคนิคต่างๆ เช่น N<sub>2</sub> adsorption-desorption, X-ray diffraction, transmission electron microscopy, atomic absorption spectroscopy, X-ray photoelectron spectroscopy, and temperature-programmed reduction โดย H<sub>2</sub> ประสิทธิภาพของตัวเร่งปฏิกิริยาที่สังเคราะห์ได้ทั้งหมดถูกนำมาศึกษาในปฏิกิริยาออกซิเดชันของคาร์บอนมอนอกไซด์และปฏิกิริยาอโตเทอร์มอลสตรีมรีฟอร์มมิงของเมทานอล พบว่าทั้งตัวเร่งปฏิกิริยาคอปเปอร์ออกไซด์บนตัวรองรับซีเรียและคอปเปอร์ออกไซด์บนตัวรองรับซีเรีย-เซอร์โคเนียแสดงประสิทธิภาพที่ดีเยี่ยมสำหรับปฏิกิริยาต่างๆ ดังกล่าว

## ACKNOWLEDGEMENTS

Firstly, I would like to express my sincere gratitude to my advisor Prof. Sujitra Wongkasemjit for the continuous support of my Ph.D study, for her patience, motivation, and knowledge. Her guidance helped me in all the time of research and writing of this thesis. I could not have imagined having a better advisor and mentor for my Ph.D study. She is more than an advisor. She is like a mother who wants to see the success of her children.

Besides my advisor, I would like to sincerely thank other research advisors, Prof. Apanee Luengnaruemitchai and Assoc. Prof. Thanyalak Chaisuwan who inspires, assists, and guides me when I face the problems. Moreover, I wish to thank my thesis committee, Assoc. Prof. Apirat Laobuthee, Asst. Prof. Manit Nithitanaku and Asst. Prof. Bussarin Ksapabutr, for their insightful comments and encouragement.

I am really grateful for the full scholarship and partial funding of the thesis work provided by Development and Promotion of Science and Technology Talents Project and the Grant for International Research Integration: Chula Research Scholar, Ratchadaphiseksompote Endowment Fund, Chulalongkorn University, Thailand, respectively.

I am also grateful to the following my university colleagues and my friends: Supakorn Tantisriyanurak, Kanapos Wangkewee, Wasupon Wongvitvichot, Nicharat Manmuanpom, Chachchaya Thunyaratchatanon and Sakollaphat Pithakratanayothin for great assistance, helpful advice, great motivation, and powerful encouragement.

Last but not the least, I would like to thank my family for supporting me spiritually throughout writing this thesis and my life in general.

## TABLE OF CONTENTS

	<b>PAGE</b>
Title Page	i
Abstract (in English)	iii
Abstract (in Thai)	iv
Acknowledgements	v
Table of Contents	vi
List of Tables	ix
List of Figures	x

### CHAPTER

<b>I</b>	<b>INTRODUCTION</b>	1
<b>II</b>	<b>THEORETICAL BACKGROUND AND LITERATURE REVIEW</b>	4
	2.1 Preferential Oxidation of CO (CO-PROX)	4
	2.2 H <sub>2</sub> Production from Methanol	5
	2.3 Catalyst	12
<b>III</b>	<b>EXPERIMENTAL</b>	23
	3.1 Objectives	23
	3.2 Experimental	23
<b>IV</b>	<b>HIGH PERFORMANCE AND STABILITY OF COPPER LOADING ON MESOPOROUS CERIA CATALYST FOR PREFERENTIAL OXIDATION OF CO IN PRESENCE OF EXCESS OF HYDROGEN</b>	28
	4.1 Abstract	28
	4.2 Introduction	29
	4.3 Experimental	30

4.4	Results and Discussion	33
4.5	Conclusions	41
4.6	Acknowledgements	42
4.7	References	42
<b>V</b>	<b>KINETICS OF Cu LOADED MESOPOROUS CeO<sub>2</sub>-ZrO<sub>2</sub> CATALYST FOR THE PREFERENTIAL OXIDATION OF CO (CO-PROX) IN THE PRESENCE OF EXCESS HYDROGEN</b>	
		57
5.1	Abstract	57
5.2	Introduction	58
5.3	Experimental	60
5.4	Results and Discussion	64
5.5	Conclusions	73
5.6	Acknowledgements	74
5.7	References	74
<b>VI</b>	<b>ACHIEVEMENT OF HYDROGEN PRODUCTION FROM AUTOTHERMAL STEAM REFORMING OF METHANOL OVER Cu-LOADED MESOPOROUS CeO<sub>2</sub> AND Cu-LOADED MESOPOROUS CeO<sub>2</sub>-ZrO<sub>2</sub> CATALYSTS</b>	
		98
6.1	Abstract	98
6.2	Introduction	99
6.3	Experimental	101
6.4	Results and Discussion	104
6.5	Conclusions	111
6.6	Acknowledgements	111
6.7	References	112



<b>VII</b>	<b>HIGH POTENTIAL OF MESOPOROUS CERIA/CERIA-ZIRCONIA SYNTHESIZED VIA NANOCASTING PATHWAY FOR CATALYTIC APPLICATIONS</b>	127
	7.1 Abstract	127
	7.2 Introduction	128
	7.3 Experimental	129
	7.4 Results and Discussion	130
	7.5 Conclusions	132
	7.6 Acknowledgements	132
	7.7 References	133
<b>VIII</b>	<b>CONCLUSIONS AND RECOMMENDATIONS</b>	138
	<b>REFERENCES</b>	140
	<b>CURRICULUM VITAE</b>	149

**LIST OF TABLES**

<b>TABLE</b>		<b>PAGE</b>
<b>CHAPTER IV</b>		
4.1	Properties of MSP CeO <sub>2</sub> and CuO/CeO <sub>2</sub> catalyst	48
4.2	Relationship of species distribution on the surface of catalysts by XPS	49
4.3	H <sub>2</sub> -TPR results of all catalysts	50
<b>CHAPTER V</b>		
5.1	Compositions and N <sub>2</sub> physisorption data of the synthesized catalysts	83
5.2	Structural parameters of CZ support and Cu-CZ catalysts calculated from XRD and SAED data	84
5.3	The amounts of Cu found in bulk and on the surface of the synthesized Cu-CZ catalysts	85
5.4	Kinetic results of CO-PROX reaction over all synthesized Cu-CZ catalyst	86
<b>CHAPTER VI</b>		
6.1	BET specific surface areas of all fresh and spent catalysts	118
6.2	Structural parameters of all fresh and spent catalysts from XRD	119
6.3	TPO results of catalysts	120
<b>CHAPTER VII</b>		
7.1	BET specific surface areas of all fresh and spent catalysts	135

## LIST OF FIGURES

FIGURE		PAGE
<b>CHAPTER II</b>		
2.1	Effect of the hydrogen-to-carbon atomic ratio in the fuel on the theoretical (maximum) fuel processing efficiency.	6
2.2	Effect of oxygen concentration in the feed on the methanol conversion and CO selectivity. Feed: 100 ml/min, 10% CH <sub>3</sub> OH, 15% H <sub>2</sub> O, O <sub>2</sub> (shown) and balance He. Catalyst: 70 wt.% CuO-CeO <sub>2</sub> , weight=0.5 g.	10
2.3	Effect of O <sub>2</sub> /CH <sub>3</sub> OH molar ratio on the catalytic performance in the OSRM reaction over CZAZOC-6. The inset in the top figure shows the variation of outlet CO concentration and RH <sub>2</sub> /RMeOH conversion ratio as a function of O <sub>2</sub> /CH <sub>3</sub> OH molar ratio.	11
2.4	Effect of H <sub>2</sub> O/CH <sub>3</sub> OH molar ratio on the catalytic performance in the OSRM reaction over CZAZOC-6. The inset in the bottom figure indicates the variation of outlet CO concentration and RH <sub>2</sub> /RMeOH conversion ratio as a function of H <sub>2</sub> O/CH <sub>3</sub> OH molar ratio .	12
2.5	Structures of mesoporous M41S materials.	14
2.6	Schematic illustration of the nanocasting pathway.	15
2.7	CO-PROX over 1% M/Ce <sub>0.63</sub> Zr <sub>0.37</sub> O <sub>2</sub> (M = Co, Cr, Cu, Ni, Zn), evolution of the CO conversion, the O <sub>2</sub> conversion and the CO <sub>2</sub> selectivity as a function of the reaction temperature.	18
2.8	CO conversion (%) at various temperatures.	19
2.9	(a) CO conversion and (b) selectivity to CO <sub>2</sub> as a function of temperature.	20
2.10	Stability testing of 3 wt% Au/CeO <sub>2</sub> and 3 wt% Au/Ce <sub>0.75</sub> Zr <sub>0.25</sub> O <sub>2</sub> catalysts at reaction temperature 350 °C.	22

<b>FIGURE</b>	<b>PAGE</b>
<b>CHAPTER IV</b>	
4.1 (A) WAXD and SAXD (inset) patterns of the synthesized MSP ceria and (B) N <sub>2</sub> adsorption-desorption isotherms and pore size distribution (inset) of the synthesized MSP ceria.	51
4.2 (A) XRD patterns at a scanning speed of 1 °min <sup>-1</sup> and a scanning speed of 0.01°min <sup>-1</sup> (inset) of (a) pure MSP ceria, (b) 3CuO/CeO <sub>2</sub> , (c) 5CuO/CeO <sub>2</sub> , (d) 7CuO/CeO <sub>2</sub> , and (e) 9CuO/CeO <sub>2</sub> ; (B) TEM image of 7Cu/MSP ceria calcined at 500 °C.	52
4.3 (A) H <sub>2</sub> -TPR profiles of (a) 3CuO/CeO <sub>2</sub> , (b) 5CuO/CeO <sub>2</sub> , (c) 7CuO/CeO <sub>2</sub> , (d) 9CuO/CeO <sub>2</sub> and pure MSP ceria (inset) and (B) The deconvolution of reduction profiles of all Cu/MSP ceria.	53
4.4 (a) CO conversion and (b) selectivity for PROX reaction using feed composition of 1% CO, 1% O <sub>2</sub> , 40% H <sub>2</sub> balance in He (c) CO conversion and (d) selectivity for PROX reaction in the present of 10 % CO <sub>2</sub> (e) CO conversion of 7CuO/CeO <sub>2</sub> for PROX reaction in various feed compositions.	54
4.5 (A) O1s XPS spectra of fresh catalysts (a) pure MSP ceria, (b) 3CuO/CeO <sub>2</sub> , (c) 5CuO/CeO <sub>2</sub> , (d) 7CuO/CeO <sub>2</sub> , (e) 9CuO/CeO <sub>2</sub> and (B) Example of deconvolution of O1s spectrum of 7CuO/CeO <sub>2</sub> .	55
4.6 (A) Ce3d XPS spectra of fresh and used (-P) catalysts (a) pure MSP ceria, (b) 3CuO/CeO <sub>2</sub> , (c) 5CuO/CeO <sub>2</sub> , (d) 7CuO/CeO <sub>2</sub> , (e) 9CuO/CeO <sub>2</sub> , (f) 7CuO/CeO <sub>2</sub> -P1, (g) 7CuO/CeO <sub>2</sub> -P2, (h) 7CuO/CeO <sub>2</sub> -P3 and (B) Example of deconvolution of Ce3d spectra of 7CuO/CeO <sub>2</sub> .	55
4.7 (A) Cu 2p XPS spectra of fresh and used (-P) catalysts (a) pure MSP ceria, (b) 3CuO/CeO <sub>2</sub> , (c) 5CuO/CeO <sub>2</sub> , (d) 7CuO/CeO <sub>2</sub> , (e) 9CuO/CeO <sub>2</sub> , (f) 7CuO/CeO <sub>2</sub> -P1, (g) 7CuO/CeO <sub>2</sub> -P2 and (B) Example of deconvolution of Cu2p spectra of 9CuO/CeO <sub>2</sub> .	56
4.8 Raman spectra of fresh and used (-P) catalysts after stability test for PROX reaction (a) fresh 7CuO/CeO <sub>2</sub> , (b) 7CuO/CeO <sub>2</sub> -P1, (c) 7CuO/CeO <sub>2</sub> -P2, (d) 7CuO/CeO <sub>2</sub> -P3.	56

<b>FIGURE</b>	<b>PAGE</b>
<b>CHAPTER V</b>	
5.1 (a) Small angle XRD patterns of the CZ support, Cu-CZ catalysts and MCM-48 (inset), TEM images of (b) the CZ support, (c) 1%Cu-CZ, (d) 3%Cu-CZ, (e) 5%Cu-CZ, (f) 7%Cu-CZ and (g) 9%Cu-CZ.	87
5.2 Wide angle XRD patterns of the CZ support and Cu-CZ catalysts.	88
5.3 (a) Ce 3d XPS spectra of the CZ support and Cu-CZ catalysts and (b) The deconvoluted Ce 3d XPS spectrum of the 7%Cu-CZ catalyst.	89
5.4 (a) O 1s XPS spectra of the CZ support and Cu-CZ catalysts and (b) The deconvoluted O 1s XPS spectrum of the 7%Cu-CZ catalyst.	90
5.5 (a) Cu 2p XPS spectra of CZ support and Cu-CZ catalysts and (b) The deconvoluted Cu 2p XPS spectrum of the 7%Cu-CZ catalyst.	91
5.6 (a) H <sub>2</sub> -TPR profiles of the CZ support (inset) and (b) Cu-CZ catalysts.	92
5.7 CO conversion and selectivity as a function of temperature of the CZ support and Cu-CZ catalysts, Gas compositions: 1 vol.% CO, 1 vol.% O <sub>2</sub> , 40 vol.% H <sub>2</sub> and He as balance.	93
5.8 CO conversion and selectivity as a function of temperature of the CZ support and Cu-CZ catalysts, Gas compositions: 1 vol % CO, 1 vol.% O <sub>2</sub> , 10 vol.% CO <sub>2</sub> , 40 vol.% H <sub>2</sub> and He as balance.	94
5.9 CO conversion and selectivity as a function of temperature of the CZ support and Cu-CZ catalysts, Gas compositions: 1 vol.% CO, 1 vol.% O <sub>2</sub> , 10 vol.% CO <sub>2</sub> , 10 vol.% H <sub>2</sub> O, 40 vol.% H <sub>2</sub> and He as balance.	94
5.10 Reaction rates at various CO concentrations of (a) 1, (b) 3, (c) 5, (d) 7, and (e) 9%Cu-CZ at the reaction temperatures of 90° and 130 °C.	95
5.11 Reaction rates at various O <sub>2</sub> concentrations of (a) 1, (b) 3, (c) 5, (d) 7, and (e) 9%Cu-CZ at the reaction temperatures of 90° and 130 °C.	96

<b>FIGURE</b>	<b>PAGE</b>
5.12 CO conversion is continuously monitored over a 72 hr period as a measure of performance stability of the 9%Cu-CZ for catalysis of the CO-PROX reaction.	97
<b>CHAPTER VI</b>	
6.1 Wide angle XRD patterns of (A) fresh Cu-C catalysts; (B) fresh Cu-CZ catalysts; (C) spent Cu-C catalysts and (D) spent Cu-CZ catalysts at various Cu contents.	121
6.2 (A) The methanol conversion of Cu-C catalysts; (B) The methanol conversion of Cu-CZ catalysts; (C) The H <sub>2</sub> yield of Cu-C catalysts; (D) The H <sub>2</sub> yield of Cu-CZ catalysts; (E) The gas selectivity of 9%Cu-C catalyst; (F) The gas selectivity of 9%Cu-CZ catalyst. (Reaction condition: H <sub>2</sub> O/CH <sub>3</sub> OH=2/1, O <sub>2</sub> 5 ml/min)	122
6.3 The effect of H <sub>2</sub> O/CH <sub>3</sub> OH (W/M) molar ratio on catalytic performance (A) The methanol conversion of 9%Cu-C catalyst; (B) The methanol conversion of 9%Cu-CZ catalyst; (C) The H <sub>2</sub> yield of 9%Cu-C catalyst; (D) The H <sub>2</sub> yield of 9%Cu-CZ catalyst. (Reaction condition: O <sub>2</sub> 5 ml/min)	123
6.4 Stability testing of 9%Cu-C and 9%Cu-CZ catalysts (A) The methanol conversion; (B) The H <sub>2</sub> yield; and (C) The CO selectivity. (Reaction conditions: H <sub>2</sub> O/CH <sub>3</sub> OH=2/1; O <sub>2</sub> 5 ml/min; reaction temperature at 350 °C for 9%Cu-C and 300°C for 9%Cu-CZ; and time-on-stream per catalyst 168 h)	124
6.5 Wide angle XRD patterns of (A) spent 9%Cu-C catalyst; (B) spent 9%Cu-CZ catalyst after stability testing for 168 h.	125
6.6 TPO profiles of (A) spent 9%Cu-C catalyst; (B) spent 9%Cu-CZ catalyst after stability testing for 168 h.	125

<b>FIGURE</b>		<b>PAGE</b>
6.7	TEM images of (A) and (B) fresh 9%Cu-C catalyst, (C) and (D) fresh 9%Cu-CZ catalyst, (E) and (F) spent 9%Cu-C catalyst, and (G) and (H) spent 9%Cu-CZ catalyst after stability testing for 168 h.	126
6.8	(A) Cu 2p XPS spectra of fresh 9%Cu-C catalyst and spent 9%Cu-C catalyst after stability testing for 168 h; and (B) Cu 2p XPS spectra of fresh 9%Cu-CZ catalyst and spent 9%Cu-CZ catalyst after stability testing for 168 h.	126
<b>CHAPTER VII</b>		
7.1	Wide angle XRD patterns of mesoporous C, mesoporous CZ, Cu-C, and Cu-CZ.	136
7.2	CO conversion as a function of temperature of Cu-C and Cu-CZ catalysts.	136
7.3	A) Methanol conversion and B) H <sub>2</sub> yield of Cu-C and Cu-CZ catalysts.	137

## **CHAPTER I**

### **INTRODUCTION**

Nowadays, the world's fossil fuel consumption has continuously risen because of the increasing of population that affects the rapid decreasing of fossil fuels. Furthermore, carbon emissions from fossil fuels are the main factor to rise global temperature and pollutions, causing the important risk of global climate change. To solve these problems, to find new energy sources which can use to replace of fossil fuel are very necessary. Hydrogen is very attractive to produce the clean energy. Hydrogen is not a primary energy source like coal and gas but it is an energy carrier. Hydrogen can be obtained from diverse resources, both renewable (hydro, wind, wave, solar, biomass) and non-renewable (coal, natural gas and nuclear) sources. The importance of hydrogen as a potential energy carrier has increased significantly over the last decade due to the development of fuel cell technology (Edwards *et al.*, 2007). Fuel cells are alternative sources for clean energy production. Fuel cells directly convert the chemical energy in hydrogen to electricity, with pure water and potentially useful heat as by products. Among the various types of fuel cells, proton exchange membrane fuel cells (PEMFC) are widely used because of their low temperature of operation (80 °C), high power density and high efficiency (Mishra *et al.*, 2011).

Generally, the hydrogen-rich gas contains 0.5-2.0 vol.% CO, which poisons the PEMFC electrodes typically made from Pt. The amount of CO in hydrogen-rich gas must be removed to a level below 10 ppm. Preferential oxidation of CO (CO-PROX) is an efficient method for CO removal from a hydrogen-rich gas mixture (Potemkin *et al.*, 2012). The PEMFC's ideal fuel is hydrogen which is stored on-board in high-pressure tanks. However, the current technology does not provide the storage of enough hydrogen to the driving range. Thus, PEMFC vehicles probably use liquid fuels to solve problems of safety and handling of hydrogen.

Methanol has been identified as a suitable liquid fuel which can produce hydrogen. A hydrogen-rich gas can be produced on-board of the vehicle by several



reactions, such as steam reforming of methanol (SRM), partial oxidation of methanol (POM), and oxidative steam reforming of methanol (OSRM) (Agrell *et al.*, 2002). However, oxidative steam reforming or autothermal steam reforming of methanol (OSRM or ASRM) provides high efficiency for H<sub>2</sub> production.

As a result, catalyst is an important factor for CO preferential oxidation (PROX) and H<sub>2</sub> production from methanol. Mostly, mesoporous materials are extensively used as catalyst or catalyst support due to its high surface area and suitable pore size as well as pore structure, allowing large molecules to penetrate inside the pore. One way to obtain mesoporous materials is to use nanocasting method with template, and cubic MCM-48, indexed in the space group of Ia3d, is an interesting hard template since it has a three-dimensional pore structure and interconnected channels which can reduce the diffusion limitations and avoid the pore-blocking of the catalysts (Monnier *et al.*, 1993).

Cerium oxide or ceria (CeO<sub>2</sub>) as a fluorite-type oxide is the most important rare-earth oxide for the oxidation reactions on account of its redox cycle between two oxidation states (Ce<sup>4+</sup>-Ce<sup>3+</sup>) and high oxygen storage capacity (OSC) (Yane *et al.*, 2014). It has also been extensively used for oxygen storage capacity and environmental catalysis. Furthermore, incorporation of zirconium oxide or zirconia (ZrO<sub>2</sub>) to CeO<sub>2</sub> exhibits even better features than pure CeO<sub>2</sub>, such as, a higher thermal resistance, a higher efficiency of the redox property, and a better oxygen storage and release capacity (Trovarelli *et al.*, 2001). Thus, CeO<sub>2</sub>-ZrO<sub>2</sub> catalyst support, one of the most popular supports, has attracted much attention from many scientists.

Copper (Cu), a transition metal, is a good candidate for catalytic industry. Cu-based catalysts are useful for several applications due to its high activity and selectivity in many reactions (Zhang *et al.*, 2014). Importantly, it is low cost when compared with noble metals. Cu-based catalyst loaded onto catalyst support is very attractive catalyst. In this study, it is thus aimed to synthesize a high surface area Cu loaded mesoporous CeO<sub>2</sub> and Cu loaded mesoporous CeO<sub>2</sub>-ZrO<sub>2</sub> catalyst via the nanocasting technique, followed by the deposition-precipitation (DP) method. The synthesized Cu loaded mesoporous CeO<sub>2</sub> and CeO<sub>2</sub>-ZrO<sub>2</sub> catalysts are then studied its potential in the preferential oxidation of CO (CO-

PROX) reaction and autothermal steam reforming of methanol (ASRM) reaction. All synthesized catalysts were comprehensively characterized using various analytical techniques, and systematically studied for their optimal conditions of each reaction.

## CHAPTER II

### LITERATURE REVIEW

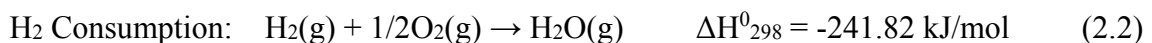
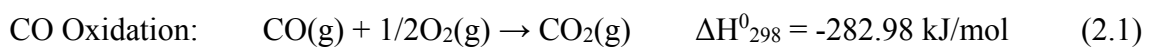
#### 2.1 Preferential Oxidation of CO (CO-PROX)

Proton exchange membrane fuel cells (PEMFC) have been extensively studied in the past decades. Typically, H<sub>2</sub> production for PEMFC is achieved by a multi-step process including steam reforming or partial oxidation of liquid fuels or catalytic reforming of hydrocarbons or oxygenated hydrocarbons followed by water-gas shift (WGS). The gas stream obtained after these processes contains about 50% H<sub>2</sub>, 20% CO<sub>2</sub>, 0.5-1% CO, 10% H<sub>2</sub>O and N<sub>2</sub>. The PEMFC anode made from Pt can be poisoned by CO in the H<sub>2</sub> rich gas at levels of 10-100 ppm (Liu *et al.*, 2004). Therefore, it is necessary to eliminate the amount of CO in the hydrogen gas stream to protect PEMFC anode. There are several different methods for CO removal from the hydrogen gas stream. The main methods are as follows (Gray *et al.*, 1998):

- i) Purification with hydrogen selective membrane
- ii) CO methanation
- iii) Pressure swing adsorption
- iv) Preferential oxidation of CO

The preferential oxidation of CO (CO-PROX) has been conceded as one of the most straightforward and cost-effective methods to achieve acceptable CO concentrations (Gamarra *et al.*, 2007). Mishra and Prasad also studied how to purify hydrogen using CO-PROX (Mishra and Prasad, 2011).

The CO-PROX reaction composes of 2 main chemical reactions which are shown in Equations 2.1 and 2.2.



In CO oxidation (Equation 1), an excess of oxygen is added to CO to generate CO<sub>2</sub> molecules, at around a factor of 2, and about 90% of CO is transformed. Then, a substantially higher oxygen excess, around a factor of 4, is used to reduce the CO concentration to less than 10 ppm. The second reaction, H<sub>2</sub> consumption reaction, as shown in Equation 2, is to allow H<sub>2</sub> to react with O<sub>2</sub> to generate H<sub>2</sub>O molecules. It is highly undesirable reaction because it reduces the activity of CO-PROX catalyst (Mishra and Prasad, 2011).

Generally, the CO conversion is calculated, based on the CO consumption in the reaction, as follows (Laguna *et al.*, 2012):

$$\text{CO conversion (\%)} = \frac{(\text{CO}_{\text{in}} - \text{CO}_{\text{out}}) \times 100}{\text{CO}_{\text{in}}} \quad (2.3)$$

The selectivity of the CO oxidation in the presence of excess H<sub>2</sub> is calculated from the oxygen mass balance, as follows (Laguna *et al.*, 2012):

$$\text{CO oxidation selectivity (\%)} = \frac{(\text{CO}_{\text{in}} - \text{CO}_{\text{out}}) \times 100}{2(\text{O}_{2\text{in}} - \text{O}_{2\text{out}})} \quad (2.4)$$

## 2.2 H<sub>2</sub> Production from Methanol

Hydrogen is not primary energy source, but it is an energy carrier (Edwards *et al.*, 2007). H<sub>2</sub> does not exist freely in nature because it is only produced from diverse resources of energy. At present, H<sub>2</sub> is considered to be an alternative transportation fuel. The importance of H<sub>2</sub> as a potential energy carrier has increased significantly over the last decade due to the development of fuel cell technology, which is the important technology in the development of zero-emission electrical vehicle (Edwards *et al.*, 2007). In fuel cells, H<sub>2</sub> reacts with O<sub>2</sub> to produce heat and electricity with only water vapor as a by-product.

Proton exchange membrane fuel cells (PEMFC) have been widely studied for a long time. What scientists mostly concern is the purity of  $H_2$  for PEMFC system and technologies for a safe and efficient storage of  $H_2$  on-board of the vehicle which are still not commercially available. Thus, many researchers study how to generate  $H_2$  on-board by using a reformer. Natural gas, gasoline, or alcohols (methanol, ethanol) as liquid fuels are the potential hydrogen sources (Mariño *et al.*, 2004). Figure 2.1 shows the efficiency of liquid fuel as function of H/C atomic ratio. The efficiency increases with increasing the H/C ratio.

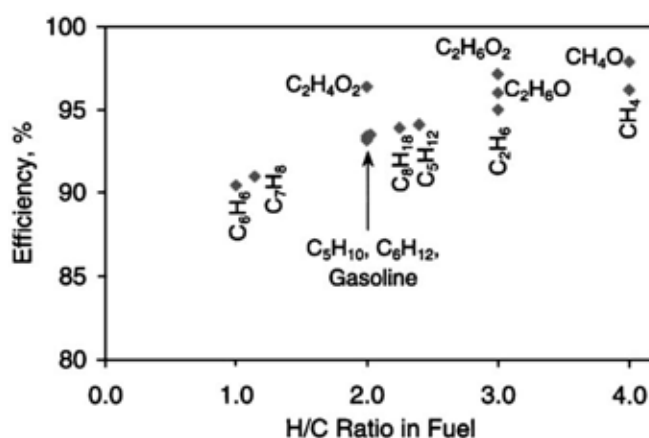


**Figure 2.1** Effect of the hydrogen-to-carbon atomic ratio in fuel on the theoretical (maximum) fuel processing efficiency (Ahmed and Krumpelt, 2001).

Among the various types of liquid fuels, methanol is a prominent candidate because it gives the highest fuel processing efficiency. Methanol has a high H/C ratio (4:1) which equals to that of methane. It is a liquid at atmospheric pressure and normal environmental temperature, unlike methane or liquefied petroleum gas (LPG). In terms of environmental impact, methanol is readily metabolized by ambient organisms in the environment and can be converted to hydrogen at lower temperatures (150°-350 °C) than most other fuels (>500 °C) because methanol does not contain carbon-carbon bonds that needs higher energy to break. Methanol is easily activated at low temperatures, causing low levels of CO formation during  $H_2$  production process (Palo *et al.*, 2007). Furthermore,

methanol can reduce the risk of coke formation during the reaction. Hydrogen can be produced from methanol by several different catalytic processes, such as methanol decomposition (MD), steam reforming of methanol (SRM), partial oxidation of methanol (POM), and oxidative steam reforming or autothermal steam reforming of methanol (OSRM or ASRM) (Turco *et al.*, 2007).

### 2.2.1 Steam Reforming of Methanol (SRM)

In the early 1960s, synthesis gas was widely produced from the steam reforming of hydrocarbons (Twigg *et al.*, 2003). SRM is an attractive process which is extensively used to produce H<sub>2</sub>. It is an endothermic reaction to produce a high yield of H<sub>2</sub>, about 75%, while maintaining a low selectivity of CO of less than 1% (Wild *et al.*, 2000). The overall reaction of SRM is shown in Equation 2.5 (Sa *et al.*, 2010).



The SRM reaction is accomplished by two side reactions: methanol decomposition, Equation 2.6, and water-gas shift, Equation 2.7



The decomposition of methanol is an endothermic reaction that produces a high yield of CO. The amount of CO must be transformed into H<sub>2</sub> and CO<sub>2</sub> by the water-gas shift reaction because CO is unsuitable for on-board PEMFC applications (Huang *et al.*, 2009). Moreover, the SRM can also lead to the formation of toxic and undesirable products which are formic acid (HCOOH), formaldehyde (CH<sub>2</sub>O), and dimethylether (CH<sub>3</sub>OCH<sub>3</sub>) since they can limit the H<sub>2</sub> production (Houteit *et al.*, 2006).

In any H<sub>2</sub> production process, there is a concern regarding carbon or coke formation, see Equations 2.8 and 2.9 (Armor, 1999), which can take place rapidly and shut down the H<sub>2</sub> production process. Therefore, it is important to control the carbon formation.



### 2.2.2 Partial Oxidation of Methanol (POM)

Partial oxidation of methanol is another attractive process of H<sub>2</sub> production for PEMFC applications. The reaction route of POM, as shown in Equation 2.10 (Alejo *et al.*, 1997), to produce H<sub>2</sub> is an exothermic reaction which does not require any heat supply.



Advantages of POM over SRM are following:

- i) It uses oxygen (or air) instead of steam as oxidant.
- ii) It is more thermodynamically favorable.
- iii) It displays a higher reaction rate.

However, a number of other reactions can occur during the operation of POM. These reactions are mainly methanol oxidation (Equation 2.11), methanol decomposition (Equation 2.12), steam reforming (Equation 2.13), water-gas shift (Equation 2.14), methanation (Equation 2.15), CO oxidation (Equation 2.16), and H<sub>2</sub> oxidation (Equation 2.17) (Ubago-Pe' rez *et al.*, 2007):

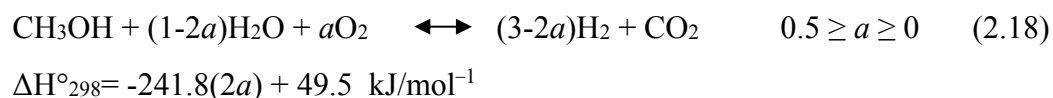




Moreover, the highly exothermic reaction of POM not only leads to the problem of removing the heat and controlling the reactor temperature, but also produces significant amount of CO.

### 2.2.3 Autothermal Steam Reforming of Methanol (ASRM)

As previously mentioned, methanol can be converted to a H<sub>2</sub>-rich stream by POM, SRM, or OSRM. The ASRM (Equation 2.18) is a combination between SRM and POM (Patel and Pant, 2007):



where  $a$  is an oxygen to methanol (O/M) molar ratio.

The POM is a highly exothermic reaction with a rapid start-up. However, this reaction gives a lower H<sub>2</sub> yield than theoretical H<sub>2</sub> concentration (67%). Furthermore, this reaction also provides a higher formation of by-product CO than SRM. On the other hand, SRM is an endothermic reaction and can give a higher theoretical H<sub>2</sub> concentration (75%) because of the additional contribution of water, while producing a low concentration of CO (<1%). External heating of the reformer in SRM reaction is required and fast start-up behavior unlike POM. Thus, the combination of POM and SRM which called the autothermal steam reforming of methanol (ASRM) was studied in order to save energy and obtain rapid start-up. In ASRM reaction, the exothermic POM supplies the heat energy which is required for the endothermic SRM. The overall heat of reaction depends on the value of  $a$  in Equation 2.18. Moreover, the reaction of CO generation with oxygen in ASRM is expected to reduce the amount of CO (Chang *et al.*, 2010).



Udani *et al.* (2009) studied SRM and ASRM over a series of coprecipitated CuO-CeO<sub>2</sub> catalysts and found that, see Figure 2.2, there was a rapid increase in the methanol conversion with increasing O<sub>2</sub> concentration. The methanol conversion with 5% of O<sub>2</sub> showed the highest conversion throughout the temperature range of 160°-300 °C. They concluded that the rate of POM was much faster than that of SRM.

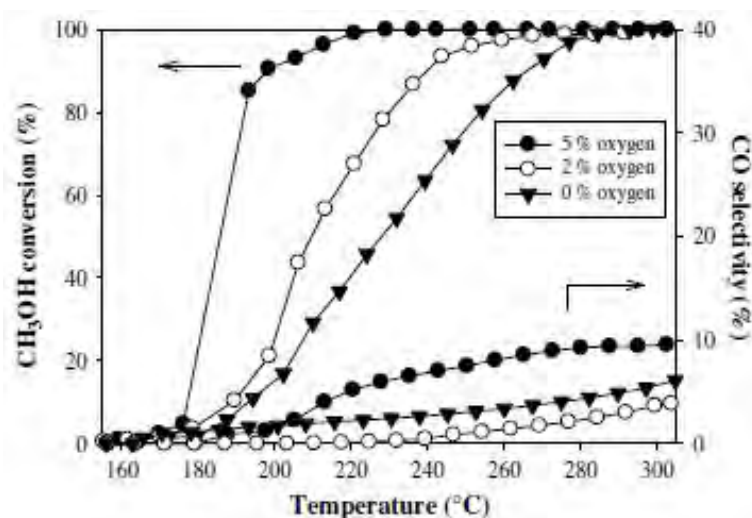


**Figure 2.2** Effect of oxygen concentration in the feed on the methanol conversion and CO selectivity. Feed: 100 ml/min, 10% CH<sub>3</sub>OH, 15% H<sub>2</sub>O, O<sub>2</sub> (shown) and balance He. Catalyst: 70 wt.% CuO-CeO<sub>2</sub>, weight=0.5 g (Udani *et al.*, 2009).

In 2001, Velu *et al.* reported that ASRM was more efficient for the selective H<sub>2</sub> production relatively at a lower temperature of around 230 °C using CuZnAl(Zr)-oxide catalysts. They studied several parameters for ASRM reaction, including effect of O<sub>2</sub>/CH<sub>3</sub>OH molar ratio, see Figure 2.3. The methanol conversion and the amount of H<sub>2</sub>, CO, and CO<sub>2</sub> increased with increasing O<sub>2</sub>/CH<sub>3</sub>OH ratio up to 0.3. They declined with further increasing in the O<sub>2</sub>/CH<sub>3</sub>OH ratio to 0.50 because they explained that H<sub>2</sub> produced in the ASRM reaction was oxidized to H<sub>2</sub>O, as shown in Equation 2.17.

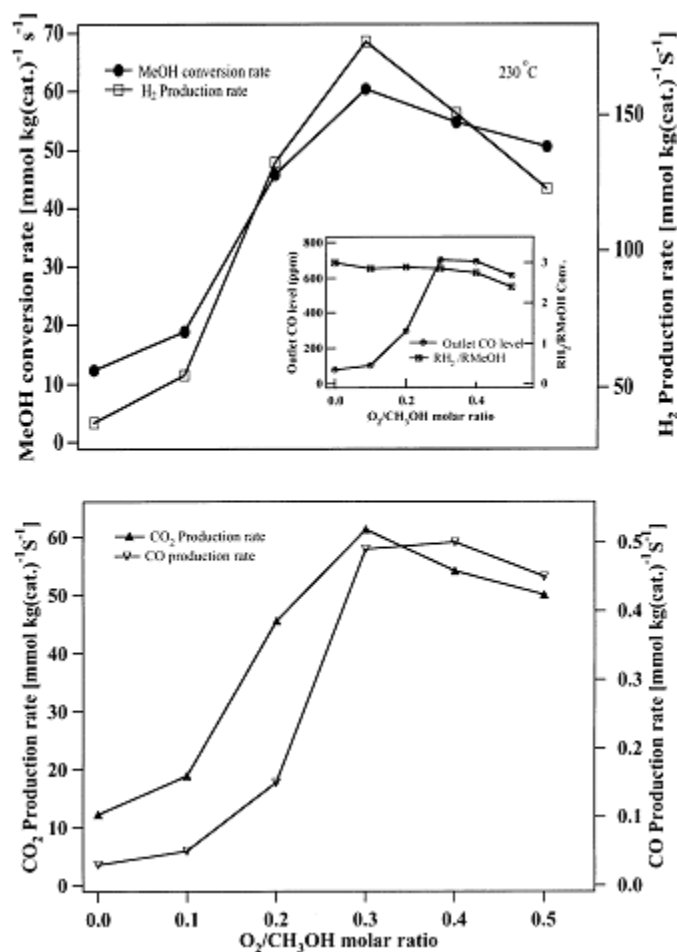


**Figure 2.3** Effect of O<sub>2</sub>/CH<sub>3</sub>OH molar ratio on the catalytic performance in the ASRM reaction over CZAZOC-6. The inset in the top figure shows the variation of outlet CO concentration and RH<sub>2</sub>/RMeOH conversion ratio as a function of O<sub>2</sub>/CH<sub>3</sub>OH molar ratio (Velu *et al.*, 2001).

Furthermore, they studied effect of H<sub>2</sub>O/CH<sub>3</sub>OH molar ratio on ASRM reaction, as shown in Figure 2.4, and found that RH<sub>2</sub>/RCH<sub>3</sub>OH conversion ratio increased from about 2.5 at lower H<sub>2</sub>O partial pressures (H<sub>2</sub>O/CH<sub>3</sub>OH ratio = 0.7) to about 3.0 with increasing the H<sub>2</sub>O/CH<sub>3</sub>OH ratio up to 1.6, resulting in a decrease of the CO content. It was referred that a higher partial pressure of H<sub>2</sub>O was favorable to reduce the outlet CO concentration due to the enhancement of the WGS reaction in ASRM process.

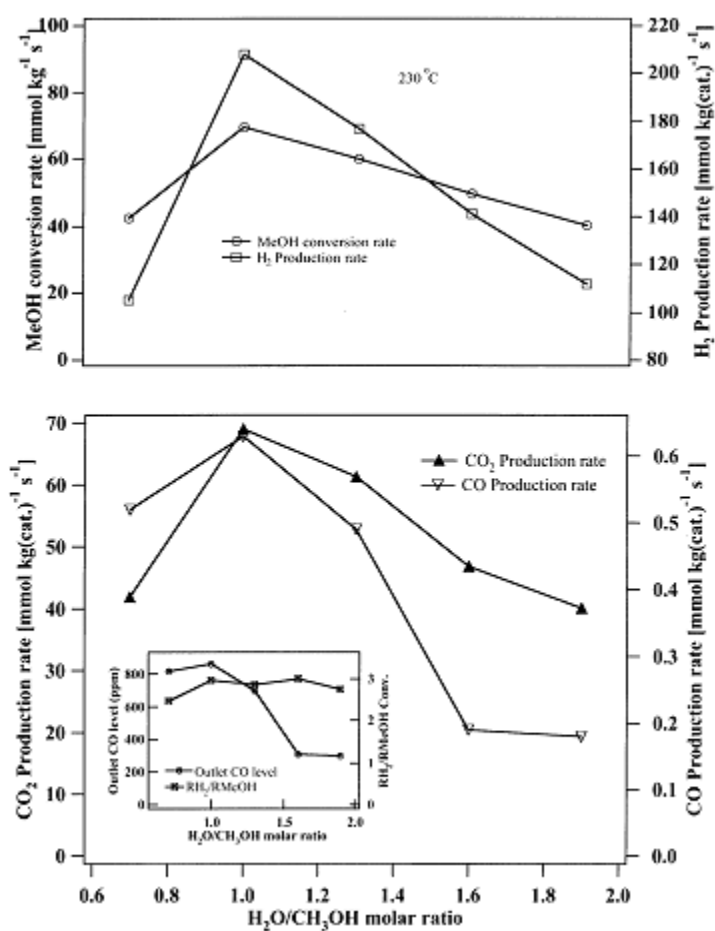


**Figure 2.4** Effect of H<sub>2</sub>O/CH<sub>3</sub>OH molar ratio on the catalytic performance in the ASRM reaction over CZAZOC-6. The inset in the bottom figure indicates the variation of outlet CO concentration and RH<sub>2</sub>/RMeOH conversion ratio as a function of H<sub>2</sub>O/CH<sub>3</sub>OH molar ratio (Velu *et al.*, 2001).

### 2.3 Catalyst

A catalyst is a substance that increases the rate of a reaction without modifying the overall standard Gibbs energy change in the reaction (Fechete *et al.*, 2012). It is not consumed during the reaction. A catalyst is appearing in the steps of a reaction mechanism, but it is not appearing in the overall chemical reaction (as it is not a reactant

or product). Furthermore, catalyst is required to increase the production yield and selectivity of any reactions. The CO-PROX and ASRM need to use catalyst to enhance their yield and selectivity. Catalysts can be classified into two categories, homogeneous and heterogeneous catalysts, depending on their relationship to the phase of the reaction. Porous material is an excellent material to utilize as heterogeneous catalysts to replace environmentally hazardous, corrosive, and difficult to separate and dispose of homogeneous catalysts (Fechete *et al.*, 2012).

### 2.3.1 Mesoporous Materials

Porous materials have been extensively studied regarding their technical applications as catalysts, catalyst supports, and adsorbents because of their ability to interact with atoms, ions, molecules, and nanoparticles not only at their surfaces, but also throughout the bulk of the materials. According to the IUPAC definition, porous materials are divided into three classes; microporous (pore size < 2 nm), mesoporous (2-50 nm), and macroporous (>50 nm) materials (Sing *et al.*, 1985). Mostly, mesoporous materials are investigated as catalyst or catalyst support because it has high surface area, suitable pore size, and pore structure which allow large molecules to penetrate inside the pore. These characteristics of mesoporous materials can overcome the limitation of microporous materials.

In 1992, Mobil scientists reported the synthesis of ordered mesoporous molecular sieves (M41S family) from liquid-crystal templates. They divided M41S family by different arrays into 3 groups, consisting of MCM-41 (hexagonal mesoporous structure), MCM-48 (cubic mesoporous structure), and MCM-50 (lamellar mesostructure), as shown in Figure 2.5 (Taguchi and Schuth, 2005). The cubic MCM-48 is the most interesting material in term of catalytic activity since it has a three-dimensional pore structure with interconnected channels which can reduce the diffusion limitations and avoid the pore-blocking of the catalysts (Monnier *et al.*, 1993). Furthermore, MCM-48 as ordered mesoporous material of silica can be used as hard template for synthesis of other mesoporous materials via nanocasting process.

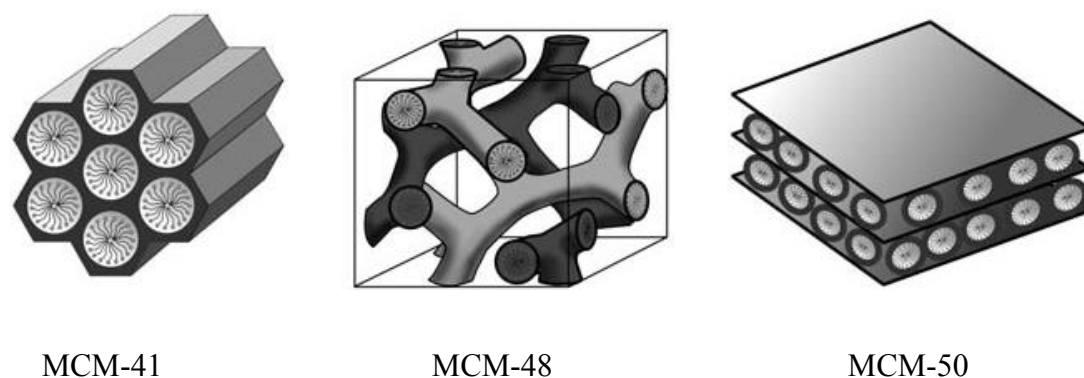


**Figure 2.5** Structures of mesoporous M41S materials (Hoffmann *et al.*, 2006).

### 2.3.2 Nanocasting Process

Although there are many synthetic pathways which have been reported for the synthesis of porous materials, the design and the synthesis of ordered nonsiliceous mesoporous materials are more attractive from an industrial perspective and their syntheses provide additional challenges. Nonsiliceous mesoporous materials, such as transition-metal and metal oxide mesoporous materials, are widely utilized as catalyst or catalyst support. Synthesis of highly ordered structure of transition-metal or metal oxide mesoporous materials is rather difficult because the hydrolysis and polymerization of alkoxides are more difficult to control.

Nanocasting process is an alternative synthesis pathway which has been developed to create mesoporous materials that are difficult to synthesize by conventional processes. Nanocasting process needs a hard template to fabricate ordered replicas (mesoporous materials). The hard template acts as a physical barrier to coalescence of the crystals during the calcination process. The strong points of the nanocasting technique are to obtain specific desired porous materials, depending on the structure of template, and ease of scale-up. Due to excellent characteristics of MCM-48, as previously mentioned, MCM-48 is chosen as a hard template for synthesis of mesoporous materials via nanocasting process. There are three main steps for nanocasting pathway to create

nanostructured materials, as shown in Figure 2.6 (Lu and Schüth, 2005 and Lu and Schüth, 2006):

- i) Formation of the template
- ii) The casting step with target precursors, including the conversion of the precursor, which is typically molecular, to a solid
- iii) Removal of the template

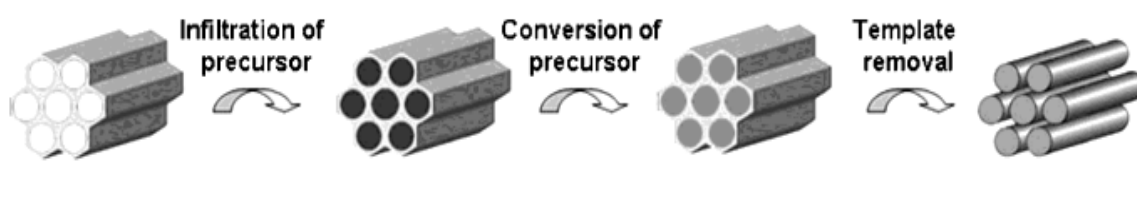


**Figure 2.6** Schematic illustration of the nanocasting pathway (Lu and Schüth, 2006).

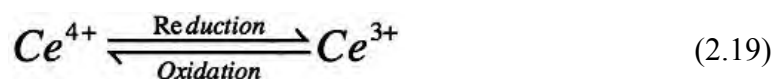
Deeprasertkul *et al.* (2014) synthesized ordered mesoporous ceria using MCM-48 as hard template via the nanocasting method. The optimal conditions to achieve the ordered mesoporous ceria were to use 50% wt of ceria precursor, 30 min stirring time, 100 °C evaporation temperature, and one filling cycle. The synthesized mesoporous ceria exhibited high surface area of 224.7 m<sup>2</sup>/g and ordered structure. Furthermore, analysis by TPR showed a larger area peak that is referred to the strong reduction at a lower temperature.

### 2.3.3 Mesoporous CeO<sub>2</sub>-ZrO<sub>2</sub> as Catalyst Support

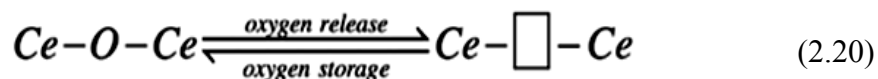
Rare earth oxides have been extensively studied in catalysis field as structural and electronic promoters to improve the activity, selectivity, and thermal stability of catalysts. The most important rare earth oxide in industrial catalysis is cerium oxide or ceria (CeO<sub>2</sub>) which has also been widely used for oxygen storage capacity and environmental catalysis. Ceria has a significant role in terms of economic relevance and tonnage for commercial catalytic processes, such as three-way catalysis (TWC) for eliminating toxic auto-exhaust gases and fluid catalytic cracking (FCC) (Trovarelli *et al.*,

1999). Two excellent characteristics for using ceria in catalysis are followed (Deeprasertkul *et al.*, 2014 and Yane *et al.*, 2014):

i) Ceria has an oxidation state between  $Ce^{3+}$  and  $Ce^{4+}$ ,  $CeO_2/Ce_2O_3$ , under oxidizing and reducing conditions facilitated via oxygen vacancies, as shown in Equation 2.19.



ii) Ceria is able to storage and release oxygen, as shown in Equation 2.20. This property of ceria is called the oxygen storage capacity (OSC).



The redox property of  $CeO_2$  strongly depends on textural properties because a decrease of surface area reduces all surface related to the redox processes (Fornasiero *et al.*, 1996).

Furthermore, incorporation of another metal to  $CeO_2$  can enhance its properties, for example, zirconium oxide ( $ZrO_2$ ), also known as zirconia, is a good candidate to combine with ceria. Zirconia has a high surface acidity and a high thermal stability. During the past several years,  $ZrO_2$  is widely used as a catalyst support. The incorporation of  $ZrO_2$  to  $CeO_2$  has been known to stabilize ceria against high temperature sintering (Zhang *et al.*, 2014). It has been also shown that the redox property of ceria is increased by incorporation of zirconia and the formation of mixed Zr–Ce oxides (Martinez-Arias *et al.*, 2002). The main characteristics which contribute to the success of ceria–zirconia include (Trovarelli *et al.*, 2001):

- i) Higher thermal resistance when compared with conventional pure  $CeO_2$
- ii) Higher reduction efficiency of the redox couple  $Ce^{4+}/Ce^{3+}$
- iii) Good oxygen storage/release capacity

Therefore, mesoporous  $CeO_2$ - $ZrO_2$  is a suitable mixed oxide for using as catalyst support or support material.

#### 2.3.4 Preparation of Supported Metal Catalysts via Deposition-Precipitation (DP)

Generally, there are many methodologies for preparing supported catalysts, such as impregnation and drying, metal-ion adsorption, DP, and chemical vapor deposition (Lee *et al.*, 2005). Deposition precipitation, a generic method to emplace metals, metal oxides, metal sulfides, or metal hydroxides as small particles onto a support material, involves in the precipitation of a metal precursor onto a suspended support material. Usually precipitation is achieved by a controlled increase of the pH in the metal salt solution (Lee *et al.*, 2005). The general advantages for the DP method include (Haruta *et al.*, 1993 and Jong, 2009):

- i) Obtaining small particle size at high metal loading
- ii) Obtaining narrow particle-size distributions
- iii) Achieving good dispersion of metal catalyst on support material

As a result, DP is extensively used for preparing supported metal catalysts.

#### 2.3.5 Cu-based Catalyst Loaded onto Catalyst Support

Due to the high cost of noble metals (such as palladium, silver, osmium, platinum, or gold) used as catalyst, researchers around the world attempt to look for other alternative catalysts. A transition metal, especially Cu, is a good candidate for catalytic industry, thus, Cu-based catalysts are useful for several applications (Zhang *et al.*, 2014). Moreover, Cu-catalysts usually exhibit high activity and selectivity in many reactions. Importantly, Cu is low cost when compared with noble metals, thus, Cu-based catalyst loaded onto catalyst support is very attractive.



### 2.3.6 Catalysts for Preferential Oxidation of CO (CO-PROX)

Marino *et al.* (2005) studied activity of supported base metal catalysts for CO-PROX. The catalysts investigated in this study were in a wide range of transition metals (Co, Cr, Cu, Ni, Zn) supported on oxides with very different acidic, basic, and redox properties (MgO, La<sub>2</sub>O<sub>3</sub>, SiO<sub>2</sub>-Al<sub>2</sub>O<sub>3</sub>, CeO<sub>2</sub>, Ce<sub>0.63</sub>Zr<sub>0.37</sub>O<sub>2</sub>). They found that the Cu-catalyst showed the best behavior (Figure 2.7) with a maximum CO conversion at temperature around 150 °C. A complete oxygen conversion was obtained at temperatures higher than 175 °C. Oxygen and CO conversions behave in a similar way in the temperature range between 50° and 150 °C, resulting in a constant selectivity.

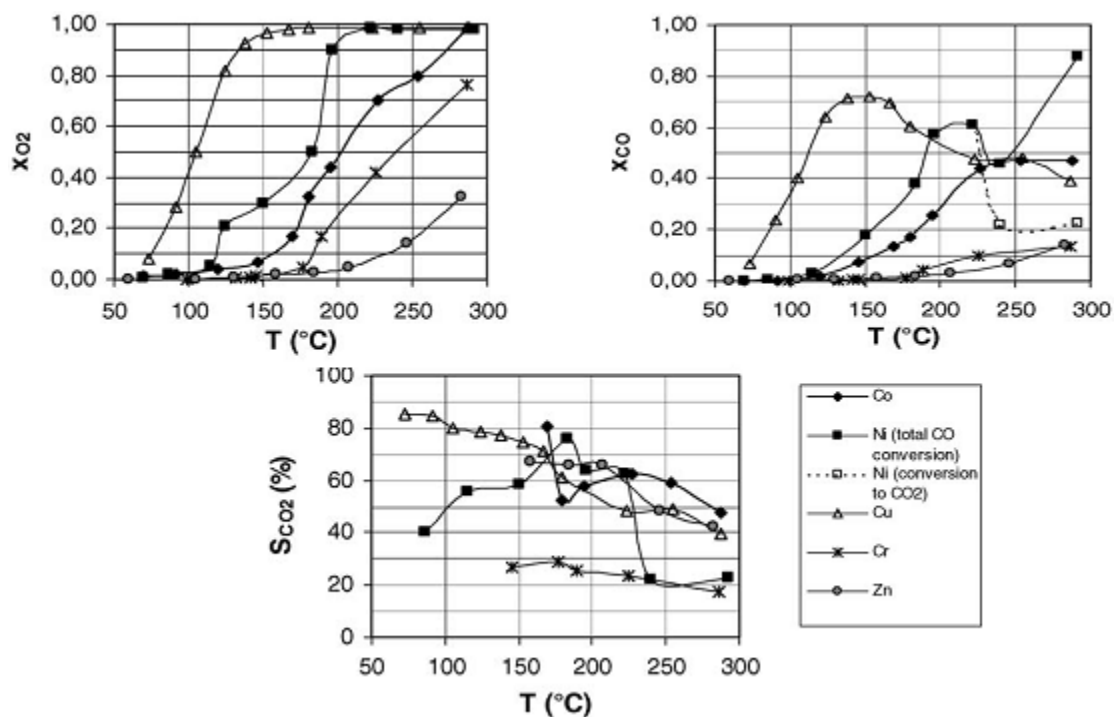


**Figure 2.7** CO-PROX over 1% M/Ce<sub>0.63</sub>Zr<sub>0.37</sub>O<sub>2</sub> (M = Co, Cr, Cu, Ni, Zn), evolution of the CO conversion, the O<sub>2</sub> conversion, and the CO<sub>2</sub> selectivity as a function of the reaction temperature (Marino *et al.*, 2005).

Caputo *et al.* (2008) synthesized CuO/CeO<sub>2</sub> catalysts with CuO content ranging from 0.5 to 8 wt.% by using wet impregnation method onto commercial ceria. Catalysts were characterized by XRD, BET analysis, UV spectroscopy, and TPR. All of catalysts were tested for CO-PROX under H<sub>2</sub>-rich conditions at 70°-210 °C, and the results showed that the active centers for CO oxidation contain Cu in the +2 oxidation state. Furthermore, they found that at temperature higher than 100 °C, some reduced Cu-sites are stabilized and promote H<sub>2</sub> oxidation, thus lowering the selectivity of the CO-PROX process. Finally, they concluded that the strong interaction between Cu and surface ceria is responsible for the formation of new species highly reducible by CO and re-oxidizable by O<sub>2</sub> at room temperature. Thus, mixed Cu-Ce material exhibiting redox properties is a good catalyst for CO-PROX reaction.

Araujo *et al.* (2012) prepared Ce<sub>1-x</sub>Cu<sub>x</sub>O<sub>2</sub> catalysts with x (mol%) = 0, 0.01, 0.03, 0.05 and 0.10 by polymeric precursor method. They obtained a very fine dispersion and strong metal-support interaction as well as favorably active Cu species. These properties are suitable for CO-PROX reaction. Furthermore, they found that under the synthetic conditions, the optimal loading for the complete CO conversion was 3% Cu, as shown in Figure 2.8.

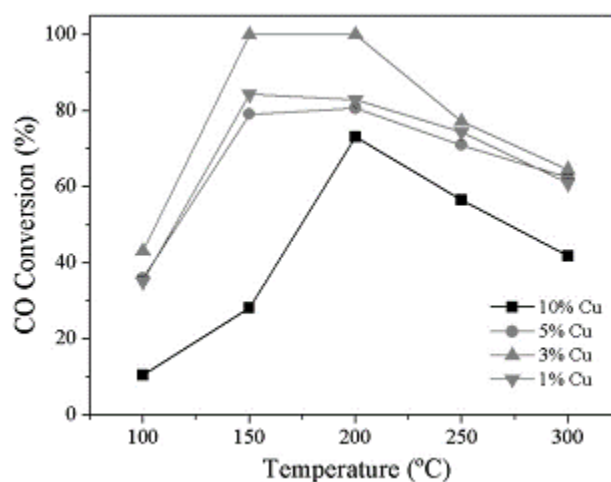


**Figure 2.8** CO conversion (%) at various temperatures (Araujo *et al.*, 2012).

Moretti *et al.* (2011) used a slow co-precipitation method in the absence of any structure directing agent for synthesis of a CuO-CeO<sub>2</sub>-ZrO<sub>2</sub> oxide system with a flower-like morphology. All samples were studied for the CO-PROX in the 40°-190 °C temperature range. They reported that CO-PROX activity and selectivity values of CuO-CeO<sub>2</sub>-ZrO<sub>2</sub> oxide system at low temperatures were very interesting. The sample (FCZCu650) which was treated at high temperature was attributed to the mobility at high temperatures of the small Cu ions, which could migrate towards the surface, thus becoming more easily reducible. Thus, FCZCu650 showed the highest catalytic activity, as shown in Figure 2.9.

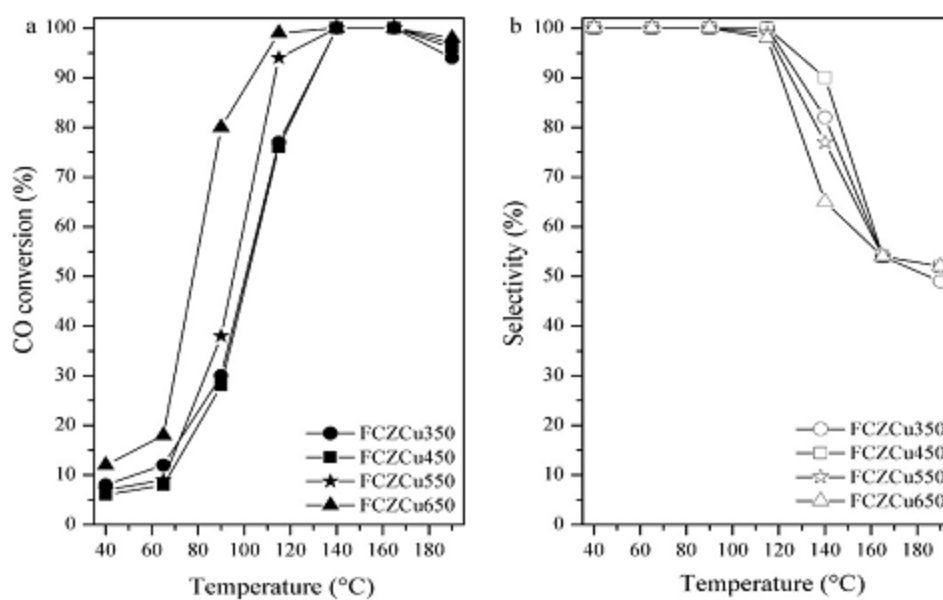


**Figure 2.9** (a) CO conversion and (b) selectivity to CO<sub>2</sub> as a function of temperature (Moretti *et al.*, 2011).

### 2.3.7 Catalysts for Autothermal Steam Reforming of Methanol (ASRM)

Shan *et al.* (2004) mentioned that CuO/CeO<sub>2</sub> catalysts were attracted because of their unique catalytic performances associated with environmental concerns, especially for CO oxidation, selective oxidation of CO under rich H<sub>2</sub> and WGS reactions. These reactions can occur during the ASRM. Due to the higher redox properties and the higher activity of Cu-based catalysts for ASRM, a high catalytic activity was expected for ASRM over CuO/CeO<sub>2</sub> catalyst. The Ce<sub>0.9</sub>Cu<sub>0.1</sub>O<sub>Y</sub> catalysts in this research were prepared by DP, coprecipitation (CP), and complexation-combustion (CC) methods. The production of H<sub>2</sub> from ASRM was tested for all catalysts. They found that methanol conversions higher than 85% with 90% H<sub>2</sub> yield from the ASRM at 240 °C were obtained when using Ce<sub>0.9</sub>Cu<sub>0.1</sub>O<sub>Y</sub> prepared by the CC method.

Pojanavaraphan *et al.* (2014) studied the synthesis of gold (Au) deposited on CeO<sub>2</sub>-ZrO<sub>2</sub> mixed oxides by CP technique for using in catalytic production of H<sub>2</sub> by ASRM reaction in the temperature range of 200°-400 °C. They reported that an active uniform Ce<sub>1-x</sub>Zr<sub>x</sub>O<sub>2</sub> solid solution appeared at a Zr/(Ce + Zr) ratio of 0.25. The catalyst at this ratio calcined at 400 °C efficiently performed Zr<sup>4+</sup> incorporation inside the Ce<sup>4+</sup> lattice to produce smaller ceria crystallites and higher surface area. The highest methanol conversion obtained was 92% at 400 °C while H<sub>2</sub> and CO concentrations were observed at 16 and 0.25%, respectively. Moreover, the stabilities of Au/CeO<sub>2</sub> and Au/CeO<sub>2</sub>-ZrO<sub>2</sub> were tested in ASRM reaction, as shown in Figure 2.10. It was also found that the inhibition of Au/CeO<sub>2</sub> activity by coke formation caused the loss of activity for the pure ceria supported catalyst. On the other hand, Au/CeO<sub>2</sub>-ZrO<sub>2</sub> activity was not significantly affected since the amount of coke formed was quite low.

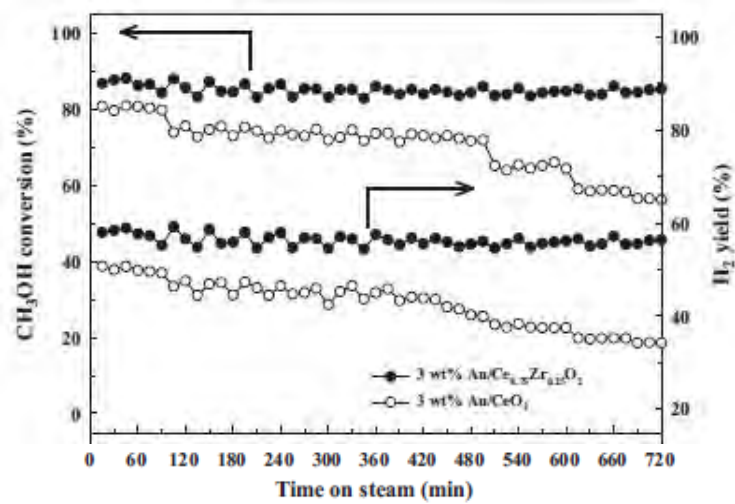


**Figure 2.10** Stability testing of 3 wt% Au/CeO<sub>2</sub> and 3 wt% Au/Ce<sub>0.75</sub>Zr<sub>0.25</sub>O<sub>2</sub> catalysts at reaction temperature of 350 °C (Pojanavaraphan *et al.*, 2014).

## CHAPTER III EXPERIMENTAL

### 3.1 Objectives

- To synthesize and characterize CuO loaded mesoporous CeO<sub>2</sub> and CuO loaded mesoporous CeO<sub>2</sub>-ZrO<sub>2</sub> catalysts
- To study catalytic activity of CuO loaded mesoporous CeO<sub>2</sub> and CuO loaded mesoporous CeO<sub>2</sub>-ZrO<sub>2</sub> catalysts for the preferential oxidation of CO (CO-PROX) reaction
- To study catalytic activity of CuO loaded mesoporous CeO<sub>2</sub> and CuO loaded mesoporous CeO<sub>2</sub>-ZrO<sub>2</sub> catalysts for autothermal steam reforming of methanol (ASRM)

### 3.2 Experimental

#### 3.2.1 Chemicals and Gases

- Fumed silica (SiO<sub>2</sub>, 99.8%, Nippon Aerosil, Japan),
- Triethanolamine (TEA, QRĕc chemical, Thailand),
- Ethylene glycol (EG, 99%, J.T. Baker, USA)
- Acetonitrile (CH<sub>3</sub>CN, 99.9%, Labscan, Thailand)
- Cetyltrimethylammonium bromide (CTAB, 96.0%, Fluka, Germany)
- Cerium(III) nitrate hexahydrate (Ce(NO<sub>3</sub>)<sub>3</sub>.6H<sub>2</sub>O, 99%, Sigma-Aldrich, Germany)
- Zirconium oxide chloride octahydrate (ZrOCl<sub>2</sub>.8H<sub>2</sub>O, 99.9%, Merck, Germany)
- Copper(II) nitrate trihydrate (Cu(NO<sub>3</sub>)<sub>2</sub>.3H<sub>2</sub>O, 99.5%, Merck, Germany)
- Sodium hydroxide (NaOH, 99%, Labscan, Thailand)
- Sodium carbonate (Na<sub>2</sub>CO<sub>3</sub>, 99.8%, Ajax, Thailand)
- Ethanol (CH<sub>3</sub>CH<sub>2</sub>OH, 99.9%, Labscan, Thailand)

- Methanol (CH<sub>3</sub>OH, 99.9%, Labscan, Thailand)
- Deionized water
- Nitrogen (N<sub>2</sub>, 99.98% purity, Thai Industrial Gases Public Company Limited (TIG), Thailand)
- Hydrogen (H<sub>2</sub>, 99.99% purity, Thai Industrial Gases Public Company Limited (TIG), Thailand)
- Oxygen (O<sub>2</sub>, 99.97% purity, Thai Industrial Gases Public Company Limited (TIG), Thailand)
- Helium (He, 99.99% purity, Thai Industrial Gases Public Company Limited (TIG), Thailand)
- Carbon dioxide (CO<sub>2</sub>, 99.99% purity, Thai Industrial Gases Public Company Limited (TIG), Thailand)
- Carbon monoxide (CO, 10% in Helium, Thailand)

### 3.2.2 Catalyst Preparation

#### 3.2.2.1 *Preparation of Silatrane*

The synthetic procedure of silatrane followed Wongkasemjit's synthetic method (Phiriyawirut *et al.*, 2003). A mixture consisting of 0.1 mol fumed silica, 0.125 mol TEA, and 100 ml EG was refluxed at 200 °C under nitrogen atmosphere for 12 h in an oil bath. The excess EG was then removed under vacuum at 110 °C to obtain a crude brown solid. The product was washed with acetonitrile, followed by vacuum-drying to result in white silatrane.

#### 3.2.2.2 *Preparation of MCM-48*

MCM-48 was prepared following Longloilert's synthetic method, using a molar composition of SiO<sub>2</sub>:CTAB:NaOH:H<sub>2</sub>O = 1:0.3:0.5:62 (Longloilert *et al.*, 2011). CTAB was dissolved in aqueous solution containing 2 M NaOH. The mixture was continuously stirred at 50 °C until the solution was homogeneously dissolved. Silatrane was added to the mixture with constant stirring at 50 °C for 1 h. Then, the mixture was transferred to a Teflon-lined stainless steel autoclave and subjected to an operating temperature of 140 °C for 16 h. The obtained

solid product was filtered and dried. The surfactant was removed by calcination at 550 °C for 6 h to obtain MCM-48.

#### *3.2.2.3 Preparation of Mesoporous CeO<sub>2</sub> Support*

Mesoporous CeO<sub>2</sub> support was synthesized via the nanocasting method using MCM-48 as template. 50 wt% Ce(NO<sub>3</sub>)<sub>3</sub>.6H<sub>2</sub>O was dissolved in 5 ml of ethanol while stirring at room temperature until a clear solution was appeared. 50 wt% MCM-48 was directly added to the solution, with continuous stirring for 30 min at room temperature. Subsequently, the removal of ethanol was performed by evaporation in an oven at 100 °C. The obtained solid was calcined at 550 °C for 6 h. The MCM-48 template was removed using 2 M NaOH at 50 °C. The resulting light yellow powder product was washed with deionized water until neutral and dried at 80 °C overnight.

#### *3.2.2.4 Preparation of Mesoporous CeO<sub>2</sub>-ZrO<sub>2</sub> Support*

Mesoporous CeO<sub>2</sub>-ZrO<sub>2</sub> support was synthesized via the nanocasting method using MCM-48 as template. Ce(NO<sub>3</sub>)<sub>3</sub>.6H<sub>2</sub>O and ZrOCl<sub>2</sub>.8H<sub>2</sub>O were dissolved in 5 ml of ethanol while stirring at room temperature until a clear solution was appeared. The molar ratio of Ce to Zr in solution was Ce:Zr = 0.75:0.25. MCM-48 was directly added to the solution, with continuous stirring for 4 h at room temperature. Subsequently, the removal of ethanol was performed by evaporation in an oven at 100 °C. The obtained solid was calcined at 550 °C for 6 h. The MCM-48 template was removed using 2 M NaOH at 50 °C. The resulting light yellow powder product was washed with deionized water until neutral and dried at 80 °C overnight.

#### *3.2.2.5 Preparation of Cu Loaded Mesoporous CeO<sub>2</sub> and Cu Loaded Mesoporous CeO<sub>2</sub>-ZrO<sub>2</sub> Catalyst*

The deposition-precipitation (DP) technique was employed to prepare Cu loaded mesoporous CeO<sub>2</sub> and Cu loaded mesoporous CeO<sub>2</sub>-ZrO<sub>2</sub> catalyst. Mesoporous catalyst support was added to an aqueous solution containing various amounts of Cu(NO<sub>3</sub>)<sub>2</sub>.3H<sub>2</sub>O (% Cu loadings of 1, 3, 5, 7, and 9% by wt.). The mixture was stirred at room temperature for 1 h. Next, 0.1 M Na<sub>2</sub>CO<sub>3</sub> as precipitating agent was added dropwise to neutralize the mixture, and the mixture was heated to 80 °C before aging for another hour. The resulting solid was washed with boiling distilled



water. Finally, it was dried at 80 °C overnight and calcined in air at 500 °C for 6 h to obtain catalysts.

### 3.2.3 Catalyst Analysis

The Brunauer-Emmett-Teller (BET) method using Quantachrome Autosorb-1 was used to determine the specific surface area, pore volume and pore size distribution of the prepared catalysts by N<sub>2</sub> adsorption-desorption at -196 °C. Small angle x-ray diffraction (SAXD, Rigaku TTRAX III) with a scanning speed of 1° min<sup>-1</sup> and CuK $\alpha$  radiation ( $\lambda$ = 1.5406 Å) in a range of  $2\theta = 1-6^\circ$  was used to characterize the mesoporous phase and the crystallinity of the prepared catalysts. Morphology and structure of the catalysts were directly observed by transmission electron microscopy (TEM) on a JEOL JEM-2100F TEM instrument operating at an accelerating voltage of 200 kV. Wide angle x-ray diffraction (WAXD) analysis of the catalysts was performed on a Rigaku Smartlab<sup>®</sup> diffractometer with a scanning speed of 1° min<sup>-1</sup> and CuK $\alpha$  radiation ( $\lambda$ = 1.5406 Å) in a range of  $2\theta = 20-80^\circ$  in order to determine the crystallinity, phase purity of the catalysts, and dispersion of Cu on mesoporous support. The crystallite size of the catalysts was also determined from the line width of the XRD peak corresponding to {111} reflection by using the Debye-Scherrer equation. The amount of Cu loading on mesoporous support was determined by atomic absorption spectrometry (AAS, VARIAN Model 300/400). X-ray photoelectron spectroscopy (XPS, Kratos AXIS Ultra DLD spectrometer) of the catalysts was applied to determine chemical compositions and oxidation states at the catalyst surface. The measurements were conducted using monochromatic AlK $\alpha$  X-ray radiation (15 kV) at a pressure lower than  $5 \times 10^{-7}$  Torr. The C1s peak was fixed at a binding energy of 284.6 eV. Raman spectra were carried out using a Senterra dispersive Raman microscope (Bruker Optics) with a 532 nm, 20 mW, argon ion laser. For each sample, the spectral range was between 4500–70 cm<sup>-1</sup>. Temperature-programmed reduction (H<sub>2</sub>-TPR) was measured to evaluate the reducibility of the prepared catalysts using 50 mg of the prepared catalysts. The sample was reduced by 5.13% H<sub>2</sub>/N<sub>2</sub> (v/v) at a heating rate of 10 °C/min. A thermal conductivity detector (TCD) was used to detect hydrogen consumption.

### 3.2.4 Catalytic Activity Measurements

#### 3.2.4.1 *Preferential Oxidation of CO (CO-PROX) Reaction*

Catalytic activity measurements of the prepared catalysts for CO-PROX reaction were carried out using a fixed bed U-tube reactor operating at a temperature range of 50°–250 °C and atmospheric pressure. A 100 mg of catalyst was packed into a U-tube between layers of glass wool. The reactant gas composition containing 1 vol.% CO, 1 vol.% O<sub>2</sub>, 40 vol.% H<sub>2</sub> balancing with He was mixed before feeding to the CO-PROX reactor. The total flow rate of the mixed gas controlled by mass flow controllers was about 50 ml min<sup>-1</sup>. The product gas stream was detected by an on-line gas chromatograph (Agilent Technologies 6890N) using a carbosphere column and a thermal conductivity detector (TCD). The effect of CO<sub>2</sub> and H<sub>2</sub>O on the performance of CO-PROX reaction was studied by adding 10 vol.% CO<sub>2</sub> and 10 vol.% H<sub>2</sub>O in the feed gas.

#### 3.2.4.2 *Oxidative Steam Reforming of Methanol (OSRM)*

The OSRM reaction was carried out in a fixed-bed reactor containing 100 mg of catalysts under atmospheric pressure at the reaction temperature of 200°–400 °C. A mixture of distilled water and methanol was injected continuously by a syringe pump at a rate of 1.5 ml/h. The mixture was vaporized to produce a vapor of methanol and steam. The vapor of mixture was carried by He as carrier gas and oxygen before entering the catalytic reactor. The O<sub>2</sub>/H<sub>2</sub>O/CH<sub>3</sub>OH feed molar ratio was constantly fixed at 0.6/2/1. The product gases (e.g. H<sub>2</sub>, CO, CO<sub>2</sub>, and CH<sub>4</sub>) from the reactor were analyzed both qualitatively and quantitatively by Hewlett Packard 5890 series II gas chromatograph (Agilent 6890N) with a packed carbosphere (80/100 mesh) column (10 ft x 1/8 in.) and a thermal conductivity detector (TCD).

**CHAPTER IV**  
**HIGH PERFORMANCE AND STABILITY OF COPPER LOADING ON**  
**MESOPOROUS CERIA CATALYST FOR PREFERENTIAL OXIDATION**  
**OF CO IN PRESENCE OF EXCESS OF HYDROGEN**

**4.1 Abstract**

Copper (Cu) supported on mesoporous (MSP) ceria catalysts were prepared by deposition-precipitation (DP) method for the preferential CO oxidation of CO in a H<sub>2</sub>-rich stream (CO-PROX). A MSP ceria support with a high surface area of 293 m<sup>2</sup>/g and ordered structure was synthesized by a nanocasting process using MCM-48 as template. All copper-MSP ceria catalysts show high dispersion of Cu and still maintain the fluorite structure of MSP ceria. Moreover, TEM imaging confirmed the three dimensional and long-range ordered pore structure of the Cu-catalysts. The reduction temperature of the Cu-catalysts decreases compared to pure MSP ceria and the reduction of Ce<sup>4+</sup> to Ce<sup>3+</sup> decreases with increasing copper content. An MSP ceria catalyst with 7 wt% Cu loading (7Cu/MSP ceria) shows the highest activity with high stability for over 48 h in various feed components, making it attractive for use as a catalyst in purification of hydrogen.

**(Keywords:** Mesoporous ceria; High surface area; Copper catalyst; Deposition-precipitation; CO-PROX reaction)

## 4.2 Introduction

Hydrogen (H<sub>2</sub>) is very attractive for use in proton exchange membrane (PEM) fuel cells as a readily available gas, a renewable energy source, a hazard-free, environmentally-friendly and efficient fuel. However, a major problem for PEM fuel cells is the need for high-purity H<sub>2</sub> (Candusso *et al.*, 2006). The preferential CO oxidation (PROX) reaction has been widely used in the purification process of H<sub>2</sub> due to its low cost and ability to reduce CO content to less than 10 ppm without excessive hydrogen consumption.

Ceria has been widely investigated for use in automotive exhaust purification, oxygen storage and release, and catalysis via conversion between Ce<sup>3+</sup> and Ce<sup>4+</sup> oxidation states (Bunluesin *et al.*, 1995; Bunluesin *et al.*, 1998; Wang *et al.*, 2002). The catalytic performance of ceria can be increased by improving its structural properties, such as surface area and crystal morphology (Beck *et al.*, 1992; Kresge *et al.*, 1992).

Mesoporous (MSP) materials provide superior performances in allowing large reactants to penetrate inside the pores due to their large pore sizes, between 2–50 nm, and high surface areas. Thus, they have attracted particular attention in many applications, including adsorption, catalysis, sensing, and as hosts for the synthesis of nanomaterials (Idakiev *et al.*, 2006). Cubic MCM-48, indexed in the space group of *Ia3d*, is a very attractive mesoporous material in terms of catalytic activity due to its three-dimensional pore structure and interconnected channels, reducing diffusion limitations and avoiding pore blockage of reactants (Monnier *et al.*, 1993).

Deeprasertkul *et al.* (2014) synthesized MSP ceria via a nanocasting method using high surface area MCM-48 as a template. The synthesized MSP ceria has high surface areas with strong reduction at lower temperature than commercial ceria. However, pure MSP CeO<sub>2</sub> still has too high a reduction temperature to be used as a catalyst in the PROX reaction. It was reported that structural modification of the CeO<sub>2</sub> lattice by doping with transition metal oxides may improve its stability and activity (Trovarelli *et al.*, 1999). For example, loading copper (Cu) onto commercial CeO<sub>2</sub> resulted in higher activity and selectivity in CO oxidation (Jacobs *et al.*, 2004; Sedmak *et al.*, 2004; Martinez-Arias *et al.*, 2006; Gamboa-Rosales *et al.*, 2011). Moreover, not

only is the Cu-catalyst tolerant to the products, CO<sub>2</sub> and H<sub>2</sub>O, from the PROX reaction (Avgouropoulos *et al.*, 2006), but also its cost is low. However, it is reported that Cu supported on commercial ceria achieves high % conversion only at high temperature (Li *et al.*, 2012). Many researchers have, thus, attempted to synthesize bimetallic Au-Cu supported on ceria to obtain high activity at low temperatures (Fonseca *et al.*, 2012). Another way to increase the activity of Cu is to dope Cu onto mesoporous ceria (Tang *et al.*, 2014). Yen *et al.* (2012) reported the CO-PROX performance of mesoporous Cu/CeO<sub>2</sub> catalyst, prepared by using MCM-48 as hard template. The Cu/CeO<sub>2</sub> catalyst with a high Cu loading (30% Cu) was studied. The maximum CO conversion was about 88% at 80 °C. However, the method employed to load Cu onto the support influences the catalytic activity. The Cu-loading was prepared by the deposition-precipitation (DP) method, which has an advantage over other methods in terms of generating a uniform particle distribution with small particle sizes (Haruta *et al.*, 1993) and a closed intimate interaction between the metal particles and the support (Bond and Thompson, 1999).

In this work, Cu loaded onto MSP ceria, with different percentages of Cu loading, using the deposition-precipitation (DP) method, was prepared and characterized, after which the catalytic activity and stability for the PROX reaction was determined using various feed components. All prepared copper catalysts were characterized by various techniques to elucidate the relationship between structure and catalytic performance.

### 4.3 Experimental

#### 4.3.1 Materials

Fumed silica (SiO<sub>2</sub>, 99.8%, Nippon Aerosil, Japan), HP grade nitrogen (N<sub>2</sub>, 99.98% purity, Thai Industrial Gases Public Company Limited (TIG), Thailand), ethylene glycol (EG, 99%, J.T. Baker, USA), triethanolamine (TEA, QRęc chemical, Thailand), acetonitrile (CH<sub>3</sub>CN, 99.9%, Labscan, Thailand), cerium(III)nitrate hexahydrate (Ce(NO<sub>3</sub>)<sub>3</sub>.6H<sub>2</sub>O, 99%, Sigma-Aldrich, Germany), ethanol (CH<sub>3</sub>CH<sub>2</sub>OH, 99.9%, Labscan, Thailand), sodium hydroxide (NaOH, 99%, Labscan, Thailand), cetyltrimethylammonium bromide (CTAB, 96.0%, Fluka, Germany),

copper(II)nitrate trihydrate ( $\text{Cu}(\text{NO}_3)_2 \cdot 3\text{H}_2\text{O}$ , 99.5%, Merck, Germany), and sodium carbonate ( $\text{Na}_2\text{CO}_3$ , 99.8%, Ajax, Thailand) were used without further purification.

#### 4.3.2 Catalyst Preparation

Following Longloilert's synthetic method (Longloilert *et al.*, 2011), CTAB, as surfactant, was dissolved in 2 M NaOH solution. The mixture was stirred at 50 °C until a clear solution was obtained, after which silatrane was added, as the silica source, until the molar composition of the mixture was 1.0SiO<sub>2</sub>:0.3CTAB:0.5NaOH:62H<sub>2</sub>O. The mixture was then stirred for 1 h before hydrothermal treatment at 140 °C for 16 h in a Teflon-lined stainless steel autoclave to obtain solid product. The solid product was collected by filtration, dried, and calcined at 550 °C for 6 h to remove all organic components.

Following Deeprasertkul's synthetic method (Deeprasertkul *et al.*, 2014), the MSP ceria was prepared via nanocasting method by mixing 50 wt% of cerium nitrate as a precursor with MCM-48 as a template in 5 ml of ethanol. After 30 min stirring, the ethanol in the mixture was removed by evaporation in an oven at 100 °C. The dried powder was calcined in air at 550 °C for 6 h to decompose the nitrate species. The silica hard template was removed by stirring 3 times with 2 M NaOH at 50 °C, washed with deionized water until neutral and dried at 100 °C.

CuO/MSP ceria catalysts were prepared by deposition-precipitation (DP) from aqueous solution of  $\text{Cu}(\text{NO}_3)_2 \cdot 3\text{H}_2\text{O}$  with different loadings of Cu (3, 5, 7 and 9 wt%). The mixture was stirred at room temperature for 1 h, heated to 80 °C, and its pH adjusted to 7 by  $\text{Na}_2\text{CO}_3$ . The mixture was then aged for 1 h to obtain a crude solid product, which was filtered, washed with warm distilled water, dried over night at 80 °C, and finally calcined in air at 500 °C for 6 h.

#### 4.3.3 Catalyst Characterization

The residual silica was determined by X-ray fluorescence spectrophotometry (XRF) technique on a PANalytical AXIOS PW 4400 and the actual content of copper loaded on MSP ceria was determined by atomic adsorption spectroscopy (VARIAN Model 300/400). Mesoporous phase morphology of the

prepared catalysts was evaluated by Small Angle X-Ray Diffraction (SAXD) (Rigaku TTRAX III) with a scanning speed of  $1^\circ \text{ min}^{-1}$  and  $\text{CuK}\alpha$  source ( $\lambda = 1.5406 \text{ \AA}$ ) in a range of  $2\theta = 2\text{--}6^\circ$ . Crystallinity was evaluated via Wide Angle X-Ray Diffraction (WAXD), performed on a Rigaku Smartlab<sup>®</sup> with a scanning speed of  $1^\circ$  and  $0.1^\circ \text{ min}^{-1}$  and  $\text{CuK}\alpha$  source ( $\lambda = 1.5406 \text{ \AA}$ ) in a range of  $2\theta = 20\text{--}80^\circ$  to investigate the metal nano-crystals and dispersions. Crystallite sizes of ceria and CuO were determined using the Scherrer equation with a Scherrer constant of 0.94 for spherical cubic crystals (Langford and Wilson, 1978). Moreover, the lattice parameter ( $a$ ) of the cubic phase was estimated as. The specific surface area and pore size distribution of the catalysts were determined by  $\text{N}_2$  adsorption-desorption isotherms (Quantachrome Autosorb-1 MP). Transmission electron microscopy (TEM) images were characterized on a JEOL JEM-2100F TEM instrument. The samples were prepared by dispersion in methanol and then the solution was dropped on a hollow carbon grid and dried at room temperature. The photographs were taken at an accelerating voltage of 200 kV. X-ray photoelectron spectroscopy (XPS) was used to characterize the surface composition and oxidation state of the surface elements measured on a Kratos AXIS Ultra DLD spectrometer with a monochromatic  $\text{Al-K}\alpha$  X-ray source (15 kV). The pressure in the analysis chamber was lower than  $5 \times 10^{-7}$  Torr. The survey spectra were observed in the binding energy (BE) between 0 to 1200 eV. The detailed spectra were obtained for the C 1s, O 1s, Ce 3d and Cu 2p regions. The charging effect was subtracted by fixing the C 1s peak at the binding energy of 284.9 eV. Raman spectra were carried out using a Senterra dispersive Raman microscope (Bruker Optics) with a 532 nm, 20 mW, argon ion laser. For each sample, the spectral range was between  $4500\text{--}70 \text{ cm}^{-1}$ .

The redox properties were evaluated by temperature-programmed reduction under hydrogen ( $\text{H}_2$ -TPR) using a 50 mg sample. The samples were pretreated in  $\text{N}_2$  at  $250^\circ \text{C}$  for 30 min, and then cooled to room temperature.  $\text{H}_2$ -TPR profiles were observed from room temperature to  $900^\circ \text{C}$  with a heating rate of  $10^\circ \text{C min}^{-1}$  in 5.13 %  $\text{H}_2/\text{N}_2$  ( $20 \text{ ml min}^{-1}$ ). Hydrogen consumption was detected by a thermal conductivity detector (TCD).

#### 4.3.4 Activity Measurement

All catalytic activity measurements for PROX were evaluated by packing 100 mg of the 80-120 mesh catalyst in a fixed-bed U-tube micro-reactor at atmospheric pressure. The activity was investigated at various temperatures (50-250 °C). The composition of feed gas (%vol) for PROX reaction was H<sub>2</sub>/O<sub>2</sub>/CO = 40/1/1, balanced in He with a total flow rate of 50 ml min<sup>-1</sup>. The influent and effluent gases were analyzed by auto-sampling using an on-line gas chromatograph (Agilent Technologies 6890N) equipped with a packed carbosphere column (80/100 mesh and 10 ft x 1/8 inch) and a thermal conductivity detector (TCD). The CO conversion or catalytic activity calculations were based on the CO consumption and the CO selectivity determined by the ratio of O<sub>2</sub> consumption for CO conversion reaction to the total O<sub>2</sub> consumption. Moreover, the effect of the feed component on the catalyst performance for the PROX reaction was studied by adding 10 vol% CO<sub>2</sub> and 10 vol% water into the influent gases while maintaining a composition of H<sub>2</sub>/O<sub>2</sub>/CO at 40/1/1 with a total flow rate of 50 ml min<sup>-1</sup>.

### 4.4 Results and Discussion

#### 4.4.1 Characterization of Pure MSP Ceria

The ordered MSP ceria synthesized via nanocasting from the MCM-48 template, the negative replica of the MCM-48 template, shows identical characteristic diffraction peaks, see the SAXD pattern in Figure 4.1A-inset at {211} and {220}, consistent with the work reported by Longloilert et al. (2011). This result confirms that the MSP ceria still retains some order from the MCM-48 template. Moreover, the crystallinity of the MSP ceria was also confirmed by WAXD in Figure 4.1A, showing peaks at  $2\theta = 29^\circ, 33.2^\circ, 47.2^\circ, 55.3^\circ, 59.1^\circ, 69.3^\circ, 76.8^\circ, \text{ and } 78.9^\circ$ , corresponding to the peaks of cubic fluorite structured ceria (Monyanon *et al.*, 2006; Caputo *et al.*, 2008). The absence of the peak at  $2\theta = 22^\circ$ , characteristic of amorphous silica, suggests absence of the silica template in the final product. Moreover, the silica template residual determined by XRF technique indicated only a small amount of silica remaining (8 %wt) in the ordered MSP ceria after removal of the template.



The N<sub>2</sub> adsorption-desorption isotherm in Figure 4.1B shows a type IV isotherm with H3 hysteresis loop, characteristic of MSP materials with slit-like pores (Alfredsson and Anderson, 1996). This isotherm shows two steps at P/P<sub>0</sub> around 0.6 and 0.9-1.0. The first step corresponds to pore-plugging (Groen *et al.*, 2003) indicating that partial channels are filled by guest species. The other step at P/P<sub>0</sub> = 0.9-1.0 is due to the textural pores between the particles (Shen *et al.*, 2005). The pore size distribution curve (inset) in Figure 4.1B presents a sharp peak with an average pore diameter of 5.8 nm, confirming the uniform sizes of pores in the prepared MSP ceria. Moreover, its BET specific surface area was determined to be 293 m<sup>2</sup>/g, which is higher than that of commercial ceria (Rhodia, S<sub>BET</sub> = 164 m<sup>2</sup>/g, average pore diameter = 4.0 nm).

#### 4.4.2 Characterization of Cu Loaded on MSP Ceria

The physical properties of the synthesized catalysts are shown in Table 4.1. The percentage of Cu loading determined by AAS measurement is very close to the theoretical value, indicating that the deposition-precipitation is a very suitable and effective method for depositing Cu onto MSP ceria (Liao *et al.*, 2013). Not surprisingly, addition of Cu decreases the BET surface area of the material, as compared to the pure ceria, in particular, 9 wt% Cu loading dramatically decreases surface area by about 31 %.

The WAXD patterns of all prepared catalysts shown in Figure 4.2A exhibit the main diffraction peaks at  $2\theta = 29^\circ, 33.2^\circ, 47.2^\circ, 55.3^\circ, 59.1^\circ, 69.3^\circ, 76.8^\circ,$  and  $78.9^\circ$ , corresponding to the fluorite-type cubic crystal structure of the ceria phase (Monyanon *et al.*, 2006; Caputo *et al.*, 2008). Interestingly, there are no diffraction peaks at  $2\theta = 35.6^\circ$  and  $38.8^\circ$  characteristic of CuO phases in all copper loading catalysts, probably due to either a high dispersion of the Cu or the low detection limit at these copper concentrations. To further support that the CuO was well-dispersed, all Cu loading catalysts were subjected to a longer WAXD scan time, as illustrated in Figure 4.2A (inset), and the results still showed no evidence of the Cu diffraction peaks, consistent that the DP method provides highly dispersed Cu on MSP ceria. This likely reflects a strong interaction between copper and ceria, as reported by Liao *et al.* (2013). Two probable mechanisms can explain the relationship between high dispersed Cu species and MSP ceria. First, the Cu atoms occupy oxygen vacancies in the MSP

ceria support. Second, the Cu atoms locate only on the pore surfaces of the MSP ceria (Dow and Huang, 1994).

The average sizes of ceria crystallites for all catalysts (Table 4.1), calculated from the diffraction peak broadening at  $2\theta = 29^\circ$  using Scherrer's equation, are not different from that of the pure MSP ceria. The average crystallite size measured for MSP ceria (3.8 nm) is very small, compared to commercial ceria (larger than 5.0 nm) (Ayastuy *et al.*, 2010; Gamboa-Rosales *et al.*, 2012), reflecting a large number of oxygen vacancies in the fluorite structure crystallites (Graham *et al.*, 1991; McBride *et al.*, 1994). The catalytic activity of ceria is proportional to the number of oxygen vacancies in the crystal (Laguna *et al.*, 2011). The lattice parameter (*a*) of all prepared catalysts, calculated from the main diffraction peaks of ceria cubic phase, showed identical values to that of pure MSP ceria, within experimental error. Moreover, the variation in the cell parameters after introducing Cu onto the ceria lattice (not shown) is negligibly different. As a result, it can be concluded that the Cu loaded on MSP ceria still retains the fluorite structure.

To seek further evidence that Cu species are highly dispersed in the MSP ceria and still retain the MSP structure, as indicated by the XRD results, TEM was carried out. However, because of the low contrast between Cu and ceria, it was not possible to detect the dispersion of CuO (Xiaodong *et al.*, 2012), as shown in Figure 4.2B. However, this figure illustrates that the morphology of 7Cu/MSP ceria still retains the long-range three-dimensional order in the pore arrangement between the nanoparticles. The average size of ceria crystallites (3.5 nm) is similar to that obtained from the WAXD analysis (3.8 nm).

Some studies report that the XPS technique is able to characterize the surface composition of ceria-based catalysts (Zsoldos *et al.*, 1996; Palermo *et al.*, 2002; Fox *et al.*, 2008; Wei *et al.*, 2011). Table 4.2 summarises the information about the amount of Cu on the surface of the catalysts, the fraction of lattice oxygen, the location of the shake-up peak and the amount of  $\text{Ce}^{3+}$  species. Each Cu containing catalyst was detected at 5 positions. Interestingly, all catalysts showed much lower Cu percentages at the surface than those obtained by AAS analysis in the bulk. As discussed previously, the XRD results showed high dispersion with no accumulated copper. It can be rationalized that most of copper species are embedded inside the

pores of MSP ceria since the average pore diameter of MSP ceria (5.79 nm) is much larger than that of Cu atoms (0.07 nm).

#### 4.4.3 Reduction Property of Cu Loaded on MSP Ceria

The H<sub>2</sub>-TPR profile of MSP ceria, shown in Figure 4.3A (inset), exhibits two reduction peaks at 320°–650 °C and 680°–880 °C. According to studies cited elsewhere (Rao and Mishra, 2003; Zhu *et al.*, 2004), these peaks correspond, respectively, to the reduction of the surface-capping oxygen and bulk-phase lattice oxygen (Rao and Mishra, 2003; Zhu *et al.*, 2004). The highest intensity of the former peak was observed on the ordered MSP ceria correlating to the high surface area (Deeprasertkul *et al.*, 2014). The reduction of CeO<sub>2</sub> can be classified into four steps (Rao and Mishra, 2003):

- (i) H<sub>2</sub> reacts with Ce<sup>4+</sup> to form hydroxyl groups.
- (ii) Oxygen vacancies and Ce<sup>3+</sup> species are generated.
- (iii) Water is removed.
- (iv) The oxygen vacancies diffuse into the bulk.

After reduction, the formed oxygen vacancies can be refilled by O<sub>2</sub> gas in order to generate Ce<sup>4+</sup> species again, thus explaining the redox behavior of the catalysts.

Furthermore, it is worth noting that pure CuO has only one TPR peak at 380°–392 °C (Xiaoyuan *et al.*, 2001). In this study, the reduction profiles of all Cu/MSP ceria were shifted to lower temperatures at 180° and 230 °C, as shown in Figure 4.3A. The reduction profiles of all Cu/MSP ceria were deconvoluted to two peaks, as illustrated in Figure 4.3B. The low temperature peak is related to highly dispersed Cu species on the surface directly interacting with the MSP ceria support. The second peak at the higher temperature is related to larger CuO clusters formed on the MSP ceria surface (Luo *et al.*, 1997; Caputo *et al.*, 2008).

The theoretical and experimental hydrogen (H<sub>2</sub>) consumptions for all samples are presented in Table 4.3. The excess H<sub>2</sub> consumption in the second peak above the theoretical H<sub>2</sub> consumption required for complete reduction of CuO (CuO + H<sub>2</sub> → Cu + H<sub>2</sub>O) relates to the H<sub>2</sub> consumption for the reduction of Ce<sup>4+</sup> to Ce<sup>3+</sup> (Luo *et al.*, 1997). As seen in Table 4.3, the amount of H<sub>2</sub> available for the reduction of ceria

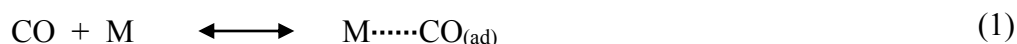
decreases, because the H<sub>2</sub> consumption of CuO increases when the Cu content in catalyst increases. As a result, it can be concluded that the reduction of Ce<sup>4+</sup> to Ce<sup>3+</sup> decreases with increasing the Cu content.

#### 4.4.4 Catalytic Performance for PROX

##### 4.4.4.1 *Effect of Feed Components*

Catalytic performances of all Cu loading catalysts were evaluated for the PROX reaction under excess H<sub>2</sub> in the temperature range of 50°–250 °C, see Figure 4.4 a-b. All Cu/MSP ceria showed higher activity than pure ceria which has T<sub>50</sub> at 310 °C. The CO-PROX mechanism over CuO/CeO<sub>2</sub> catalysts can be explained by the following reactions as shown in equation (1), (2), (3) and (4) (Dow and Huang, 1994; Goldstein and Mitchell, 2011; Royer and Duprez, 2011).

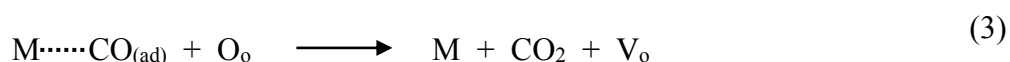
a) CO is adsorbed on M:



b) M is reduced by CO<sub>(ad)</sub>:



c) CO<sub>(ad)</sub> reacts with the lattice oxygen:



d) CO reacts with the lattice oxygen:



where M denotes CuO or Cu<sub>2</sub>O, O<sub>o</sub> denotes the lattice oxygen of CeO<sub>2</sub> and V<sub>o</sub> denotes oxygen vacancies.

The catalysts with 7 and 9% Cu loadings achieve 100% conversion at 110 °C while the others reach 100% conversion at 130 °C. At low temperature, the catalytic activity is proportional to the amount of the lattice oxygen at the surface (see Table 4.2), which can provide oxygen to CO molecule easily (Martinez-Arias *et al.*, 2009), resulting in the higher activity. Moreover, all catalysts

provide CO conversion greater than 90 % at temperatures below 170 °C. The oxygen selectivity towards CO<sub>2</sub> decreases with temperature; in particular, 9% Cu/MSP ceria shows a dramatic decrease of selectivity. At temperatures below 110 °C, all catalysts, except 9Cu/CeO<sub>2</sub>, have selectivities above 80 %. The CO conversions and selectivities of all catalysts show a similar behavior. The catalytic activity increases with increasing temperature at low temperatures. On the other hand, the CO conversion and selectivity decreases at high temperatures because the rate of H<sub>2</sub> oxidation is higher than the rate of CO oxidation (Monyanon *et al.*, 2006). As previously indicated, 3Cu/CeO<sub>2</sub>, 5Cu/CeO<sub>2</sub> and 7Cu/CeO<sub>2</sub>, providing higher activity and selectivity, were thus chosen to further study the effect of CO<sub>2</sub> in the PROX reaction.

It was found that the activities and selectivities of all studied catalysts were shifted to the higher temperature in the presence of CO<sub>2</sub>, as shown in Figure 4.4 c-d. The decrease in the catalytic performance might be due to the competitive adsorption of CO and CO<sub>2</sub> (Avgouropoulos and Loannides, 2003) and the formation of carbonates on interfacial ceria sites, resulting in diminishing CuO-CeO<sub>2</sub> interfacial redox activity (Gamarra and Martinez-Arias, 2009). All catalysts showed 100 % conversion at 130 °C with different reaction rates. The 7Cu/CeO<sub>2</sub> has the highest rate at temperatures below the maximum % conversion temperature. The selectivities of all catalysts were slightly different at temperatures below 170 °C. Moreover, 7Cu/CeO<sub>2</sub> showed the lowest H<sub>2</sub> consumption (not shown) of 1% at 130 °C while 3Cu/CeO<sub>2</sub> and 5Cu/CeO<sub>2</sub> consumed about 7 %. Therefore, 7Cu/CeO<sub>2</sub> was used to study the effect of both 10% CO<sub>2</sub> and H<sub>2</sub>O in the PROX reaction, results of which are shown in Figure 4.4e. The activity is strongly shifted to the higher temperature, as compared to when the feed is free of both gases. Moreover, the position of 100% CO conversion was also shifted to 150 °C. This phenomenon can be explained by the competitive adsorption of CO and CO<sub>2</sub> and the blocking effect of water (Avgouropoulos and Loannides, 2003).

#### 4.4.4.2 Stability of 7Cu/CeO<sub>2</sub> Catalyst

From previous results, 7Cu/CeO<sub>2</sub> shows the best performance in the PROX reaction under various feed streams. The time-on-stream performance of 7Cu/CeO<sub>2</sub> catalyst in a feed free of CO<sub>2</sub> and water and the presence of CO<sub>2</sub> was

collected at 130 °C, while in the presence of CO<sub>2</sub> and H<sub>2</sub>O, the catalysis was performed at 150 °C. The CO conversion of 7Cu/CeO<sub>2</sub> catalyst was maintained at 100 % for a period of 48 h in all feed streams (not shown), showing both an impressive performance and stability of the catalyst. Moreover, the elemental oxidation states of both fresh and used catalysts from the tests (denoted as – P3, P2, and P1 for the systems containing both CO<sub>2</sub> and water, only CO<sub>2</sub>, and no CO<sub>2</sub> and water, respectively) were analyzed by XPS to confirm the stability of these catalysts.

The O 1s spectra of all catalysts are presented in Figure 4.5. The surface oxygen consists of 2 peaks, corresponding to 2 species. The first peak at binding energy (BE) of about 530-533 eV is assigned to adsorbed oxygen or oxygen in the hydroxy-like groups (Wang *et al.*, 2008), while the second peak at BE around 527-529 eV belongs to the lattice oxygen in ceria and CuO. The amount of the lattice oxygen seems to be proportional to the presence of Cu. All fresh catalysts show higher amounts of lattice oxygen than the used catalysts, as can be seen in Table 4.2.

The Ce 3d region spectra were deconvoluted to eight peaks, as shown in Figure 4.6. The Ce 3d core level spectra corresponding to Ce<sup>4+</sup> oxidation state are composed of six contributions, viz. v, u, v', u', v'', and u'', and the four peaks, consisting of v<sup>0</sup>, u<sup>0</sup>, v', and u', correspond to Ce<sup>3+</sup> ions. The amount of Ce<sup>3+</sup> on the surfaces of the ceria based catalysts, as summarized in Table 4.2, can be estimated using the following equation (Alvaro *et al.*, 2011).

$$\text{Ce}^{3+}(\%) = [\Sigma(\text{Ce}^{3+})/\Sigma(\text{Ce}^{3+}+\text{Ce}^{4+})]\times 100 \quad (5)$$

All fresh and used catalysts show high amounts of Ce<sup>3+</sup> around 37–40 % probably due to either the photo-reduction of ceria in the analysis chamber or the thermal treatment during the preparation (Galtayries *et al.*, 1998). The amount of Ce<sup>3+</sup> after going through the PROX reaction, resulting from the reduction of Ce<sup>4+</sup> to Ce<sup>3+</sup>, (7CuO/CeO<sub>2</sub>-P1, 7CuO/CeO<sub>2</sub>-P2 and 7CuO/CeO<sub>2</sub>-P3) is slightly increased from the corresponding value for fresh catalyst.

In Figure 4.7, the Cu 2p core level spectra for all samples present three main peaks of Cu2p<sub>3/2</sub>, shake-up, and Cu 2p<sub>1/2</sub> at around 933, 939–947, and 953 eV, respectively. The shake-up satellite peak indicates the existence of the Cu<sup>2+</sup> oxidation state while the Cu 2p<sub>3/2</sub> peak represents both Cu<sup>+</sup> and Cu<sup>2+</sup> species

which are generally difficult to distinguish (Avgouropoulos and Loannides, 2003). The decreasing ratio between the intensities of the shake-up satellite and the Cu 2p<sub>3/2</sub> peaks with the shift of satellite peak toward the lower BE after the PROX reaction, corresponds to the reduction of Cu<sup>2+</sup> to a lower oxidation or metallic state (Liao *et al.*, 2013). However, the ratio of I<sub>Cu,sat</sub>/I<sub>Cu,2p3/2</sub> and the satellite peak position of the used catalysts are slightly different from the fresh catalysts, as shown in Table 4.2. There is not only a little change in the Cu 2p core level spectra, but also a slight difference in the Ce 3d region of the used and the fresh catalysts. This may indicate that the reaction takes place inside the pores of MSP ceria, resulting in a slight change in the metal species at the surface.

Moreover, the structure of catalyst after the stability test was characterized by Raman spectroscopy to observe the vibrational mode characteristic of groups of atoms (Radovic *et al.*, 2007). The results (not shown) indicate that the fresh 7Cu/CeO<sub>2</sub> exhibits four peaks at 110, 452, 585, and 1107 cm<sup>-1</sup>. The main Raman peak of 7CuO/CeO<sub>2</sub>-P1, 7CuO/CeO<sub>2</sub>-P2 and 7CuO/CeO<sub>2</sub>-P3 appears at 449, 449 and 448 cm<sup>-1</sup>, respectively, as shown in Figure 4.8, and is related to a triply degenerate F<sub>2g</sub> mode (Souza *et al.*, 2010). The used catalyst shows a systematic shift of the F<sub>2g</sub> mode to lower frequencies due to lattice expansion, resulting from the occurrence of oxygen vacancies, while two Ce<sup>3+</sup> ions (ionic radius 1.143 Å) replace two Ce<sup>4+</sup> ions (ionic radius 0.970 Å) in the oxidation of CO (Shannon, 1976; Kim, 1989; Hong and Virkar 1995; Bishop *et al.*, 2009). The increase of Ce<sup>3+</sup> after the PROX reaction was also confirmed by XPS analysis, as summarized in Table 4.2. In particular, the used catalyst in the presence of 10 % CO<sub>2</sub> and 10 % H<sub>2</sub>O showed the largest change in Raman shift, indicating more vacancies generated due to the occurrence of the water-gas shift reaction. This reaction becomes more important at higher temperatures and higher humidity, resulting in a substantial increase in the number of oxygen vacancies, which is confirmed by the increase of activity in the PROX reaction (Laguna *et al.*, 2011). At high temperatures, the activity of the catalyst that has CO<sub>2</sub> and H<sub>2</sub>O in the feed is higher than the activity of the catalyst that has only CO<sub>2</sub>.

The distortion of the fluorite structure can be confirmed by XRD (not shown). The average cell parameter of the cubic crystal structure of the used catalyst is slightly changed due to the reduction of Ce<sup>4+</sup> to Ce<sup>3+</sup> during the CO-PROX

reaction, but the variation in the cell parameters calculated from each plane is larger, compared to the fresh catalyst. Moreover, the lattice parameter between the fresh and the used catalysts are slightly different. However, it can be concluded that the synthesized Cu/MSP ceria is highly stable since despite the above small changes, it maintains the basic cubic structure during the PROX reaction.

#### 4.5 Conclusions

The MSP ceria synthesized by nanocasting shows highly ordered structure, a high surface area of 293 m<sup>2</sup>/g, and small crystallite sizes, producing a large number of oxygen vacancies in the crystal. All Cu loaded catalysts exhibit a high dispersion of Cu and maintain the fluorite structure of MSP ceria, as confirmed by XRD. Moreover, the TEM image also confirms the long-range three-dimensional order of the pore structure. XPS analysis indicates lower Cu content on the surface than that in the bulk as analyzed by AAS analysis, indicating penetration of copper precursor into the pores of MSP ceria. The reduction temperature of Cu catalysts is shifted to lower temperatures than that of the pure MSP ceria. Moreover, the reduction of Ce<sup>4+</sup> to Ce<sup>3+</sup> is inversely proportion to the copper content.

Among all synthesized Cu/MSP ceria, 7Cu/CeO<sub>2</sub> presents 100% conversion at 110 °C and 87% selectivity toward CO<sub>2</sub> in excess H<sub>2</sub> and a feed free of CO<sub>2</sub> and H<sub>2</sub>O. In the presence of 10 % CO<sub>2</sub> or 10 % CO<sub>2</sub> with 10 % H<sub>2</sub>O, the catalytic activity of 7Cu/CeO<sub>2</sub> provides 100% CO conversion at higher temperatures (130° and 150 °C, respectively) due to the competitive adsorption of CO and CO<sub>2</sub>, and the blocking effect of H<sub>2</sub>O. Moreover, 7Cu/CeO<sub>2</sub> is a highly stable catalyst over 48 h, either in a feed free of CO<sub>2</sub> and H<sub>2</sub>O, or in the presence of CO<sub>2</sub>, or the presence of CO<sub>2</sub> and H<sub>2</sub>O, as confirmed by XRD, Raman spectrometer, and XPS analysis.



## 4.6 Acknowledgements

This research is financially supported by the Ratchadapisake Sompote Endowment Fund, and the Center of Excellence for Petrochemical and Materials Technology, Chulalongkorn University, Thailand. The authors would like to thank Mr. John M. Jackson for proof-reading this paper.

## 4.7 References

- Alfredsson, V. and Anderson, W.M. (1996) Structure of MCM-48 revealed by transmission electron microscopy. Chemistry of Materials, 8, 1141-1146.
- Alvaro, R.C., Ana, A.D., Elisa, M., Aldo, T., Loretta, S., Maurizio, L., Antonio, J.L., and Enrique, R.C. (2011) CuO/CeO<sub>2</sub> supported on Zr doped SBA-15 as catalysts for preferential CO oxidation (CO-PROX). Journal of Power Sources, 196, 4382-4387.
- Avgouropoulos, G., Papavasiliou, J., Tabakova, T., Idakiev, V., and Ioannides, T. (2006) A comparative study of ceria-supported gold and copper oxide catalysts for preferential CO oxidation reaction. Chemical Engineering Journal, 124, 41-45.
- Avgouropoulos, J. and Ioannides, T. (2003) Selective CO oxidation over CuO-CeO<sub>2</sub> catalysts prepared via the urea-nitrate combustion method. Applied Catalysis A, 244, 155-167.
- Ayastuy, J.L., Gurbani, A., Gonzalez-Marcos, M.P., and Gutierrez-Ortiz, M.A. (2010) Effect of copper loading on copper-ceria catalysts performance in CO selective oxidation for fuel cell applications. International Journal of Hydrogen Energy, 35, 1232-1244.
- Beck, J.S., Vartuli, J.C., Roth, W.J., Leonowica, M.E., Kresge, C.T., Schmitt, K.D., Chu, C.T.W., and Olson, D.H. (1992) A new family of mesoporous molecular sieves prepared with liquid crystal templates. Journal of the American Chemical Society, 114, 10834-10843.

- Bishop, S.R., Duncan, K.L., and Wachsman, E.D. (2009) Defect equilibria and chemical expansion in non-stoichiometric undoped and gadolinium-doped cerium oxide. Electrochimica Acta, 54, 1436-1443.
- Bond, G.C. and Thompson, D.T. (1999) Catalysis by Gold. Catalysis Reviews, 41, 319-388.
- Bunluesin, T., Cordatos, H., and Gorte, R.J. (1995) A study of CO oxidation kinetics on Rh/Ceria. Journal of Catalysis, 157, 222-226.
- Bunluesin, T., Gorte, R.J., and Graham, G.W. (1998) Studies of the water-gas-shift reaction on ceria-supported Pt, Pd, and Rh: implications for oxygen-storage properties. Applied Catalysis B, 15, 107-114.
- Candusso, D., Harel, F., Bernardinis, A.D., Francois, X., Pera, M.C., Hissel, D., Schott, P., and Coquery, G. (2006) Characterisation and modelling of a 5 kW PEMFC for transportation applications. International Journal of Hydrogen Energy, 31, 1019-1030.
- Caputo, T., Lisi, L., Pirone, R., and Russo, G. (2008) On the role of redox properties of CuO/CeO<sub>2</sub> catalysts in the preferential oxidation of CO in H<sub>2</sub>-rich gases. Applied Catalysis A, 348, 42-53.
- Deeprasertkul, C., Longloilert, R., Chaisuwan, T., and Wongkasemjit, S. (2014) Impressive low reduction temperature of synthesized mesoporous ceria via nanocasting. Materials Letters, 130, 218-222.
- Dow, W.P. and Huang, T.J. (1994) Effect of oxygen vacancy of yttria-stabilized zirconia support on carbon monoxide oxidation over copper catalyst. Journal of Catalysis, 147, 322-332.
- Fonseca, J.D.S.L., Ferreira, H.S., Bion, N., Pirault-Roy, L., Rangel, M.D.C., Duprez, D., and Epron, F. (2012) Cooperative effect between copper and gold on ceria for CO-PROX reaction. Catalysis Today, 180, 34-41.
- Fox, E.B., Velu, S., Engelhard, M.H., Chin, Y.H., Miller, J.T., Kropf, J., and Song, C.S. (2008) Characterization of CeO<sub>2</sub>-supported Cu-Pd bimetallic catalyst for the oxygen-assisted water-gas shift reaction. Journal of Catalysis, 260, 358-370.

- Haruta, M., Tsubota, S., Kobayashi, T., Kageyama, H., Genet, M.J., and Delmon, B. (1993) Low-temperature oxidation of CO over gold supported on TiO<sub>2</sub>, alpha-Fe<sub>2</sub>O<sub>3</sub>, and Co<sub>3</sub>O<sub>4</sub>. Journal of Catalysis, 144, 175-192.
- Hong, S.J. and Virkar, A.V. (1995) Lattice parameters and densities of rare-earth oxide doped ceria electrolytes. Journal of the American Ceramic Society, 78, 433-439.
- Galtayries, A., Sporken, R., Riga, J., Blanchard, G., and Caudano, R. (1998) XPS comparative study of ceria/zirconia mixed oxides: powders and thin film characterization. Journal of Electron Spectroscopy and Related Phenomena, 88, 951-956.
- Gamarra, D. and Martinez-Arias, A. (2009) Preferential oxidation of CO in rich H<sub>2</sub> over CuO/CeO<sub>2</sub>: *Operando*-DRIFTS analysis of deactivating effect of CO<sub>2</sub> and H<sub>2</sub>O. Journal of Catalysis, 263, 189-195.
- Gamboa-Rosales, N.K., Ayastuy, J.L., Gonzalez-Marcos, M.P., and Gutierrez-Ortiz, M.A. (2011) Effect of Au promoter in CuO/CeO<sub>2</sub> catalysts for the oxygen-assisted WGS reaction. Catalysis Today, 176, 63-71.
- Gamboa-Rosales, N.K., Ayastuy, J.L., Gonzalez-Marcos, M.P., and Gutierrez-Ortiz, M.A. (2012) Oxygen-enhanced water gas shift over ceria-supported Au-Cu bimetallic catalysts prepared by wet impregnation and deposition-precipitation. International Journal of Hydrogen Energy, 37, 7005-7016.
- Goldstein, E.A. and Mitchell, R.E. (2011) Chemical kinetics of copper oxide reduction with carbon monoxide. Proceedings of the Combustion Institute, 33, 2803-2810.
- Graham, G.W., Weber, W.H., Peters, C.R., and Usman, R. (1991) Empirical method for determining CeO<sub>2</sub>-particle size in catalysts by raman spectroscopy. Journal of Catalysis, 130, 310-313.
- Groen, J.C., Peffer, L.A.A., and Perez-Ramirez, J. (2003) Pore size determination in modified micro and mesoporous materials. Pitfalls and limitations in gas adsorption data analysis. Microporous and Mesoporous Materials, 60, 1-17.
- Idakiev, V., Tabakova, T., Naydenov, A., Yuan, Z.Y., and Su, B.L. (2006) Gold catalysts supported on mesoporous zirconia for low-temperature water-gas shift reaction. Applied Catalysis B, 63, 178-186.

- Jacobs, G., Khalid, S., Patterson, P.M., Sparks, D.E., and Davis, B.H. (2004) Water-gas shift catalysis: kinetic isotope effect identifies surface formates in rate limiting step for Pt/ceria catalysts. Applied Catalysis A, 268, 255-266.
- Kim, D.J. (1989) Lattice parameter, ionic conductivities, and solubility limits in fluorite structure MO<sub>2</sub> oxides (M=Hf<sup>4+</sup>, Zr<sup>4+</sup>, Ce<sup>4+</sup>, Th<sup>4+</sup>, U<sup>4+</sup>). Journal of the American Ceramic Society, 72, 1415-1421.
- Kresge, C.T., Leonowica, M.E., Roth, W.J., Vartuli, J.C., and Beck, J.S. (1992) Ordered mesoporous molecular sieves synthesized by a liquid-crystal template mechanism. Letters to Nature, 359, 710-712.
- Laguna, O.H., Centeno, M.A., Boutonnet, M., and Odriozola, J.A. (2011) Fe-doped ceria solids synthesized by the microemulsion method for CO oxidation reactions. Applied Catalysis B, 106, 621-629.
- Langford, J. and Wilson, A. (1978) Scherrer after Sixty Years: A Survey and Some New Results in the Determination of Crystallite Size. Journal of Applied Crystallography, 11, 102-113.
- Li, X., Quek, X.Y., Ligthart, D.A.J.M., Guo, M., Zhang, Y., Li, C., Yang, Q., and Hensen, E.J.M. (2012) CO-PROX reactions on copper cerium oxide catalysts prepared by melt infiltration. Applied Catalysis B, 123, 424-432.
- Liao, X., Chu, W., Dai, X., and Pitchon, V. (2013) Bimetallic Au–Cu supported on ceria for PROX reaction: Effects of Cu/Au atomic ratios and thermal pretreatments. Applied Catalysis B, 142, 25-37.
- Longloilert R., Chaisuwan T., Luengnaruemitchai A., and Wongkasemjit S. (2011) Synthesis of MCM-48 from silatrane via sol-gel process. Journal of Sol-Gel Science and Technology, 58, 427-435.
- Luo, M.F., Zhong, Y.J., Yuan, X.X., and Zheng, X. (1997) TPR and TPD studies of CuO/CeO<sub>2</sub> catalysts for low temperature CO oxidation. Applied Catalysis A, 162, 121-131.
- Martinez-Arias, A., Gamarra, D., Fernandez-Garcia, M., Hornes, A., Bera, P., Koppany, Z.S., and Schay, Z. (2009) Redox-catalytic correlations in oxidised copper-ceria CO-PROX catalysts. Catalysis Today, 143, 211-217.

- Martinez-Arias, A., Hungria, A.B., Munuera, G., and Gamarra, D. (2006) Preferential oxidation of CO in rich H<sub>2</sub> over CuO/CeO<sub>2</sub>: Details of selectivity and deactivation under the reactant stream. Applied Catalysis B, 65, 207-216.
- McBride, J.R., Haas, K.C., Poindexter, B.D., and Weber, W.H. (1994) Raman and x-ray studies of Ce<sub>1-x</sub>RE<sub>x</sub>O<sub>2-y</sub>, where RE = La, Pr, Nd, Eu, Gd, and Tb. Journal of Applied Physics, 76, 2435-2441.
- Monnier, A., Schuth, F., Huo, Q., Kumar, D., Margolese, D., Maxwell, R.S., Stucky, M., Krishnamurty, G.D., Petroff, P., Firouzi, A., and Janicke, M. (1993) Cooperative formation of inorganic-organic interfaces in the synthesis of silicate mesostructures. Science, 261, 1299-1303.
- Monyanon, S., Pongstabodee, S., and Luengnaruemitchai, A. (2006) Catalytic activity of Pt–Au/CeO<sub>2</sub> catalyst for the preferential oxidation of CO in H<sub>2</sub>-rich stream. Journal of Power Sources, 163, 547-554.
- Palermo, A., Williams, F.J., and Lambert, R.M. (2002) In situ control of the composition and performance of a bimetallic alloy catalyst: The selective hydrogenation of acetylene over Pt/Pb. Journal of Physical Chemistry B, 106, 10215-10219.
- Radovic, M., Dohcevic-Mitrovic, Z., Scepanovic, M., Grujic-Brojcin, M., Matovic, B., Boskovic, S., and Popovic, Z.V. (2007) Raman study of Ba-doped ceria nanopowders. Science of Sintering, 39, 281-286.
- Rao, G.R. and Mishra, B.G. (2003) Structural, redox and catalytic chemistry of ceria based materials. Bulletin of the Catalysis Society of India, 2, 122-134.
- Royer, S. and Duprez, D. (2011) Catalytic oxidation of carbon monoxide over transition metal oxides. ChemCatChem, 3, 24-65.
- Sedmak, G., Hocevar, S., and Levec, J. (2004) Transient kinetic model of CO oxidation over a nanostructured Cu<sub>0.1</sub>Ce<sub>0.9</sub>O<sub>2-y</sub> catalyst. Journal of Catalysis, 222, 87-99.
- Shannon, R.D. (1976) Revised effective ionic radii and systematic studies of interatomic distances in halides and chalcogenides. Acta Crystallographica Section A, 32, 751-767.

- Shen, W., Dong, X., Zhu, Y., Chen, H., and Shi, J. (2005) Mesoporous CeO<sub>2</sub> and CuO-loaded mesoporous CeO<sub>2</sub>: Synthesis, characterization, and CO catalytic oxidation property. Microporous and Mesoporous Materials, 85, 157-162.
- Souza, E.C.C., Brito, H.F., and Muccillo, E.N.S. (2010) Optical and electrical characterization of samaria-doped ceria. Journal of Alloys and Compounds, 491, 460-464.
- Tang, C., Sun, J., Yao, X., Cao, Y., Liu, L., Ge, C., Gao, F., and Dong, L. (2014) Efficient fabrication of active CuO-CeO<sub>2</sub>/SBA-15 catalysts for preferential oxidation of CO by solid state impregnation. Applied Catalysis B, 146, 201-212.
- Trovarelli, A., Leitenburg, C.D., Boaro, M., and Dolcetti, G. (1999) The utilization of ceria in industrial catalysis. Catalysis Today, 50, 353-367.
- Wang, X., Gorte, R.J., and Wagner, J.P. (2002) Deactivation mechanisms for Pd/ceria during the water-gas-shift reaction. Journal of Catalysis, 212, 225-230.
- Wang, X., Kang, Q., and Li, D. (2008) Low-temperature catalytic combustion of chlorobenzene over MnO<sub>x</sub>-CeO<sub>2</sub> mixed oxide catalysts. Catalysis Communications, 9, 2158-2162.
- Wei, Y.C., Liu, C.W., Chang, W.J., and Wang, K.W. (2011) Promotion of Pt-Ru/C catalysts driven by heat treated induced surface segregation for methanol oxidation reaction. Journal of Alloys and Compounds, 509, 535-541.
- Xiaodong, M., Xi, F., Xuan, H., Hongwen, G., Lu, L., Jie, G., Huiqin, C., and Ting, Z. (2012) Mesoporous CuO/CeO<sub>2</sub> bimetal oxides: One-pot synthesis, characterization and their application in catalytic destruction of 1,2-dichlorobenzene. Microporous and Mesoporous Materials, 158, 214-218.
- Xiaoyuan, J., Guanglie, L., Renxian, Z., Jianxin, M., Yu, C., and Xiaoming, Z. (2001) Studies of pore structure, temperature-programmed reduction performance, and micro-structure of CuO/CeO<sub>2</sub> catalysts. Applied Surface Science, 173, 208-220.
- Yen, H., Seo, Y., Kaliaguine, S., and Kleitz, F. (2012) Tailored mesostructured copper/ceria catalysts with enhanced performance for preferential oxidation of CO at low temperature. Angewandte Chemie International Edition, 51, 12032-12035.

Zhu, H., Qin, Z., Shan, W., Shen, W., and Wang, J. (2004) Pd/CeO<sub>2</sub>-TiO<sub>2</sub> catalyst for CO oxidation at low temperature: a TPR study with H<sub>2</sub> and CO as reducing agents. Journal of Catalysis, 225, 267-277.

Zsoldos, Z., Gardin, F., Hilaire, L., and Guzzi, L. (1996) Genesis of cobalt oxide-induced surface structure in PtCo<sub>x</sub>/Al<sub>2</sub>O<sub>3</sub> catalysts. Journal of Molecular Catalysis A: Chemical, 111, 113-122.

**Table 4.1** Properties of MSP CeO<sub>2</sub> and CuO/CeO<sub>2</sub> catalyst

Catalyst	Cu(%) <sup>t</sup>	Cu(%) <sup>a</sup>	S <sub>BET</sub> (m <sup>2</sup> /g)	Average size of ceria particles (nm)	Lattice parameter (Å)
MSP CeO <sub>2</sub>	-	-	293	3.8	5.3983±0.015
3CuO/CeO <sub>2</sub>	3.0	2.9	257	3.8	5.3999±0.016
5CuO/CeO <sub>2</sub>	5.0	5.0	240	3.8	5.3863±0.014
7CuO/CeO <sub>2</sub>	7.0	7.0	230	3.8	5.3810±0.009
9CuO/CeO <sub>2</sub>	9.0	9.1	202	3.8	5.3818±0.015

<sup>t</sup> Theoretical value

<sup>a</sup> from AAS

**Table 4.2** Relationship of species distribution on the surface of catalysts by XPS

Catalyst	Cu on surface (%)	$O_{\text{lattice}} / (O_{\text{OH}} + O_{\text{abs}})$	$I_{\text{Cu,sat}} / I_{\text{Cu}2p3/2}$	Position of shake up (Cu-2p)	$\text{Ce}^{3+} 3d_{5/2}$ (%)
MSP $\text{CeO}_2$	-	1.51	-	-	38
3CuO/ $\text{CeO}_2$	1.3	0.99	0.51	941.5	39
5CuO/ $\text{CeO}_2$	2.3	1.14	0.50	941.6	39
7CuO/ $\text{CeO}_2$	4.3	1.30	0.49	941.9	38
9CuO/ $\text{CeO}_2$	5.9	1.25	0.50	942.0	37
7CuO/ $\text{CeO}_2$ -P1	-	0.28	0.48	941.9	38
7CuO/ $\text{CeO}_2$ -P2	-	0.51	0.46	941.7	40
7CuO/ $\text{CeO}_2$ -P3	-	0.34	0.47	941.9	39



**Table 4.3** H<sub>2</sub>-TPR results of all catalysts

Catalyst	H <sub>2</sub> uptake of 1° peak	H <sub>2</sub> uptake of 2° peak	Theoretical H <sub>2</sub> uptake ( $\mu\text{molg}^{-1}$ ) Cu <sup>2+</sup> to Cu <sup>0</sup>	H <sub>2</sub> uptake of MSP CeO <sub>2</sub> ( $\mu\text{molg}^{-1}$ ) Ce <sup>4+</sup> to Ce <sup>3+</sup>
3CuO/CeO <sub>2</sub>	450	1134	487	647
5CuO/CeO <sub>2</sub>	673	1202	828	374
7CuO/CeO <sub>2</sub>	948	1314	1184	130
9CuO/CeO <sub>2</sub>	1048	1589	1556	33

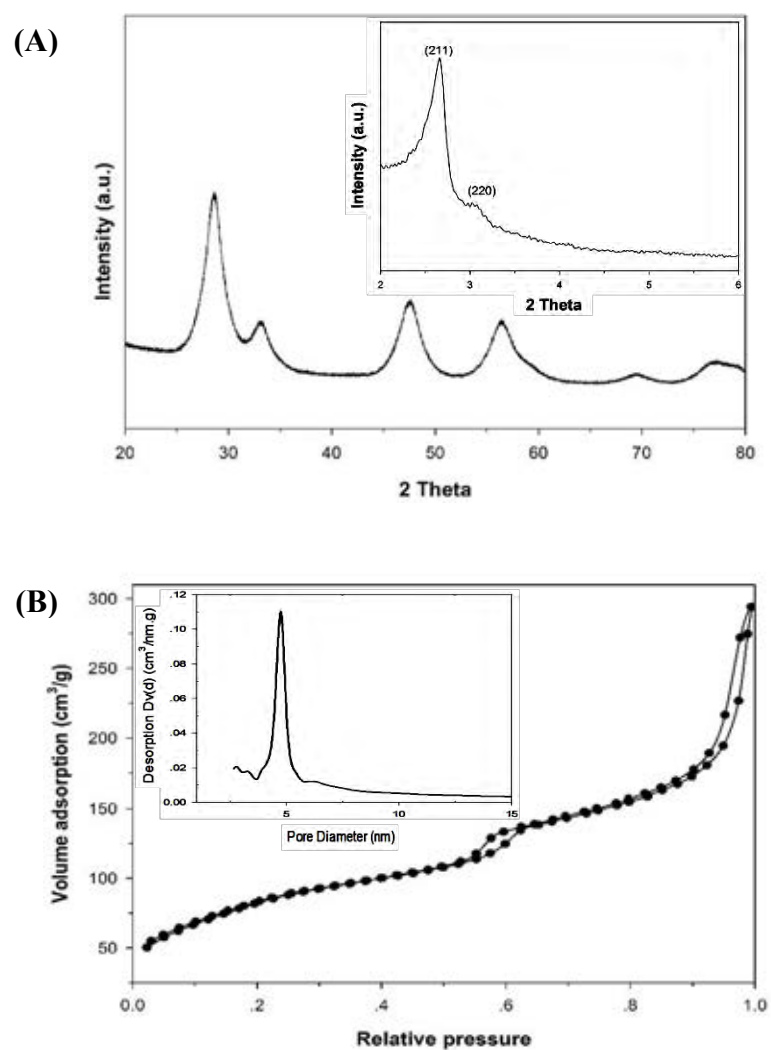


**Figure 4.1** (A) WAXD and SAXD (inset) patterns of the synthesized MSP ceria and (B) N<sub>2</sub> adsorption-desorption isotherms and pore size distribution (inset) of the synthesized MSP ceria.

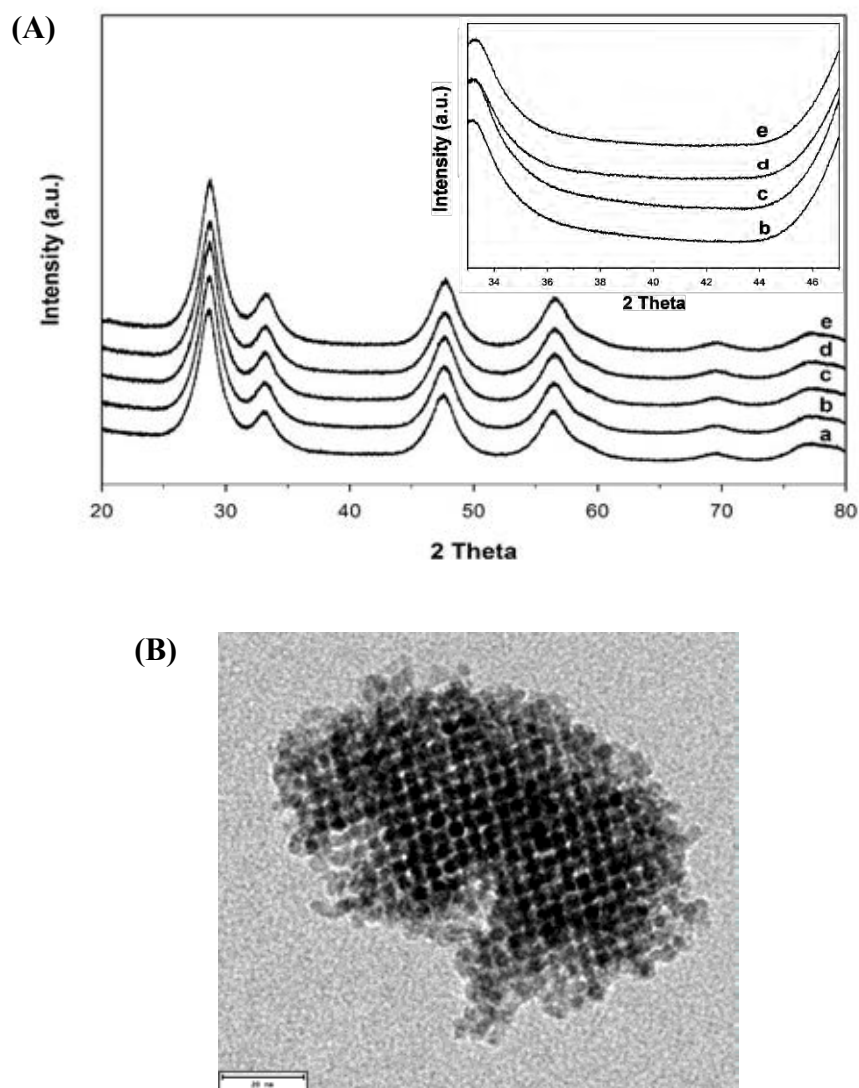


**Figure 4.2** (A) XRD patterns at a scanning speed of  $1^\circ\text{min}^{-1}$  and a scanning speed of  $0.01^\circ\text{min}^{-1}$  (inset) of (a) pure MSP ceria, (b)  $3\text{CuO/CeO}_2$ , (c)  $5\text{CuO/CeO}_2$ , (d)  $7\text{CuO/CeO}_2$ , and (e)  $9\text{CuO/CeO}_2$ ; (B) TEM image of  $7\text{Cu/MSP}$  ceria calcined at  $500^\circ\text{C}$ .

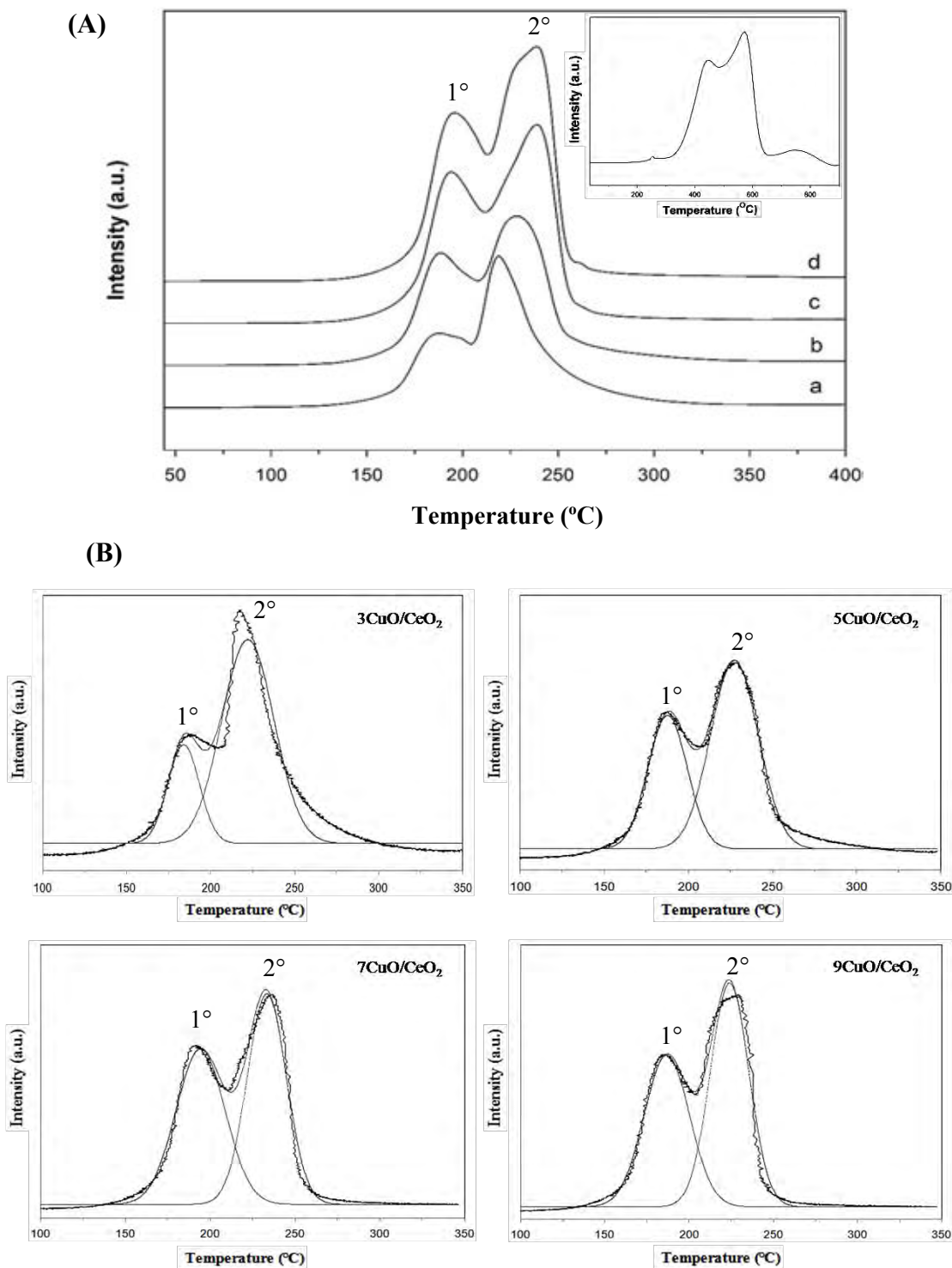


**Figure 4.3** (A) H<sub>2</sub>-TPR profiles of (a) 3CuO/CeO<sub>2</sub>, (b) 5CuO/CeO<sub>2</sub>, (c) 7CuO/CeO<sub>2</sub>, (d) 9CuO/CeO<sub>2</sub> and pure MSP ceria (inset); (B) The deconvolution of reduction profiles of all Cu/MSP ceria.

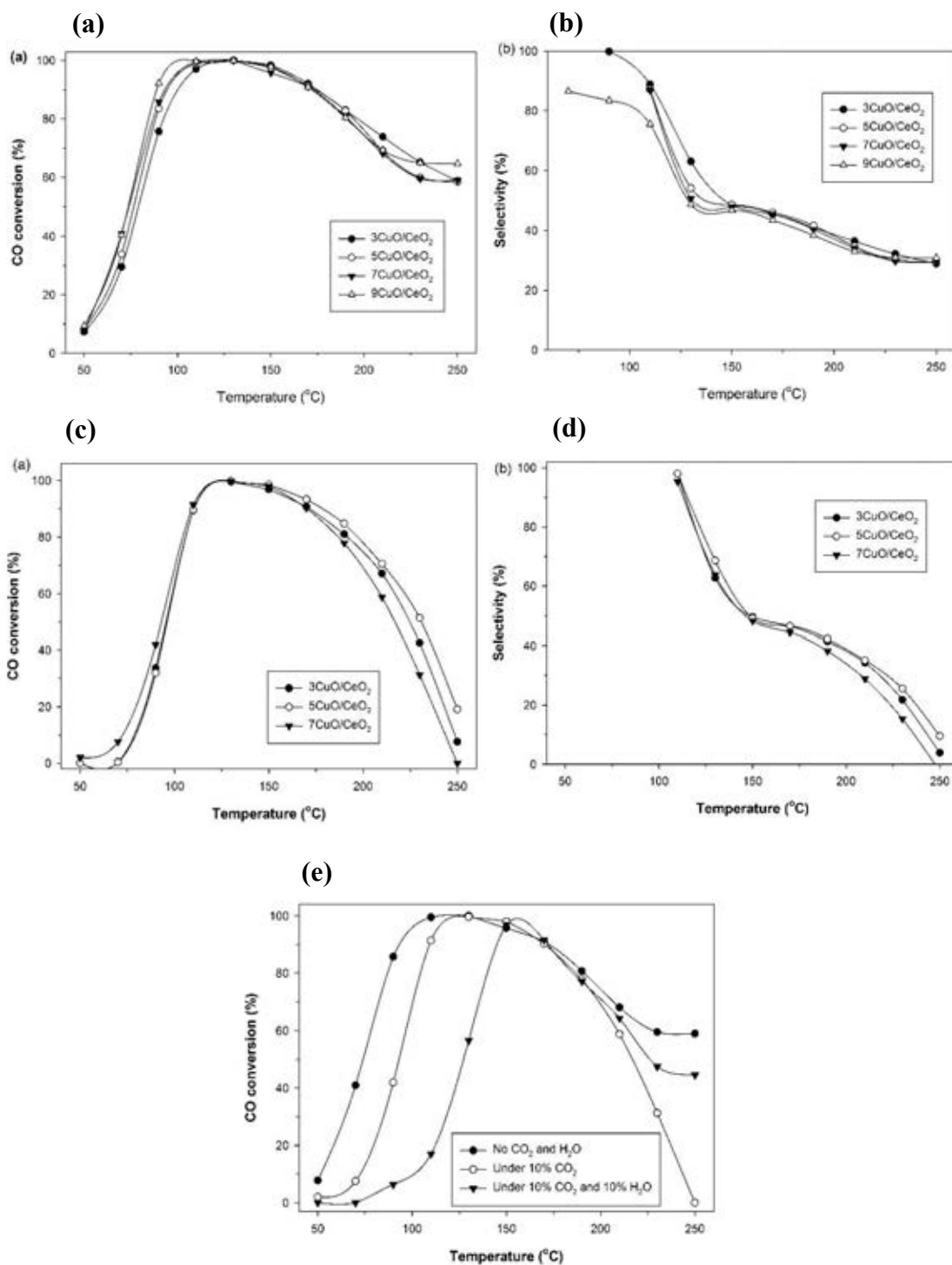


**Figure 4.4** (a) CO conversion and (b) selectivity for PROX reaction using feed composition of 1% CO, 1% O<sub>2</sub>, 40% H<sub>2</sub> balance in He (c) CO conversion and (d) selectivity for PROX reaction in the present of 10 % CO<sub>2</sub> (e) CO conversion of 7CuO/CeO<sub>2</sub> for PROX reaction in various feed compositions.

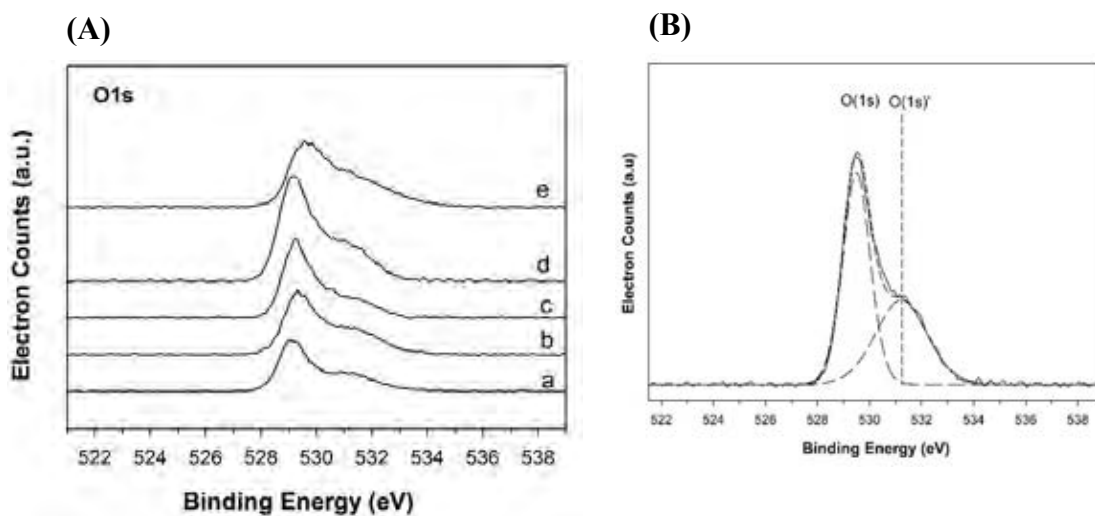


**Figure 4.5** (A) O1s XPS spectra of fresh catalysts (a) pure MSP ceria, (b) 3CuO/CeO<sub>2</sub>, (c) 5CuO/CeO<sub>2</sub>, (d) 7CuO/CeO<sub>2</sub>, (e) 9CuO/CeO<sub>2</sub>; (B) Example of deconvolution of O1s spectrum of 7CuO/CeO<sub>2</sub>.

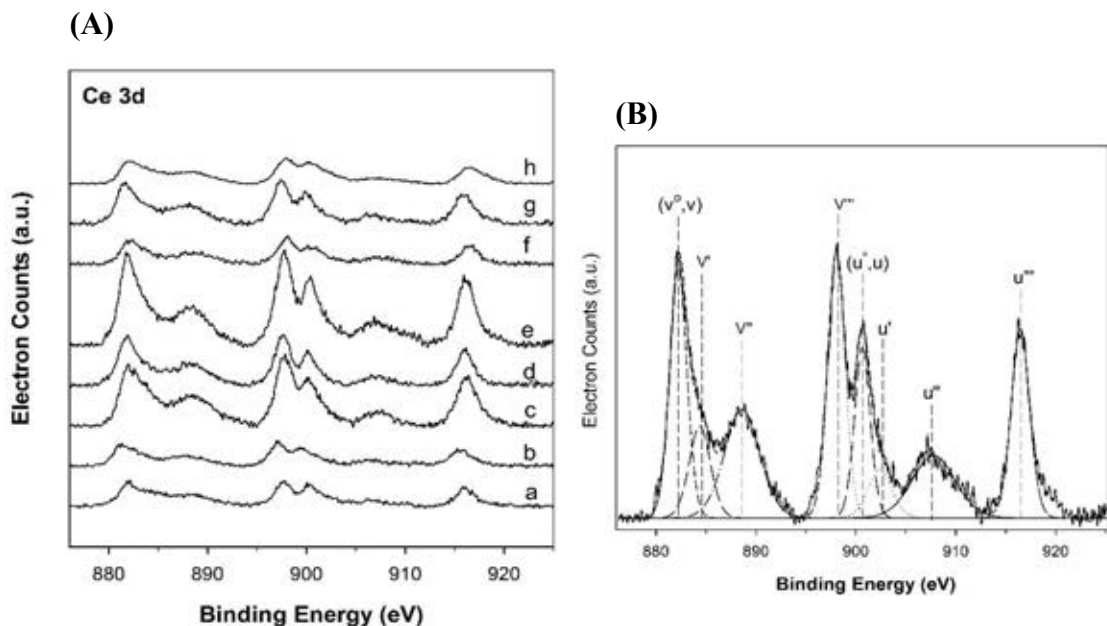


**Figure 4.6** (A) Ce3d XPS spectra of fresh and used (-P) catalysts (a) pure MSP ceria, (b) 3CuO/CeO<sub>2</sub>, (c) 5CuO/CeO<sub>2</sub>, (d) 7CuO/CeO<sub>2</sub>, (e) 9CuO/CeO<sub>2</sub>, (f) 7CuO/CeO<sub>2</sub>-P1, (g) 7CuO/CeO<sub>2</sub>-P2, (h) 7CuO/CeO<sub>2</sub>-P3; (B) Example of deconvolution of Ce3d spectra of 7CuO/CeO<sub>2</sub>.

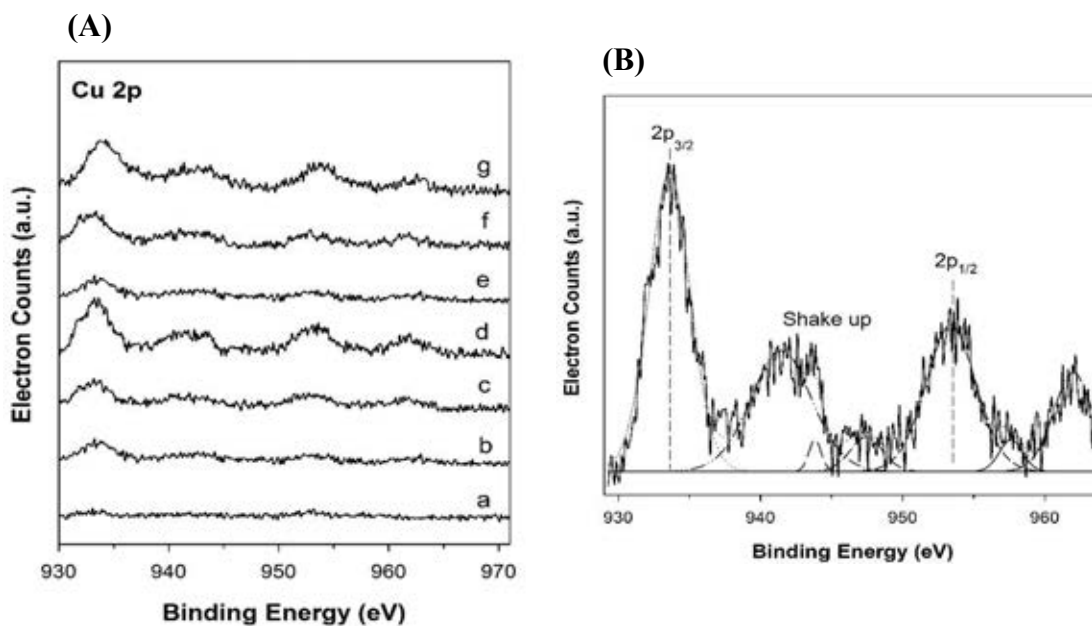


**Figure 4.7** (A) Cu 2p XPS spectra of fresh and used (-P) catalysts (a) pure MSP ceria, (b) 3CuO/CeO<sub>2</sub>, (c) 5CuO/CeO<sub>2</sub>, (d) 7CuO/CeO<sub>2</sub>, (e) 9CuO/CeO<sub>2</sub>, (f) 7CuO/CeO<sub>2</sub>-P1, (g) 7CuO/CeO<sub>2</sub>-P2; (B) Example of deconvolution of Cu2p spectra of 9CuO/CeO<sub>2</sub>.

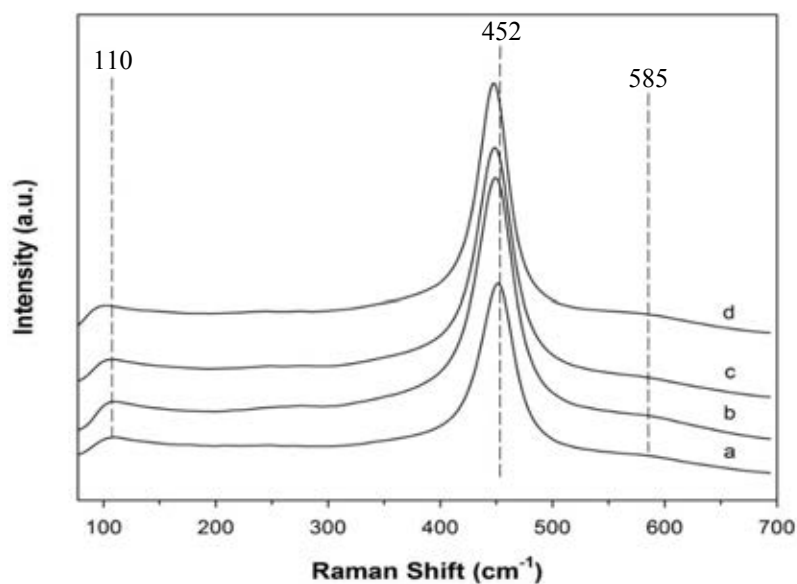


**Figure 4.8** Raman spectra of fresh and used (-P) catalysts after stability test for PROX reaction (a) fresh 7CuO/CeO<sub>2</sub>, (b) 7CuO/CeO<sub>2</sub>-P1, (c) 7CuO/CeO<sub>2</sub>-P2, (d) 7CuO/CeO<sub>2</sub>-P3.

**CHAPTER V**  
**KINETICS OF Cu LOADED MESOPOROUS CeO<sub>2</sub>-ZrO<sub>2</sub> CATALYST FOR**  
**THE PREFERENTIAL OXIDATION OF CO (CO-PROX) IN THE**  
**PRESENCE OF EXCESS HYDROGEN**

**5.1 Abstract**

Copper (Cu) loaded mesoporous ceria-zirconia (CeO<sub>2</sub>-ZrO<sub>2</sub>) catalysts (Cu-CZ) are successfully synthesized for preferential oxidation of CO (CO-PROX). Mesoporous CeO<sub>2</sub>-ZrO<sub>2</sub> with high specific surface area and crystalline structure is prepared for the first time via a nanocasting process. Deposition-precipitation methodology is chosen to load various Cu contents (1 to 9 wt %) on the prepared mesoporous CeO<sub>2</sub>-ZrO<sub>2</sub> support. All synthesized catalysts exhibit high activity with 95-100% CO conversion and over 50% selectivity at temperatures below 150°C. Furthermore, the effects on catalytic activity of CO<sub>2</sub> concentrations alone, and CO<sub>2</sub> in the presence of H<sub>2</sub>O are studied. We find that the presence of CO<sub>2</sub> and CO<sub>2</sub> with H<sub>2</sub>O in the feed gas slightly diminishes the performance of the catalysts. The 9%Cu-CZ catalyst provides the lowest activation energy, resulting in the best catalytic performance as well as complete CO conversion within 72 h.

**(Keywords:** Mesoporous CeO<sub>2</sub>-ZrO<sub>2</sub>; Cu-CeO<sub>2</sub>-ZrO<sub>2</sub>; Nanocasting process; Deposition-precipitation method; Preferential oxidation of CO)



## 5.2 Introduction

Fuel cell technology has extensively been investigated and developed for various applications. Of particular interest here are proton exchange membrane fuel cells (PEMFC) (Song *et al.*, 2002). PEMFCs are fueled with hydrogen produced by several processes which involve catalytic decomposition of hydrocarbons or oxygenated hydrocarbons followed by water–gas shift (WGS) reaction (Rostrup-Nielsen *et al.*, 2002; Fu *et al.*, 2003). Generally, significant amounts of CO<sub>2</sub> (15-25 vol %), CO (0.5-2 vol.%) and H<sub>2</sub>O are obtained in the gas stream along with production of H<sub>2</sub> (45-75 vol.%) (Avgouropoulos *et al.*, 2002), causing a problem since PEMFC electrodes are generally made from Pt, which can be easily poisoned by CO even at levels of 10-100 ppm. To achieve a high performance of PEMFC, CO must be removed to levels below 10 ppm from the hydrogen-rich gas feed. The simplest and least expensive method to reduce the CO concentration is via the preferential catalytic oxidation of CO (CO-PROX) (Marino *et al.*, 2005). Many supported noble metal catalysts have been studied and used to treat the H<sub>2</sub>-rich CO-PROX feed, including Pt, Pd, Ir, Rh and Ru (Huang and Yu, 1991; Oh and Sinkevitch, 1993; Liu *et al.*, 1994; Son *et al.*, 2002; Zhang *et al.*, 2002; Snytnikov *et al.*, 2003; Marino *et al.*, 2004). Nguyen *et al.* (2015) investigated the CO-PROX performance of platinum-group metals supported on ceria, and found that Pt-CeO<sub>2</sub> was the most active and selective catalyst. Snytnikov *et al.* (2003) studied the selective oxidation of CO in excess hydrogen over Pt-, Ru- and Pd-supported on Sibunit (porous carbonaceous material) catalysts and found that Ru and Pt catalysts were the best active and selective catalysts. Following works (Sakurai and Haruta, 1995; Haruta, 2004), which discovered strong, low-temperature catalytic activity for CO oxidation of gold nanoparticles on reducible oxide supports, including Au/Al<sub>2</sub>O<sub>3</sub>, Au/Fe<sub>2</sub>O<sub>3</sub>, Au/TiO<sub>2</sub>, Au/Ti-SBA-15, Au/CeO<sub>2</sub>, and Au/MnO<sub>2</sub>-TiO<sub>2</sub>. Jardim *et al.* (2014) demonstrated that gold supported on Ni-doped ceria exhibits superior catalytic performance for the CO-PROX reaction at ambient temperature. However, although, both Pt- and Au-based catalysts provide high activity and stability for catalysis of the CO-PROX reaction, their high expense and sensitivity to sulfur poisoning are important drawbacks (Zhang *et al.*, 2002). Here we build on prior discoveries that less expensive Cu particles supported on ceria also

demonstrate good efficiency and superior properties, such as high catalytic activity for CO oxidation as well as resistance to poisoning (Huang *et al.*, 1989; Liu *et al.*, 1994; Avgouropoulos *et al.*, 2001).

Although ceria ( $\text{CeO}_2$ ) as a fluorite-type oxide is the most important rare-earth oxide for the oxidation reactions on account of its redox cycle between two oxidation states ( $\text{Ce}^{4+}$ - $\text{Ce}^{3+}$ ) and high oxygen storage capacity (OSC) (Madier *et al.*, 1999; Shan *et al.*, 2003), the incorporation of zirconia ( $\text{ZrO}_2$ ) into  $\text{CeO}_2$  exhibits even better features than pure  $\text{CeO}_2$ , such as higher thermal resistance, more efficient redox function, and better oxygen storage and release capacity (Trovarelli *et al.*, 2001). Thus,  $\text{CeO}_2$ - $\text{ZrO}_2$  catalyst supports are one of the extensively-studied systems. Thus, several previous works have confirmed high performance of the Cu-Ce-Zr catalyst system for the CO-PROX reaction. For instance, Ayastuy *et al.* (2012) obtained complete CO oxidation at low temperature over  $\text{CuO/Ce}_x\text{Zr}_{1-x}\text{O}_2$  catalysts synthesized by the conventional wetness impregnation method; Moretti *et al.* (2015) prepared 3-D flower of a Ce-Zr-Cu mixed oxide catalyst for CO-PROX by slow co-precipitation, and found complete CO conversion of 100% with the maximum selectivity of 98% was achieved in the temperature range of 115°-160°C.

Generally, the fundamental characteristics required of a catalyst support include high surface area, large pore volume, and broad pore size distribution. Mesoporous materials can fulfill these properties exhibiting 2-50 nm pore sizes and high surface area (Li and Zhao, 2013). One so-called “nanocasting” technique capable to achieve mesoporous catalyst supports is to use mesoporous silica as a hard template. The template acts as a physical barrier to coalescence of the crystals during the calcination process. The strong points of the nanocasting method are the ability to tailor specific porous materials, depending on the structure of the template as well as ease of scale up (Abdollahzadeh-Ghom *et al.*, 2011).

MCM-48, mesoporous silica, is suitable as a hard template because it has a three-dimensional and cubic-crystalline pore structure coupled with high surface area (Schumacher *et al.*, 2000; Rossinol *et al.*, 2005; Longloilert *et al.*, 2011). Yen *et al.* (2012) synthesized a mesoporous  $\text{CeO}_2$  catalyst support using MCM-48 as a hard

template, and found that, after loading 30% Cu content onto it, the catalyst presented a maximum CO conversion of around 88% at 80°C in the presence of rich H<sub>2</sub>.

Until now, no study has shown synthesis of a mesoporous CeO<sub>2</sub>-ZrO<sub>2</sub> catalyst support via the nanocasting technique. In this study, we report successful synthesis of a high surface area Cu loaded mesoporous CeO<sub>2</sub>-ZrO<sub>2</sub> catalyst via the nanocasting technique, followed by the deposition-precipitation (DP) method, and study its potential to obtain complete CO conversion in the CO-PROX reaction over the temperature range of 50°-250 °C. The effects of Cu content, the presence of CO<sub>2</sub>, and the presence of CO<sub>2</sub> with H<sub>2</sub>O on the catalyst performance were investigated. All synthesized catalysts were comprehensively characterized using pertinent analytical techniques.

### 5.3 Experimental

#### 5.3.1 Chemicals

Fumed silica (SiO<sub>2</sub>, 99.8%, Nippon Aerosil, Japan), triethanolamine (TEA, QRĕc chemical, Thailand), ethylene glycol (EG, 99%, J.T. Baker, USA), HP grade nitrogen (N<sub>2</sub>, 99.98% purity, Thai Industrial Gases Public Company Limited (TIG), Thailand), acetonitrile (CH<sub>3</sub>CN, 99.9%, Labscan, Thailand), cetyltrimethylammonium bromide (CTAB, 96.0%, Fluka, Germany), cerium(III) nitrate hexahydrate (Ce(NO<sub>3</sub>)<sub>3</sub>.6H<sub>2</sub>O, 99%, Sigma-Aldrich, Germany), zirconium oxide chloride octahydrate (ZrOCl<sub>2</sub>.8H<sub>2</sub>O, 99.9%, Merck, Germany), copper(II) nitrate trihydrate (Cu(NO<sub>3</sub>)<sub>2</sub>.3H<sub>2</sub>O, 99.5%, Merck, Germany), ethanol (CH<sub>3</sub>CH<sub>2</sub>OH, 99.9%, Labscan, Thailand), sodium hydroxide (NaOH, 99%, Labscan, Thailand), and sodium carbonate (Na<sub>2</sub>CO<sub>3</sub>, 99.8%, Ajax, Thailand) were used without further purification.

#### 5.3.2 Catalyst Preparation

##### 5.3.2.1 *Preparation of Silatrane*

The synthetic procedure to obtain silatrane followed Wongkasemjit's synthetic method (Phiriyawirut *et al.*, 2003). A mixture consisting of

0.1 mol fumed silica, 0.125 mol TEA, and 100 ml EG was refluxed at 200°C under nitrogen atmosphere for 12 h in an oil bath. The excess EG was then removed under vacuum at 110°C to obtain a crude brown solid. The product was washed with acetonitrile, followed by vacuum-drying to result in white silatrane.

#### 5.3.2.2 Preparation of MCM-48

MCM-48 was prepared following Longloilert's synthetic method, using a molar composition of  $\text{SiO}_2:\text{CTAB}:\text{NaOH}:\text{H}_2\text{O} = 1:0.3:0.5:62$  (Longloilert *et al.*, 2011). CTAB was dissolved in aqueous solution containing 2 M NaOH. The mixture was continuously stirred at 50°C until the solution was homogeneously dissolved. Silatrane was added to the mixture with constant stirring at 50 °C for 1 h. Then, the mixture was transferred to a Teflon-lined stainless steel autoclave and subjected to an operating temperature of 140 °C for 16 h. The obtained solid product was filtered and dried. The surfactant was removed by calcination at 550 °C for 6 h to obtain MCM-48.

#### 5.3.2.3 Preparation of Mesoporous $\text{CeO}_2\text{-ZrO}_2$

Mesoporous  $\text{CeO}_2\text{-ZrO}_2$  was synthesized via the nanocasting method using MCM-48 as template.  $\text{Ce}(\text{NO}_3)_3 \cdot 6\text{H}_2\text{O}$  and  $\text{ZrOCl}_2 \cdot 8\text{H}_2\text{O}$  were dissolved in 5 ml of ethanol while stirring at room temperature until a clear solution was appeared. The molar ratio of Ce to Zr in solution was  $\text{Ce}:\text{Zr} = 0.75:0.25$ . MCM-48 was directly added to the solution, with continuous stirring for 4 h at room temperature. Subsequently, the removal of ethanol was performed by evaporation in an oven at 100°C. The obtained solid was calcined at 550 °C for 6 h. The MCM-48 template was removed using 2 M NaOH at 50 °C. The resulting light yellow powder product was washed with deionized water until neutral and dried at 80 °C overnight.

#### 5.3.2.4 Preparation of Cu Loaded Mesoporous $\text{CeO}_2\text{-ZrO}_2$ Catalyst

The deposition-precipitation (DP) technique was employed to prepare Cu loaded mesoporous  $\text{CeO}_2\text{-ZrO}_2$  catalyst. Mesoporous  $\text{CeO}_2\text{-ZrO}_2$  catalyst support was added to an aqueous solution containing various amounts of  $\text{Cu}(\text{NO}_3)_2 \cdot 3\text{H}_2\text{O}$  (%Cu loadings of 1, 3, 5, 7, and 9% by wt.). The mixture was stirred at room temperature for 1 h. Next,  $\text{Na}_2\text{CO}_3$  as precipitating agent was added dropwise to neutralize the mixture, which was then heated to 80°C before aging for another hour.

The resulting solid was filtered and washed with boiling distilled water. Finally, it was dried at 80°C overnight and calcined in air at 500 °C for 6 h to obtain Cu-CeO<sub>2</sub>-ZrO<sub>2</sub> catalysts.

### 5.3.3 Catalyst Analysis

The Brunauer-Emmett-Teller (BET) method using a Quantachrome Autosorb-1 was applied to determine the specific surface area, pore volume and pore size distribution of the prepared catalysts by N<sub>2</sub> adsorption-desorption at -196°C. Small angle x-ray diffraction (SAXD, Rigaku TTRAX III) with a scanning speed of 1°min<sup>-1</sup> and CuK $\alpha$  radiation ( $\lambda$ = 1.5406 Å) in a range of  $2\theta = 1-6^\circ$  was used to characterize the mesoporous phase and the crystallinity of the prepared catalysts. Morphology and structure of the catalysts were directly observed by transmission electron microscopy (TEM) on a JEOL JEM-2100F TEM instrument operating at an accelerating voltage of 200 kV. Wide angle x-ray diffraction (WAXD) analysis of the catalysts was performed on a Rigaku Smartlab<sup>®</sup> diffractometer with a scanning speed of 1° min<sup>-1</sup> and CuK $\alpha$  radiation ( $\lambda$ = 1.5406 Å) in a range of  $2\theta = 20-80^\circ$  in order to determine the crystallinity, phase purity of the catalysts, and dispersion of Cu on mesoporous CeO<sub>2</sub>-ZrO<sub>2</sub>. The crystallite size of the catalysts was also determined from the line width of the XRD peak corresponding to {111} reflection by using the Scherrer's equation. The amount of Cu loading on mesoporous CeO<sub>2</sub>-ZrO<sub>2</sub> was determined by atomic absorption spectrometry (AAS, VARIAN Model 300/400). X-ray photoelectron spectroscopy (XPS, Kratos AXIS Ultra DLD spectrometer) of the catalysts was applied to determine chemical compositions and oxidation states at the catalyst surface. The measurements were conducted using monochromatic Al K $\alpha$  X-ray radiation (1486.6 eV) at a pressure lower than  $5 \times 10^{-7}$  Torr. The C1s peak was fixed at a binding energy of 284.6 eV. High resolution spectra were recorded with dwell times at 119.8, 331.5, and 142.5 ms for Ce 3d, O 1s, and Cu 2p, respectively, step sizes of 0.1 eV, and a pass energy of 20 eV. Temperature-programmed reduction (H<sub>2</sub>-TPR) was measured to evaluate the reducibility of the prepared catalysts using 50 mg of the prepared catalysts. The sample was reduced by 5.13% H<sub>2</sub>/N<sub>2</sub> (v/v) at a

heating rate of 10°C/min. A thermal conductivity detector (TCD) was used to detect hydrogen consumption.

#### 5.3.4 Catalytic Activity Measurements

Catalytic activity measurements of the prepared catalysts for CO-PROX reaction were carried out using a fixed bed U-tube reactor operating at a temperature range of 50°-250 °C and atmospheric pressure. A 100 mg of catalyst was packed into a U-tube between layers of glass wool. The reactant gas composition containing 1, 1, and 40 vol% of CO, O<sub>2</sub>, and H<sub>2</sub>, respectively, balancing with He was mixed before feeding to the CO-PROX reactor. The total flow rate of the mixed gas controlled by mass flow controllers was about 50 ml min<sup>-1</sup>. The product gas stream was detected by an on-line gas chromatograph (Agilent Technologies 6890N) using a carbosphere column and a thermal conductivity detector (TCD). The effect of CO<sub>2</sub> and H<sub>2</sub>O on the performance of CO-PROX reaction was studied by adding 10 vol.% CO<sub>2</sub> and 10 vol.% H<sub>2</sub>O in the feed gas. The CO conversion and selectivity (eq. 1 and 2) were calculated, based on the CO consumption in the CO-PROX reaction (Zeng *et al.*, 2013).

$$CO \text{ Conversion } (\%) = \frac{[CO_{in}] - [CO_{out}]}{[CO_{in}]} \times 100 \quad (1)$$

$$Selectivity (\%) = 0.5 \times \frac{[CO_{in}] - [CO_{out}]}{[O_{2,in}] - [O_{2,out}]} \times 100 \quad (2)$$

#### 5.3.5 Kinetic Study

The apparatus employed for kinetic of the CO-PROX reaction over the synthesized Cu- CZ catalysts consisted of a fixed bed U- tube reactor, gas flow measuring system, and on-line analytical system. A fresh catalyst sample (0.1 g) was packed into the reactor. The reactant gases fed into the reactor comprised CO, O<sub>2</sub>, and H<sub>2</sub>, balanced with He using a total flow rate of 50 ml/min. The amounts of CO and O<sub>2</sub> were varied at reaction temperatures of 90° and 130 °C and at atmospheric pressure. Subsequently, the product gas stream was evaluated by on-line gas chromatography

(Agilent Technologies 6890N) using a carbosphere column and a thermal conductivity detector (TCD).

## 5.4 Results and Discussion

### 5.4.1 Catalyst Characterization

#### 5.4.1.1 Textural and Structural Studies

The BET specific surface areas ( $S_{\text{BET}}$ ), the total pore volume ( $V_{\text{pore}}$ ), and the average pore diameter ( $d_{\text{pore}}$ ) of the synthesized catalysts are summarized in Table 5.1. The synthesized  $\text{Ce}_{0.75}\text{Zr}_{0.25}\text{O}_2$  (CZ) catalyst support notably exhibits the highest specific surface area of  $256 \text{ m}^2\text{g}^{-1}$  with mesopore diameter (3.80 nm) in the mesoporous range (2-50 nm) (Sing *et al.*, 1985). Increase of Cu content loaded onto the mesoporous CZ support systematically decreases the specific surface area of the catalysts. This result suggests that the presence of CuO blocks the pores of CZ and obstructs  $\text{N}_2$  adsorption in the BET experiment (Araujo *et al.*, 2012). Interestingly, the Cu loading does not significantly change the pore diameter, suggesting that the CuO crystallites are too small in size and too sparsely distributed within the pores to affect the measured pore diameter, or that a sufficient fraction of them are located at the entrance to pores hence blocking access to the interior pore surfaces.

Figure 5.1a illustrates the SAXD patterns of the synthesized CZ support and all Cu-CZ catalysts. The CZ support, which is the negative replica of the MCM-48 template, was prepared by the nanocasting process, shows similar characteristic peaks at  $\{211\}$  and  $\{220\}$  to MCM-48. However, the main reflection of CZ is slightly shifted to a smaller angle, resulting from having a larger pore size than the pores of MCM-48 (2.42 nm) (Abdollahzadeh-Ghom *et al.*, 2011). Comparing the SAXD results for the CZ support and the Cu-CZ catalysts, it is found that the latter all provide similar diffraction patterns although their patterns are not as sharp as that of MCM-48. It could be deduced that the CZ support and the Cu-CZ catalysts each maintain some order from the MCM-48 template, as further confirmed by TEM analysis.

The TEM images of the CZ support and the Cu-CZ catalysts shown in Figure 5.1b-5.1g confirm that the long-range order in the pores is still maintained even when Cu is loaded onto the CZ support.

To observe the phase structure of all synthesized samples, WAXD patterns were taken over a  $2\theta$  range of  $20^\circ$  and  $80^\circ$ , as shown in Figure 5.2. Our CZ support exhibits the diffraction peaks at  $28.71^\circ$ ,  $33.31^\circ$ ,  $47.96^\circ$ ,  $56.95^\circ$ ,  $59.24^\circ$ ,  $70.00^\circ$  and  $76.93^\circ$  which, according to PDF-Card No. 00-002-1311, correspond to  $\{1\ 1\ 1\}$ ,  $\{2\ 0\ 0\}$ ,  $\{2\ 2\ 0\}$ ,  $\{3\ 1\ 1\}$ ,  $\{2\ 2\ 2\}$ ,  $\{4\ 0\ 0\}$ , and  $\{3\ 3\ 1\}$  reflections, respectively representative of the fluorite cubic structure. These diffraction peaks appear at higher  $2\theta$  when compared with the diffraction peaks of pure  $\text{CeO}_2$ , which occur at  $28.5^\circ$ ,  $33.1^\circ$ ,  $47.6^\circ$ ,  $56.5^\circ$  and  $59.2^\circ$ , respectively (Atribak *et al.*, 2008). The shift of these peaks reflects the substitution of the large  $\text{Ce}^{4+}$  cations (0.097 nm) or  $\text{Ce}^{3+}$  cations with the smaller  $\text{Zr}^{4+}$  cations (0.084 nm). Furthermore, no diffraction peaks corresponding to  $\text{ZrO}_2$  appear in the XRD pattern, consistent with the incorporation of  $\text{ZrO}_2$  into the  $\text{CeO}_2$  or  $\text{Ce}_2\text{O}_3$  lattice i.e. with formation of a homogeneous mixed oxide (Adamski *et al.*, 2007; Atribak *et al.*, 2010; Moser *et al.*, 2015; Nousir *et al.*, 2015).

The addition of Cu into the CZ support does not change the diffraction pattern and the intensities of the CZ support peaks. Furthermore, each diffractogram of the Cu-CZ catalysts shows no diffraction peaks from CuO crystallites. This suggests that CuO is finely dispersed on the surface of the CZ support or a solid solution was formed by substituting  $\text{Ce}^{4+}$  with  $\text{Cu}^{2+}$  species (Li *et al.*, 2000; Chen *et al.*, 2009; Delimaris *et al.*, 2009). The absence of the CuO diffraction peak can also indicate that CuO crystallites are very small (Shan *et al.*, 2003; Pojanavaraphan *et al.*, 2014). The crystallite size and the unit cell parameters of both the CZ support and the Cu-CZ catalysts are presented in Table 5.2. The crystallite sizes of the pure CZ support and the Cu-CZ catalysts calculated from Scherrer's equation are found to be very similar. Thus, the insertion of Cu into CZ support does not disrupt the fluorite cubic structure of the CZ support, as confirmed by the evaluated unit cell parameter of the CZ support. The unit cell parameters of the pure CZ support and Cu-CZ catalysts calculated from Bragg's equation are also similar. These results are further corroborated by small-angle electron diffraction (SAED) data from TEM, as shown in Table 5.2.



#### 5.4.1.2 Distribution of Loaded Copper

As displayed in Table 5.3, the amount of Cu loading onto the CZ support was estimated by AAS and XPS analysis in both bulk and on the catalyst surface, respectively. Comparing the amounts of Cu found in bulk and on surface of all catalysts, it appears that higher Cu contents are implanted inside the pores of the CZ support. Combining the XRD, AAS and XPS results, it can be inferred that the deposition-precipitation (DP) technique is a successful method for preparation of Cu-CZ catalysts.

#### 5.4.1.3 X-ray Photoelectron Spectroscopy (XPS)

Analysis of the oxidation state analysis of catalyst surfaces was carried out using the XPS technique. Figure 5.3 presents the Ce 3d spectra of the CZ support and Cu-CZ catalysts. The Ce 3d spectra exhibit eight characteristic peaks corresponding to four pairs of spin-orbit doublets. The four peaks at 881.9, 884.0, 887.9, and 897.9 eV labeled as  $v$ ,  $v'$ ,  $v''$ , and  $v'''$ , respectively, are attributed to Ce 3d<sub>5/2</sub>, while the other four peaks at 900.4, 902.6, 906.7, and 916.3 eV marked as  $u$ ,  $u'$ ,  $u''$ , and  $u'''$ , respectively, are assigned to Ce 3d<sub>3/2</sub>. The  $v$ ,  $v''$ ,  $v'''$ ,  $u$ ,  $u''$ , and  $u'''$  peaks belong to the 3d<sup>10</sup>4f<sup>0</sup> electronic state of Ce<sup>4+</sup> ions, whereas the  $v'$  and  $u'$  peaks refer to the 3d<sup>10</sup>4f<sup>1</sup> state of the Ce<sup>3+</sup> ions (Jeong *et al.*, 2015; Mullins, 2015). The cohabitation of Ce<sup>3+</sup> and Ce<sup>4+</sup> species is indicated by these peaks. Moreover, it is reported that the formation of Ce<sup>3+</sup> species accompanies the generation of oxygen vacancies on the ceria surface. Thus, an increase in oxygen vacancy sites on the surface of Cu-CZ catalysts is indicated by reason of an increase in Ce<sup>3+</sup>. Thus, it can be implied that oxygen migrates from the bulk to the catalyst surface (Paier *et al.*, 2013; Guo *et al.*, 2014).

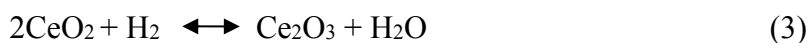
In Figure 5.4, XPS spectra in the O 1s region of the CZ support and Cu-CZ catalysts are exhibited. All samples show two asymmetric peaks at 529.1 and 530.6 corresponding to lattice oxygen in the ceria and copper oxides and defect oxygen on the catalyst surface, respectively (Sing *et al.*, 1985). Furthermore, it is observed that the amount of the lattice oxygen seems to be proportional to the presence of Cu. According to the studies reported elsewhere (Zhao *et al.*, 2007; Laguna *et al.*, 2010), it has been deduced that defect oxygen promotes oxygen mobility in the

catalysts and provides well-dispersed metal on the support surface, as also shown in our XRD study.

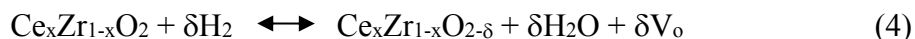
The Cu 2p region spectra are shown in Figure 5.5. The prominent peak at 932.6 eV is assigned to Cu 2p<sub>3/2</sub>, while Cu 2p<sub>1/2</sub> corresponds to the peak located at 952.5 eV. Another peak, attributed to a shake-up peak, appears between 933.5 and 948.0 eV. The intensities of the Cu 2p<sub>3/2</sub> and shake-up peaks increase with increasing the Cu content loaded onto the CZ support. The shake-up peak is characteristic of Cu<sup>2+</sup> species (CuO), whereas the Cu 2p<sub>3/2</sub> peak at 932.6 eV is characteristic of Cu<sup>1+</sup> species (Cu<sub>2</sub>O) (Kundakovic and Flytzani-Stephanopoulos, 1998; Zhang *et al.*, 2014). Based on the results found by Biesinger *et al.* (2010), the shake-up peak is generated because the outgoing photoelectron interacts with a valence electron which is then excited to a higher-energy level. Subsequent decrease in kinetic energy of the shaken-up core electron generates a satellite structure with higher binding energy relative to the core level value. Therefore, these satellite electrons are part of the total Cu 2p emission and should be included in estimation of the total Cu. According to the XPS result, it can be confirmed that Ce<sup>4+</sup>, Ce<sup>3+</sup>, Cu<sup>2+</sup>, and Cu<sup>+</sup> species are present in all Cu-CZ catalysts.

#### 5.4.1.4 Temperature-Programmed Reduction (H<sub>2</sub>-TPR)

Several authors (Monteiro *et al.*, 1995; Leitenburg *et al.*, 1996; Kaspar *et al.*, 1999; Bozo *et al.*, 2000; Fally *et al.*, 2000) report that there are two generally distinguishable peaks observed in H<sub>2</sub>-TPR of CeO<sub>2</sub> (see eq. (3)) (Trovarelli *et al.*, 1995). The first peak appearing at lower temperature is assigned to the surface reduction of CeO<sub>2</sub> while the second peak is attributed to the reduction of bulk CeO<sub>2</sub>.



For the reduction of the CZ support, as indicated in Eq. (4), oxygen anions react to form water molecules ( $\delta\text{H}_2\text{O}$ ), accompanied by creation of oxygen vacancies ( $\delta\text{V}_\text{o}$ ), which encourages the mobility of oxygen from the bulk to the surface. H<sub>2</sub> consumption is increased only via the reduction of Ce<sup>4+</sup> to Ce<sup>3+</sup>, because Zr<sup>4+</sup> is a non-reducible oxide (Li *et al.*, 2010).



The H<sub>2</sub>-TPR experiment provides a measure of the reducibility of the CZ support as a mixed oxide. Figure 5.6a presents the H<sub>2</sub>-TPR profile of the CZ support. The H<sub>2</sub> uptake peak appears in the range of 400-645°C as a result of the addition of ZrO<sub>2</sub> to CeO<sub>2</sub> (Leitenburg *et al.*, 1996). The H<sub>2</sub>-TPR profile exhibits only a single large H<sub>2</sub> consumption peak, which represents the reduction of bulk CeO<sub>2</sub>, comprising several layers of the mixed oxide. It is suggested that the insertion of ZrO<sub>2</sub> into the CeO<sub>2</sub> lattice encourages the reduction of the bulk ceria and enhances the oxygen anion mobility (Little, 1966; Kaspar *et al.*, 1999; Bozo *et al.*, 2000; Fally *et al.*, 2000).

H<sub>2</sub>-TPR profiles of the Cu-CZ catalysts are shown in Figure 5.6b. All catalysts except 1%Cu-CZ show two prominent reduction peaks. The first peak, ranging from 145°C to 200°C, is attributed to the reduction of finely dispersed CuO strongly interacting with the surface of the CZ support. The second peak, in the range from 210°C to 300°C, is ascribed to the reduction of isolated CuO particles, non-associated with the CZ support (Ratnasamy *et al.*, 2004; Djinojic *et al.*, 2008). Basically, the peak area of H<sub>2</sub>-TPR is proportionally related to the amount of H<sub>2</sub> consumption. Figure 5.6b shows that increase in the amount of Cu from 1 to 9%Cu-CZ systematically increases the H<sub>2</sub> consumption. It can be deduced that the redox properties increase with increasing Cu content loaded onto the CZ support, consistent with the study of Radik *et al.* (2013), who showed that Cu loading can promote oxygen mobility.

## 5.4.2 Catalytic Activity for the CO-PROX Reaction

### 5.4.2.1 *Effect of Cu Content*

The CO-PROX performance of the CZ support and all Cu-CZ catalysts was studied in term of CO conversion (eq. (1)) and selectivity (eq. (2)). Results are shown in Figure 5.7. The CZ supports loaded with different Cu contents generate much higher CO conversions than the pure CZ support. With increasing Cu content, the maximum CO conversions obtained for each catalyst increase, and the temperature to reach the maximum conversion decreases. Moreover, the reaction

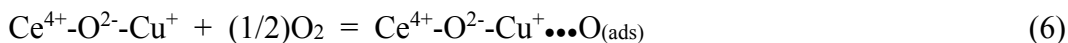
temperatures at which 50% conversion occurs depend on the amount of Cu loading. We find that 9% Cu-CZ generates 50% conversion at the lowest temperature, following 7, 5, 3 and 1% Cu-CZ, respectively as shown in Figure 5.7. Specifically, 1% Cu-CZ generated 95% conversion at 170°C, 3% Cu-CZ generated 99% at 150°C, and 5, 7 and 9% Cu-CZ generated 100% at 130°C. For comparison, the previous work reported by Yen *et al.* (2012) showed maximum CO conversion of only around 88% at 80°C in excess H<sub>2</sub> over a 30%Cu/CeO<sub>2</sub> catalyst. In our previous work (Jampa *et al.*, 2017a), we also succeeded in the preparation of mesoporous Cu-CeO<sub>2</sub> catalyst which provided 100% CO conversion at the temperature of 110°C lower than that of Cu-CZ in this study. From BET, SAXD and TEM results, it indicates that the mesoporous Cu-CeO<sub>2</sub> has more ordered structure and higher surface area than those of mesoporous Cu-CZ. As a resulting, catalytic performance of Cu-CeO<sub>2</sub> shows a little bit higher than that of Cu-CZ. However, the incorporation of ZrO<sub>2</sub> to CeO<sub>2</sub> can improve catalytic performance for autothermal steam reforming of methanol (ASRM) operated with high temperature (Jampa *et al.*, 2017b). The mesoporous Cu-CZ exhibits lower CO selectivity than that of the mesoporous Cu-CeO<sub>2</sub> catalyst during ARSM reaction.

Typically, CuO acts as catalyst by adsorbing CO molecules after which redox reaction converts CO to CO<sub>2</sub> and Cu<sup>2+</sup> to Cu<sup>1+</sup>. CeO<sub>2</sub> provides lattice oxygens in converting CO molecules to CO<sub>2</sub>. Oxygen likely competes with CO for adsorption on the catalyst and oxygen vacancies are located at the copper-ceria interface (Royer and Duprez, 2011). Gas phase oxygen can thus re-oxidize the surface metal atoms and repopulate oxygen vacancies on the CZ support (Mars and Krevelen, 1954). Also evidence suggests (Royer and Duprez, 2011) that electronic interaction between the Cu<sup>2+</sup>/Cu<sup>+</sup> and Ce<sup>4+</sup>/Ce<sup>3+</sup> redox couples facilitates the electron transfer that accompanies the oxidation reaction. The addition of Zr to CeO<sub>2</sub> enhances the thermal stability and oxygen mobility of the system. Incorporating the above observations, the CO-PROX mechanism over Cu-CZ catalysts can therefore be represented using eq. (5)-(9) (Dow and Huang, 1994; Goldstein and Mitchell, 2011; Royer and Duprez, 2011).

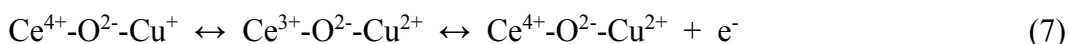
a) Adsorption of CO on the catalyst:



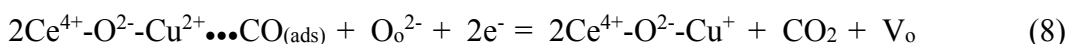
b) Adsorption of oxygen on the catalyst:



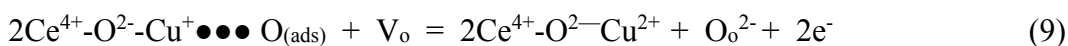
c) Electron transfer between  $\text{Cu}^{2+}/\text{Cu}^+$  and  $\text{Ce}^{4+}/\text{Ce}^{3+}$  redox couples:



d) CO undergoes redox reaction with  $\text{Cu}^{2+}$  and lattice oxygen ( $\text{O}_\text{o}^{2-}$ ):



e) Adsorbed oxygen re-oxidizes  $\text{Cu}^+$  and repopulates oxygen vacancies ( $\text{V}_\text{o}$ ) on the CZ support:



The above mechanism implies that uniform and intimate Cu dispersion on the CZ support surface is a key factor in enhancing catalytic performance for the CO-PROX reaction, which is limited by the presence of bulk CuO, since bulk CuO is inactive for the CO-PROX reaction due to diminished capability to adsorb CO (Marino *et al.*, 2005). However, in the present work, the latter problem does not occur, as confirmed by the XRD results, and by the fact that the activity of Cu-CZ catalysts increases with increasing Cu content from 1 to 9 wt.% at low temperatures, as shown in Figure 5.7, indicating that the increase of Cu content does not increase the content of bulk CuO. Furthermore, Davo-Quinonero *et al.* (2016) proposed another mechanism occurring in CO-PROX reaction over  $\text{CuO}/\text{CeO}_2$  and  $\text{CuO}/\text{CeO}_2\text{-ZrO}_2$  catalysts, viz. the formation of bicarbonates via hydroxyl groups located on the catalyst surface. As carbon-based intermediates, these bicarbonates cause faster CO oxidation rates, compared to those generated via carbonates. This mechanism proposes that CO chemisorption at the  $\text{CuO-CeO}_2$  interface produces  $\text{Cu}^+\text{-CO}$  carbonyl species which then react with surface hydroxyls ( $-\text{OH}$ ) at the chemisorption sites to generate surface bicarbonates ( $-\text{CO}_2\text{OH}$ ). The resulting surface bicarbonates are rapidly converted to  $\text{CO}_2$ .

Figure 5.7 indicates that the maximum CO conversions of all Cu-CZ catalysts are in the range of 95-100% at temperatures between 130 °C to 170

°C. and the selectivity is higher than 50% at temperatures below 150°C. The high activity and selectivity is suggested to arise from well-dispersed CuO species on the high surface area of the mesoporous CZ support.

#### 5.4.2.2 Effect of CO<sub>2</sub>

Figure 5.8 illustrates the influence of 10 vol.% CO<sub>2</sub> in the system. It was found that the maximum CO conversion of the catalysts slightly decreases, accompanied by a shift to a higher temperature (130°C to 150°C for 3, 5, 7 and 9%Cu-CZ). Moreover, the selectivities of all catalysts also drop. The decrease of CO oxidation performance, as evident in Figure 5.8, may be explained as follows; competitive adsorption of CO and CO<sub>2</sub> on the CZ surface as carbonate molecules, causes steric hindrance of oxygen mobility on the CZ surface. As a result, the presence of CO<sub>2</sub> has an inhibiting effect on the CO-PROX performance (Marino *et al.*, 2005; Gamarra and Martinez-Arias, 2009).

#### 5.4.2.3 Effect of Combined CO<sub>2</sub> and H<sub>2</sub>O

The effect on the CO-PROX reaction of addition of 10 vol.% CO<sub>2</sub> and 10 vol.% H<sub>2</sub>O to the feed gas was investigated and the results are shown in Figure 5.9. At low temperatures, the activity of all catalysts is evidently decreased. The position of maximum CO conversion is shifted to a higher temperature (170°C to 190°C for 1%Cu-CZ and 130°C to 170°C for 3, 5, 7 and 9%Cu-CZ). This is due not only to the competitive adsorption of CO and CO<sub>2</sub>, but also to the blocking effect of water, as described elsewhere (Moretti *et al.*, 2008; Gamarra and Martinez-Arias, 2009). Liu *et al.* (2004) also reported the effect of CO<sub>2</sub> and H<sub>2</sub>O addition on CO-PROX activity. They found that maximum CO conversion over CuO/CeO<sub>2</sub> and Zr doped CuO/CeO<sub>2</sub> catalysts in the presence of CO<sub>2</sub> and H<sub>2</sub>O occurred at reaction temperatures around 200 and 225°C, respectively, higher than that in our results, as seen in Figure 5.9.

### 5.4.3 Kinetic Analysis of the CO-PROX Reaction

Various catalysts, viz. 1, 3, 5, 7, and 9%Cu-CZ, were used to study the kinetics for the CO-PROX reaction in excess hydrogen. Figures 10, 11 show the reaction rates at various CO and O<sub>2</sub> feedstock concentrations, respectively. It can be observed that the reaction rate increases with increasing amount of Cu in the catalysts,

with increasing reaction temperature, and increases in the CO and O<sub>2</sub> feed concentrations, reflecting the positive effects of CO and O<sub>2</sub> on the CO-PROX reactivity (Lu *et al.*, 2013). Kinetic data on CO-PROX reaction rate for all prepared Cu- CZ catalysts, comprising the rate constant (k) at two different reaction temperatures, the power exponents in the rate expression, the activation energy (E<sub>a</sub>), and the Arrhenius constant (A), are summarized in Table 5.4. The reaction rate (r) was represented by  $r = k[CO]^x [O_2]^y$ . The power law expressions for the reaction rates of all catalysts were determined via fits to the experimental results as follows:

$$\begin{aligned} r &= k[CO]^{0.80} [O_2]^{0.27} && \text{for 1\%Cu-CZ,} \\ r &= k[CO]^{0.79} [O_2]^{0.22} && \text{for 3\%Cu-CZ,} \\ r &= k[CO]^{0.90} [O_2]^{0.25} && \text{for 5\%Cu-CZ,} \\ r &= k[CO]^{1.03} [O_2]^{0.44} && \text{for 7\%Cu-CZ, and} \\ r &= k[CO]^{0.94} [O_2]^{0.49} && \text{for 9\%Cu-CZ.} \end{aligned}$$

Evidently the increasing levels of Cu in the catalyst systematically enhances the reaction rate, manifested as systematic increases of the [O<sub>2</sub>] and [CO] power law exponents in the CO-PROX reaction rate equation.

The rate constants at 90° and 130 °C of each catalyst were calculated via the reaction rate equation, as presented in Table 5.4. It is found that the change of the k value depends on the reaction temperature and the Cu content. Moreover, the activation energy for CO-PROX over Cu-CZ catalysts was calculated by eq. 10 (House, 1966):

$$\ln\left(\frac{k_1}{k_2}\right) = \frac{E_a}{R} \left(\frac{1}{T_1} - \frac{1}{T_2}\right) \quad (10)$$

where k<sub>1</sub> and k<sub>2</sub> are the rate constants at 90° and 130 °C, respectively, E<sub>a</sub> is the activation energy, R is the gas constant (8.314 JK<sup>-1</sup>mol<sup>-1</sup>), T<sub>1</sub> and T<sub>2</sub> are the reaction temperatures at 90° (363.15 K) and 130 °C (403.15 K), respectively.

As shown in Table 5.4, the apparent activation energy follows the order of 1%Cu-CZ (43.6 kJmol<sup>-1</sup>) > 3%Cu-CZ (21.7 kJmol<sup>-1</sup>) > 5%Cu-CZ (10.7 kJmol<sup>-1</sup>) > 7%Cu-CZ (9.5 kJmol<sup>-1</sup>) > 9%Cu-CZ (8.9 kJmol<sup>-1</sup>). From these results, we conclude that higher Cu content in the catalyst provides an easier route for the CO-PROX reaction to take place, implying better catalytic performance, consistent with the

catalytic activity results shown in Figure 5.7. This conclusion is further supported by values of the Arrhenius constant of each catalyst, estimated via eq. 11 (Rodríguez-Aragon and Lopez-Fidalgo, 2005):

$$k = A \exp\left(\frac{-E_a}{RT}\right) \quad (11)$$

where  $k$  is the rate constant,  $A$  is the Arrhenius constant,  $E_a$  is the activation energy,  $R$  is the gas constant ( $8.314 \text{ JK}^{-1}\text{mol}^{-1}$ ),  $T$  is the reaction temperature. As indicated in Table 5.4,  $A$  values for the various catalysts, viz. 1, 3, 5, 7, and 9% Cu-CZ, are, respectively 0.62, 1.21, 1.99, 1.44, and 1.66 in units of  $(\text{mol}\cdot\text{dm}^{-3})^{(1-x-y)}$ .

#### 5.4.4 Stability of 9%Cu-CZ Catalyst

The 9%Cu-CZ catalyst was chosen to evaluate catalytic stability for the CO-PROX reaction due to having the best catalytic performance under diverse feed compositions, as shown by our experimental results. The stability test was performed by continuously monitoring the % CO conversion over a period of 72 h at a reaction temperature of 130 °C, using a reactant gas composition of 1:1:40 CO:O<sub>2</sub>:H<sub>2</sub> (vol%). The result is shown in Figure 5.12, from which it can be concluded that the CO conversion using the 9%Cu-CZ catalyst maintained a level of 99% conversion with no sign of reduction in activity over the 72 h testing period.

## 5.5 Conclusions

In this work, Cu loaded mesoporous CeO<sub>2</sub>-ZrO<sub>2</sub> catalysts containing different amounts of Cu were successfully synthesized via nanocasting and deposition-precipitation techniques, using MCM-48 as a hard template. The resulting CZ supports provided an ordered pore structure and a high surface area of around 256 m<sup>2</sup>g<sup>-1</sup>. Wide angle XRD spectra indicated the incorporation of ZrO<sub>2</sub> into the CeO<sub>2</sub> lattice. The Cu-CZ catalysts containing different Cu contents still maintained a significant degree of the order of the CZ support with high specific surface area. A lesser amount of Cu was found on the surface than in the pores of the CZ support. Using XPS analysis, the oxidation states on the catalysts surface consist of Ce<sup>4+</sup>, Ce<sup>3+</sup>, Cu<sup>2+</sup> and Cu<sup>+</sup> species.



The reducing power of the Cu-CZ catalysts extended to lower temperatures compared to the pure CZ support. Increase of Cu content in the CZ support systematically enhances the redox properties of the catalyst.

The catalytic activity of Cu-CZ catalysts was investigated for the preferential CO oxidation (CO-PROX) in the presence of a H<sub>2</sub>-rich stream in the temperature range of 50-250°C. All Cu-CZ catalysts showed maximum CO conversion in the range of 95-100% at lower temperatures and the selectivity was more than 50% at temperatures below 150°C. The activity of the Cu-CZ catalysts increases with increasing Cu content from 1 to 9 wt%. The presence of CO<sub>2</sub> or CO<sub>2</sub> plus H<sub>2</sub>O in the feed gas had an inhibiting effect on the CO-PROX performance. Furthermore, the kinetic analysis confirms that the 9%Cu-CZ catalyst with the lowest activation energy and largest Arrhenius constant shows the best catalytic performance for the CO-PROX reaction and maintains a 99% CO conversion level over a testing period of 72 h.

## 5.6 Acknowledgements

This research is financially supported by the Grant for International Research Integration: Chula Research Scholar, Ratchadaphiseksompot Endowment Fund, Chulalongkorn University, Thailand, Thailand Research Fund (Senior Research Scholar), and Development and Promotion of Science and Technology Talents Project.

## 5.7 References

- Abdollahzadeh-Ghom, S., Zamani, C., Andreu, T., Epifani, M., and Morante, J.R. (2011) Improvement of oxygen storage capacity using mesoporous ceria-zirconia solid solutions. *Applied Catalysis B*, 108, 32-38.
- Adamski, A., Tabor, E., Gil, B., and Sojka, Z. (2007) Interaction of NO and NO<sub>2</sub> with the surface of Ce<sub>x</sub>Zr<sub>1-x</sub>O<sub>2</sub> solid solutions-Influence of the phase composition. *Catalysis Today*, 119, 114-119.

- Araujo, V.D., Bellido, J.D.A., Bernardi, M.I.B., Assaf, J.M., and Assaf, E.M. (2012) CuO-CeO<sub>2</sub> catalysts synthesized in one-step: Characterization and PROX performance. International Journal of Hydrogen Energy, 37, 5498-5507.
- Atribak, I., Bueno-Lopez, A., and Garcia-Garcia, A. (2008) Thermally stable ceria-zirconia catalysts for soot oxidation by O<sub>2</sub>. Catalysis Communications, 9, 250-255.
- Atribak, I., Guillen-Hurtado, N., Bueno-Lopez, A., and Garcia-Garcia, A. (2010) Influence of the physico-chemical properties of CeO<sub>2</sub>-ZrO<sub>2</sub> mixed oxides on the catalytic oxidation of NO to NO<sub>2</sub>. Applied Surface Science, 256, 7706-7712.
- Avgouropoulos, G., Ioannides, T., Matralis, H.K., Batista, J., and Hocevar, S. (2001) CuO-CeO<sub>2</sub> mixed oxide catalysts for the selective oxidation of carbon monoxide in excess hydrogen. Catalysis Letters, 73, 33-40.
- Avgouropoulos, G., Ioannides, T., Papadopoulou, C.H., Batista, J., Hocevar, S., and Matralis, H.K. (2002) A comparative study of Pt/ $\gamma$ -Al<sub>2</sub>O<sub>3</sub>, Au/ $\alpha$ -Fe<sub>2</sub>O<sub>3</sub> and CuO-CeO<sub>2</sub> catalysts for the selective oxidation of carbon monoxide in excess hydrogen. Catalysis Today, 75, 157-167.
- Ayastuy, J.L., Gurbani, A., Gonzalez-Marcos, M.P., and Gutierrez-Ortiz, M.A. (2012) Selective CO oxidation in H<sub>2</sub> streams on CuO/Ce<sub>x</sub>Zr<sub>1-x</sub>O<sub>2</sub> catalysts: Correlation between activity and low temperature reducibility. International Journal of Hydrogen Energy, 37, 1993-2006.
- Bozo, C., Guilhaume, N., Garbowski, E., and Primet, M. (2000) Combustion of methane on CeO<sub>2</sub>-ZrO<sub>2</sub> based catalysts. Catalysis Today, 59, 33-45.
- Biesinger, M.C., Laua, L.W.M., Gersonb, A.R., and Smart, R.S.C. (2010) Resolving surface chemical states in XPS analysis of first row transition metals, oxides and hydroxides: Sc, Ti, V, Cu and Zn. Applied Surface Science, 257, 87-98.
- Chen, J., Zhu, J., Zhan, Y., Lin, X., Cai, G., Wei, K., and Zheng, Q. (2009) Characterization and catalytic performance of Cu/CeO<sub>2</sub> and Cu/MgO-CeO<sub>2</sub> catalysts for NO reduction by CO. Applied Catalysis A, 363, 208-215.

- Davó-Quiñonero, A., Navlani-García, M., Lozano-Castelló, D., Bueno-López, A., and Anderson, J. (2016) Role of Hydroxyl Groups in the Preferential Oxidation of CO over Copper Oxide–Cerium Oxide Catalysts. *ACS Catalysis*, 6, 1723-1731.
- Delimaris, D. and Ioannides, T. (2009) VOC oxidation over CuO-CeO<sub>2</sub> catalysts prepared by a combustion method. *Applied Catalysis B*, 89, 295-302.
- Djinovic, P., Batista, J., and Pintar, A. (2008) Calcination temperature and CuO loading dependence on CuO-CeO<sub>2</sub> catalyst activity for water-gas shift reaction. *Applied Catalysis A*, 347, 23-33.
- Dow, W.P. and Huang, T.J. (1994) Effect of oxygen vacancy of yttria-stabilized zirconia support on carbon monoxide oxidation over copper catalyst. *Journal of Catalysis*, 147, 322-332.
- Fally, F., Perrichon, V., Vidal, H., Kaspar, J., Blanco, G., Pintado, J.M., Bernal, S., Colon, G., Daturi, M., and Lavalley, J.C. (2000) Modification of the oxygen storage capacity of CeO<sub>2</sub>-ZrO<sub>2</sub> mixed oxides after redox cycling aging. *Catalysis Today*, 59, 373-386.
- Fu, Q., Saltsburg, H., and Flytzani-Stephanopoulos, M. (2003) Active nonmetallic Au and Pt species on ceria-based water-gas shift catalysts. *Science*, 301, 935-938.
- Gamarra, D. and Martinez-Arias, A. (2009) Preferential oxidation of CO in rich H<sub>2</sub> over CuO/CeO<sub>2</sub>: *Operando*-DRIFTS analysis of deactivating effect of CO<sub>2</sub> and H<sub>2</sub>O. *Journal of Catalysis*, 263, 189-195.
- Goldstein, E.A. and Mitchell, R.E. (2011) Chemical kinetics of copper oxide reduction with carbon monoxide. *Proceedings of the Combustion Institute*, 33, 2803-2810.
- Guo, R., Zhen, W., Pan, W., Zhou, Y., Hong, J., Xu, H., Jin, Q., Ding, C., and Guo, S. (2014) Effect of Cu doping on the SCR activity of CeO<sub>2</sub> catalyst prepared by citric acid method. *Journal of Industrial and Engineering Chemistry*, 20, 1577-1580.
- Haruta, M. (2004) Gold as a novel catalyst in the 21<sup>st</sup> century: Preparation, working mechanism and applications. *Gold Bulletin*, 37, 27-36.

- Huang, T., Yu, T., and Chang, S. (1989) Effect of calcination atmosphere on CuO/ $\gamma$ -Al<sub>2</sub>O<sub>3</sub> catalyst for carbon monoxide oxidation. Applied Catalysis, 52, 157-163.
- Huang, T. and Yu, T. (1991) Calcination conditions on copper/alumina catalysts for carbon monoxide oxidation and nitric oxide reduction. Applied Catalysis, 71, 275-282.
- House, J.E. (1966) Principle of chemical kinetics. USA: Academic Press.
- Jampa, S., Wangkawe, K., Tantisriyanurak, S., Changpradit, J., Jamieson, A.M., Chaisuwan, T., Luengnaruemitchai, A., and Wongkasemjit, S. (2017a) High performance and stability of copper loading on mesoporous ceria catalyst for preferential oxidation of CO in presence of excess of hydrogen. International Journal of Hydrogen Energy, 42, 5537-5548.
- Jampa, S., Jamieson, A.M., Chaisuwan, T., Luengnaruemitchai, A., and Wongkasemjit, S. (2017b) Achievement of hydrogen production from autothermal steam reforming of methanol over Cu-loaded mesoporous CeO<sub>2</sub> and Cu-loaded mesoporous CeO<sub>2</sub>-ZrO<sub>2</sub> catalysts. International Journal of Hydrogen Energy, 42, 15073-15084.
- Jardim, E.O., Rico-Francés, S., Coloma, F., Ramos-Fernández, E.V., Silvestre-Albero, J., and Sepúlveda-Escribano, A. (2014) Superior performance of gold supported on doped CeO<sub>2</sub> catalysts for the preferential CO oxidation (PROX). Applied Catalysis A, 487, 119-129.
- Jeong, D., Jang, W., Na, H., Shim, J., Jha, A., and Roh, H. (2015) Comparative study on cubic and tetragonal Cu-CeO<sub>2</sub>-ZrO<sub>2</sub> catalysts for water gas shift reaction. Journal of Industrial and Engineering Chemistry, 27, 35-39.
- Kaspar, J., Fornasiero, P., and Graziani, M. (1999) Use of CeO<sub>2</sub>-based oxides in the three-way catalysis. Catalysis Today, 50, 285-298.
- Kundakovic, L.J. and Flytzani-Stephanopoulos, M. (1998) Reduction characteristics of copper oxide in cerium and zirconium oxide systems. Applied Catalysis A, 171, 13-29.
- Laguna, O.H., Centeno, M.A., Arzamendi, G., Gandia, L.M., Romero-Sarria, F., and Odriozola, J.A. (2010) Iron-modified ceria and Au/ceria catalysts for Total

- and Preferential Oxidation of CO (TOX and PROX). Catalysis Today, 157, 55-59.
- Leitenburg, C., Trovarelli, A., Llorca, J., Cavani, F., and Bini, G. (1996) The effect of doping CeO<sub>2</sub> with zirconium in the oxidation of isobutene. Applied Catalysis A, 139, 161-173.
- Li, G., Wang, Q., Zhao, B., and Zhao, R. (2010) Modification of Ce<sub>0.67</sub>Zr<sub>0.33</sub>O<sub>2</sub> mixed oxides by coprecipitated/impregnated Co: Effect on the surface and catalytic behavior of Pd only three-way catalyst. Journal of Molecular Catalysis A: Chemical, 326, 69-74.
- Li, W. and Zhao, D. (2013) An overview of the synthesis of ordered mesoporous materials. Chemical Communications, 49, 943-946.
- Li, Y., Fu, Q., and Flytzani-Stephanopoulos, M. (2000) Low-temperature water-gas shift reaction over Cu- and Ni-loaded cerium oxide catalysts. Applied Catalysis B, 27, 179-191.
- Little, L.H. (1966) Infrared spectra of adsorbed species. London: Academic Press.
- Liu, W., Sarofin, A., and Flytzani-Stephanopoulos, M. (1994) Reduction of sulfur dioxide by carbon monoxide to elemental sulfur over composite oxide catalysts. Applied Catalysis B, 4, 167-186.
- Liu, Y., Fu, Q., and Stephanopoulos M.F. (2004) Preferential oxidation of CO in H<sub>2</sub> over CuO-CeO<sub>2</sub> catalysts. Catalysis Today, 93-95, 241-246.
- Longloilert, R., Chaisuwan, T., Luengnaruemitchai, A., and Wongkasemjit, S. (2011) Synthesis of MCM-48 from silatrane via sol-gel process. Journal of Sol-Gel Science and Technology, 58, 427-435.
- Lu, J., Sun, C., Li, N., Jia, A., and Luo, M. (2013) Kinetic study of CO oxidation over CuO/MO<sub>2</sub> (M = Si, Ti and Ce) catalysts. Applied Surface Science, 287, 124-134.
- Madier, Y., Descorme, C., Le Govic, A.M., and Duprez, D. (1999) Oxygen mobility in CeO<sub>2</sub> and Ce<sub>x</sub>Zr<sub>(1-x)</sub>O<sub>2</sub> compounds: Study by CO transient oxidation and <sup>18</sup>O/<sup>16</sup>O isotopic exchange. Journal of Physical Chemistry B, 103, 10999-11006.

- Marino, F., Descorme, C., and Duprez, D. (2004) Noble metal catalysts for the preferential oxidation of carbon monoxide in the presence of hydrogen (PROX). Applied Catalysis B, 54, 59-66.
- Marino, F., Descorme, C., and Duprez, D. (2005) Supported base metal catalysts for the preferential oxidation of carbon monoxide in the presence of excess hydrogen (PROX). Applied Catalysis B, 58, 175-183.
- Mars, P. and Krevelen, D.W. (1954) Oxidations carried out by means of vanadium oxide catalysts. Chemical Engineering Science, 3, 41-59.
- Monteiro, R.S., Noronha, F.B., Dieguez, L.C., and Schmal, M. (1995) Characterization of Pd-CeO<sub>2</sub> interaction on alumina support and hydrogenation of 1,3-butadiene. Applied Catalysis A, 131, 89-106.
- Moretti, E., Lenarda, M., Storaro, L., Talon, A., Montanari, T., Busca, G., Rodríguez-Castellón, E., Jimenez-Lopez, A., Turco, M., Bagnasco, G., and Frattini, R. (2008) One-step synthesis of a structurally organized mesoporous CuO-CeO<sub>2</sub>-Al<sub>2</sub>O<sub>3</sub> system for the preferential CO oxidation. Applied Catalysis A, 335, 46-55.
- Moretti, E., Storaro, L., Talon, A., Riello, P., Molina, A., and Rodríguez-Castellón, E. (2015) 3-D flower like Ce-Zr-Cu mixed oxide systems in the CO preferential oxidation (CO-PROX): Effect of catalyst composition. Applied Catalysis B, 168-169, 385-395.
- Moser, M., Vile, G., Colussi, S., Krumeich, F., Teschner, D., Szentmiklosi, L., Trocarelli, A., and Perez-Ramirez, J. (2015) Structure and reactivity of ceria-zirconia catalysts for bromine and chlorine production via the oxidation of hydrogen halides. Journal of Catalysis, 331, 128-137.
- Mullins, D.R. (2015) The surface chemistry of cerium oxide. Surface Science Reports, 70, 42-85.
- Nguyen, T., Morfin, F., Aouine, M., Bosselet, F., Rousset, J., and Piccolo, L. (2015) Trends in the CO oxidation and PROX performances of the platinum-group metals supported on ceria. Catalysis Today, 253, 106-114.
- Nousir, S., Maache, R., Azalim, S., Agnaou, M., Brahmi, R., and Bensitel, M. (2015) Synthesis and investigation of the physico-chemical properties of catalysts

- based on mixed oxides  $Ce_xZr_{1-x}O_2$ . Arabian Journal of Chemistry, 8, 222-227.
- Oh, S.H. and Sinkevitch, R.M. (1993) Carbon monoxide removal from hydrogen-rich fuel cell feed streams by selective catalytic oxidation. Journal of Catalysis, 142, 254-262.
- Paier, J., Penschke, C., and Sauer, J. (2013) Oxygen defects and surface chemistry of ceria: quantum chemical studies compared to experiment. Chemical Reviews, 113, 3949-3985.
- Phiriyawirut, P., Magaraphan, R., Jamieson, A.M., and Wongkasemjit, S. (2003) Morphology study of MFI zeolite synthesized directly from silatrane and alumatrane via the sol-gel process and microwave heating. Microporous Mesoporous Materials, 64, 83-93.
- Pojanavaraphan, C., Nakaranuwattana, W., Luengnaruemitchai, A., and Gulari, E. (2014) Effect of support composition and metal loading on  $Au/Ce_{1-x}Zr_xO_2$  catalysts for the oxidative steam reforming of methanol. Chemical Engineering Journal, 240, 99-108.
- Radlik, M., Adamowska, M., Łamacz, A., Krzton, A., Costa, P., and Turek, W. (2013) Study of the surface evolution of nitrogen species on  $CuO/CeZrO_2$  catalysts. Reaction Kinetics, Mechanisms, and Catalysis, 109, 43-56.
- Ratnasamy, P., Srinivas, D., Satyanarayana, C.V.V., Manikandan, P., Kumaran, R.S.S., Sachin, M., and Shetti, V.N. (2004) Influence of the support on the preferential oxidation of CO in hydrogen-rich steam reformates over the  $CuO-CeO_2-ZrO_2$  system. Journal of Catalysis, 221, 455-465.
- Rodriguez-Aragon, L.J. and Lopez-Fidalgo, J. (2005) Optimal designs for the Arrhenius equation. Chemometrics and Intelligent Laboratory Systems, 77, 131-138.
- Rossinyol, E., Arbiol, J., Peiro, F., Cornet, A., Morante, J.R., Tian, B., Bo, T., and Zhao, D. (2005) Nanostructured metal oxides synthesized by hard template method for gas sensing applications. Sensors and Actuators, B, 109, 57-63.
- Rostrup-Nielsen, J.R., Sehested, J., and Norskov, J.K. (2002) Hydrogen and synthesis gas by steam and  $CO_2$  reforming. Advances in Catalysis, 47, 65-139.

- Royer, S. and Duprez, D. (2011) Catalytic oxidation of carbon monoxide over transition metal oxides. ChemCatChem, 3, 24-65.
- Sakurai, H. and Haruta, M. (1995) Carbon dioxide and carbon monoxide hydrogenation over gold supported on titanium, iron, and zinc oxides. Applied Catalysis A, 127, 93-105.
- Schumacher, K., Ravikovitch, P.I., Chesne, A., Neimark, A.V., and Unger, K.K. (2000) Characterization of MCM-48 materials. Langmuir, 16, 4648-4654.
- Shan, W., Shen, W., and Li, C. (2003) Structural characteristics and redox behaviors of  $Ce_{1-x}Cu_xO_y$  solid solutions. Chemistry of Materials, 15, 4761-4767.
- Sing, K.S.W., Everett, D.H., Haul, R.A.W., Moscou, L., Pierotti, R.A., Rouquerol, J., and Siemieniewska, T. (1985) Reporting physisorption data for gas/solid systems with special reference to the determination of surface area and porosity. Pure and Applied Chemistry, 57, 603-619.
- Snytnikov, P.V., Sobyenin, V.A., Belyaev, V.D., Tsyrlunikov, P.G., Shitova, N.B., and Shlyapin, D.A. (2003) Selective oxidation of carbon monoxide in excess hydrogen over Pt-, Ru- and Pd-supported catalysts. Applied Catalysis A, 239, 49-56.
- Son, I.H., Shamsuzzoha, M., and Lane, A.M. (2002) Promotion of Pt/ $\gamma$ - $Al_2O_3$  by new pretreatment for low-temperature preferential oxidation of CO in  $H_2$  for PEM fuel cells. Journal of Catalysis, 210, 460-465.
- Song, C. (2002) Fuel processing for low-temperature and high-temperature fuel cells challenges, and opportunities for sustainable development in the 21st century. Catalysis Today, 77, 17-49.
- Trovarelli, A., Boaro, M., Rocchini, E., Leitenburg, C., and Dolcetti, G. (2001) Some recent developments in the characterization of ceria-based catalysts. Journal of Alloys and Compounds, 323, 584-591.
- Trovarelli, A., Leitenburg, C., Dolcetti, G., and Lorca, J.L. (1995)  $CO_2$  methanation under transient and steady-state conditions over Rh/ $CeO_2$  and  $CeO_2$ -Promoted Rh/ $SiO_2$ : The role of surface and bulk ceria. Journal of Catalysis, 151, 111-124.
- Yen, H., Seo, Y., Kaliaguine, S., and Kleitz, F. (2012) Tailored mesostructured copper/ceria catalysts with enhanced performance for preferential oxidation



of CO at low temperature. Angewandte Chemie International Edition, 51, 12032-12035.

Zeng, S., Zhang, W., Sliwa, M., and Su, H. (2013) Comparative study of CeO<sub>2</sub>/CuO and CuO/CeO<sub>2</sub> catalysts on catalytic performance for preferential CO oxidation. International Journal of Hydrogen Energy, 38, 3597-3605.

Zhang, Q., Xu, L., Ning, P., Gu, J., and Guan, Q. (2014) Surface characterization studies of CuO-CeO<sub>2</sub>-ZrO<sub>2</sub> catalysts for selective catalytic reduction of NO with NH<sub>3</sub>. Applied Surface Science, 317, 955-961.

Zhang, S., Huang, W., Qiu, X., Li, B., Zheng, X., and Wu, S. (2002) Comparative study on catalytic properties for low-temperature CO oxidation of Cu/CeO<sub>2</sub> and CuO/CeO<sub>2</sub> prepared *via* solvated metal atom impregnation and conventional impregnation. Catalysis Letters, 80, 41-46.

Zhao, M., Shen, M., and Wang, J. (2007) Effect of surface area and bulk structure on oxygen storage capacity of Ce<sub>0.67</sub>Zr<sub>0.33</sub>O<sub>2</sub>. Journal of Catalysis, 248, 258-267.

**Table 5.1** Compositions and N<sub>2</sub> physisorption data of the synthesized catalysts

Sample composition	Sample abbreviation	BET specific surface area S <sub>BET</sub> (m <sup>2</sup> g <sup>-1</sup> )	Mesopore volume <sup>a</sup> V <sub>pore</sub> (cm <sup>3</sup> g <sup>-1</sup> )	Mesopore diameter <sup>a</sup> d <sub>pore</sub> (nm)
Ce <sub>0.75</sub> Zr <sub>0.25</sub> O <sub>2</sub>	CZ	256	0.46	3.80
1 wt.%Cu-Ce <sub>0.75</sub> Zr <sub>0.25</sub> O <sub>2</sub>	1%Cu-CZ	204	0.34	3.63
3 wt.%Cu-Ce <sub>0.75</sub> Zr <sub>0.25</sub> O <sub>2</sub>	3%Cu-CZ	203	0.33	3.61
5 wt.%Cu-Ce <sub>0.75</sub> Zr <sub>0.25</sub> O <sub>2</sub>	5%Cu-CZ	188	0.30	3.64
7 wt.%Cu-Ce <sub>0.75</sub> Zr <sub>0.25</sub> O <sub>2</sub>	7%Cu-CZ	179	0.37	3.62
9 wt.%Cu-Ce <sub>0.75</sub> Zr <sub>0.25</sub> O <sub>2</sub>	9%Cu-CZ	165	0.31	3.61

**Table 5.2** Structural parameters of CZ support and Cu-CZ catalysts calculated from XRD and SAED data

Catalyst	Average crystallite size of CZ support <sup>a</sup> (nm)	Unit cell parameter of CZ support <sup>b</sup> (nm)	Unit cell parameter of CZ support <sup>c</sup> (nm)
CZ	3.750	0.5382	0.5452
1%Cu-CZ	3.645	0.5376	0.5437
3%Cu-CZ	3.620	0.5371	0.5421
5%Cu-CZ	3.571	0.5371	0.5400
7%Cu-CZ	3.657	0.5368	0.5401
9%Cu-CZ	3.330	0.5384	0.5405

<sup>a</sup> Average crystallite size of CZ support calculated from XRD data at {1 1 1} plane using Scherrer's equation

<sup>b</sup> Unit cell parameter of CZ support calculated from XRD data at {1 1 1} plane using Bragg's equation

<sup>c</sup> Unit cell parameter of CZ support calculated from SAED data of TEM using Bragg's equation

**Table 5.3** The amounts of Cu found in bulk and on the surface of the synthesized Cu-CZ catalysts

Catalyst	Cu <sup>a</sup> (wt.%)	Cu in bulk <sup>b</sup> (wt.%)	Cu on surface <sup>c</sup> (wt.%)
CZ	-	-	-
1%Cu-CZ	1.00	0.894	0.473
3%Cu-CZ	3.00	2.881	1.277
5%Cu-CZ	5.00	5.042	2.177
7%Cu-CZ	7.00	6.983	3.220
9%Cu-CZ	9.00	9.175	3.947

<sup>a</sup> By theoretical calculation

<sup>b</sup> By Atomic Absorption Spectrometry (AAS)

<sup>c</sup> By X-ray Photoelectron Spectroscopy (XPS)

**Table 5.4** Kinetic results of CO-PROX reaction over all synthesized Cu-CZ catalyst

Sample	<sup>a</sup> k <sub>1</sub> ×10 <sup>-4</sup>	<sup>a</sup> k <sub>2</sub> ×10 <sup>-4</sup>	x	y	Power rate expression	Activation energy (kJ mol <sup>-1</sup> )	Arrhenius constant (A)
1%Cu-CZ	0.92	3.87	0.80	0.27	$r = k[CO]^{0.80} [O_2]^{0.27}$	43.60	0.62
3%Cu-CZ	1.74	3.56	0.79	0.22	$r = k[CO]^{0.79} [O_2]^{0.22}$	21.73	1.21
5%Cu-CZ	8.17	11.63	0.90	0.25	$r = k[CO]^{0.90} [O_2]^{0.25}$	10.73	1.99
7%Cu-CZ	112.60	154.03	1.03	0.44	$r = k[CO]^{1.03} [O_2]^{0.44}$	9.53	1.44
9%Cu-CZ	81.36	109.12	0.94	0.49	$r = k[CO]^{0.94} [O_2]^{0.49}$	8.93	1.66

<sup>a</sup>Unit of rate constant (k) = (mol dm<sup>-3</sup>)<sup>(1-x-y)</sup>s<sup>-1</sup>

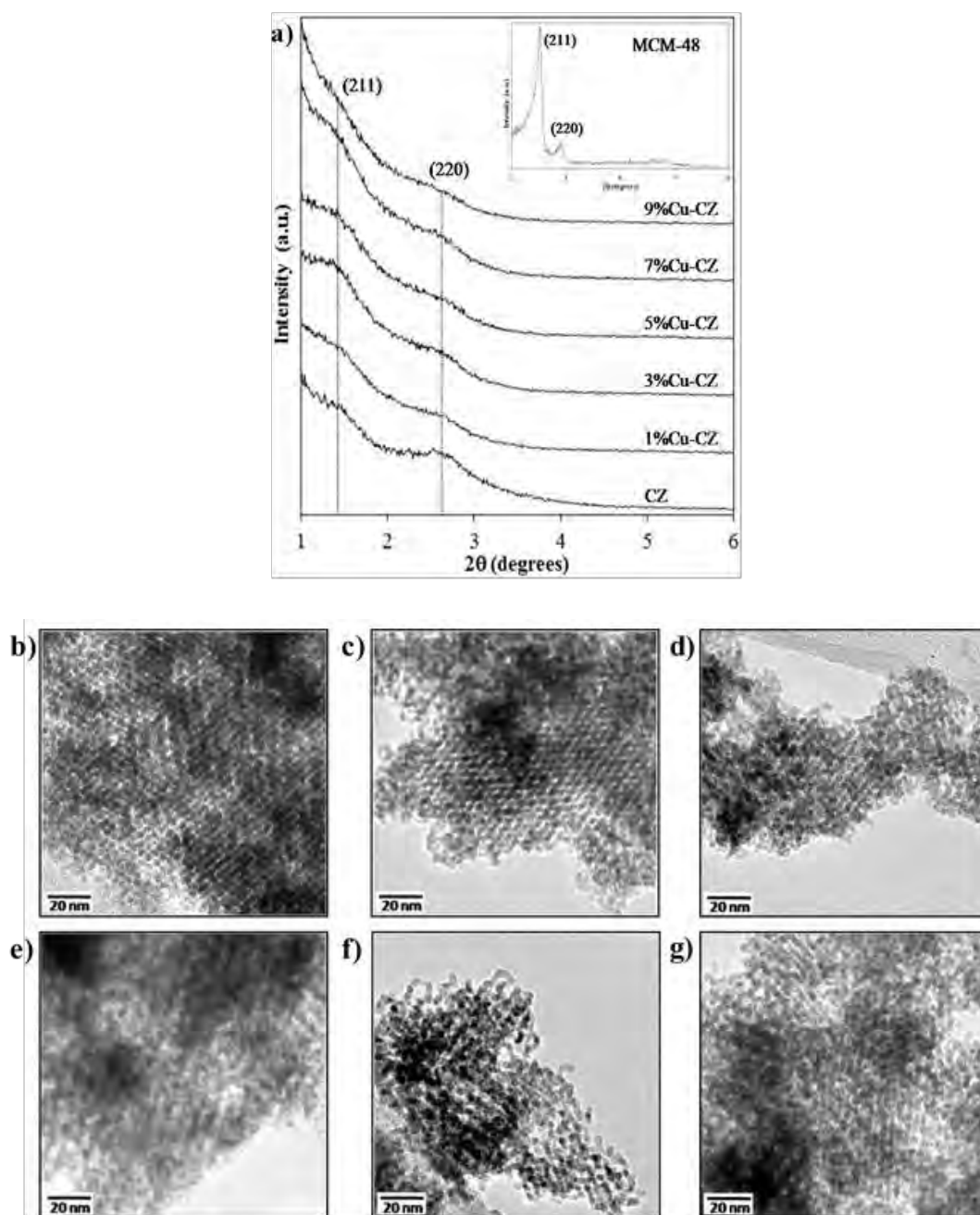


**Figure 5.1** (a) Small angle XRD patterns of the CZ support, Cu-CZ catalysts and MCM-48 (inset), TEM images of (b) the CZ support, (c) 1%Cu-CZ, (d) 3%Cu-CZ, (e) 5%Cu-CZ, (f) 7%Cu-CZ and (g) 9%Cu-CZ.

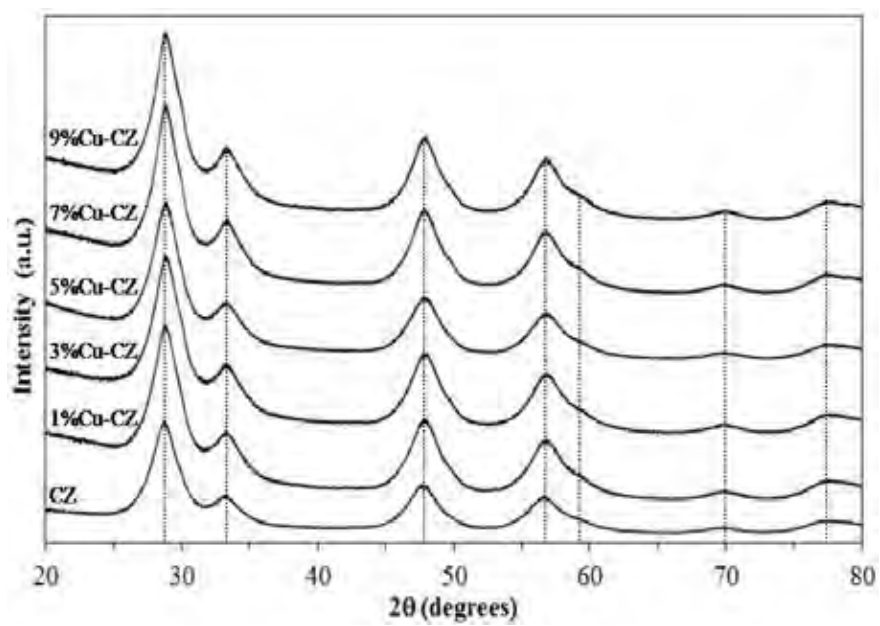


**Figure 5.2** Wide angle XRD patterns of the CZ support and Cu-CZ catalysts.

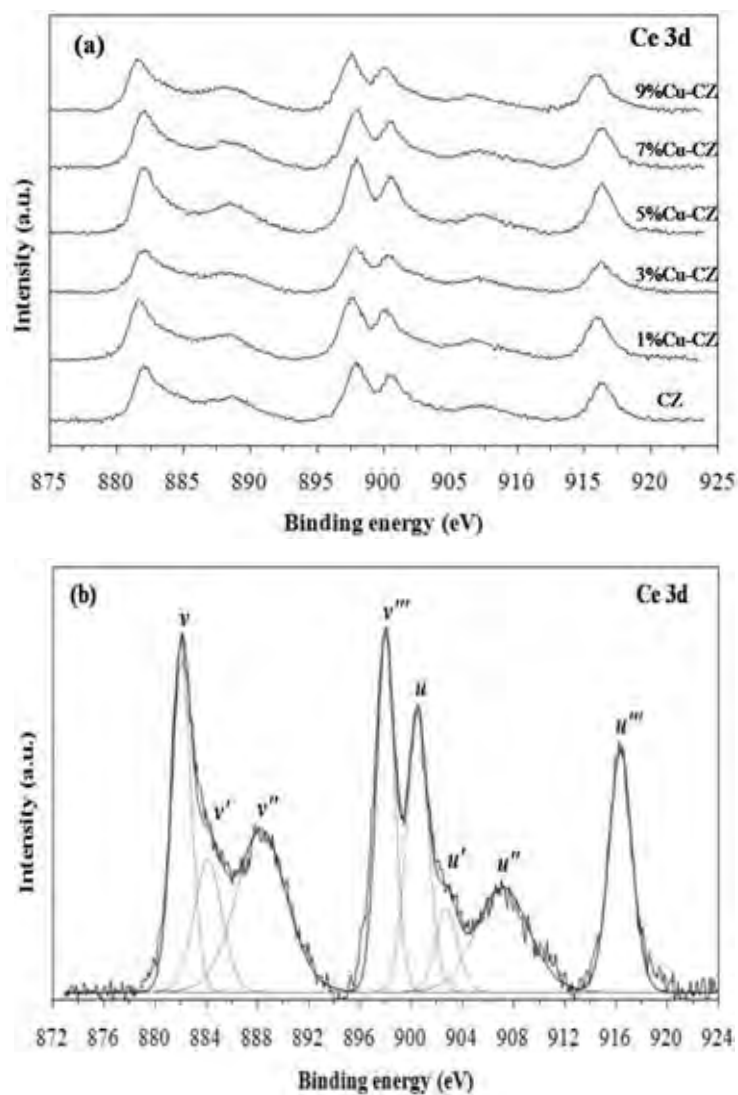


**Figure 5.3** (a) Ce 3d XPS spectra of the CZ support and Cu-CZ catalysts and (b) The deconvoluted Ce 3d XPS spectrum of the 7%Cu-CZ catalyst.



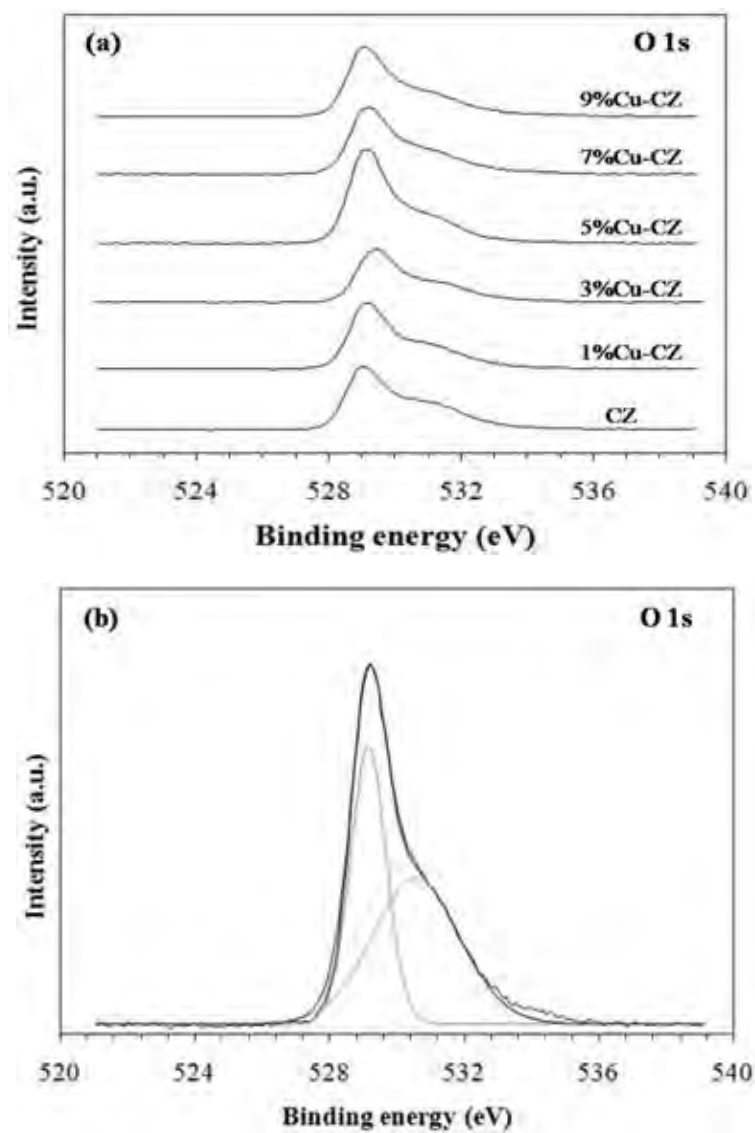


**Figure 5.4** (a) O 1s XPS spectra of the CZ support and Cu-CZ catalysts and (b) The deconvoluted O 1s XPS spectrum of the 7%Cu-CZ catalyst.

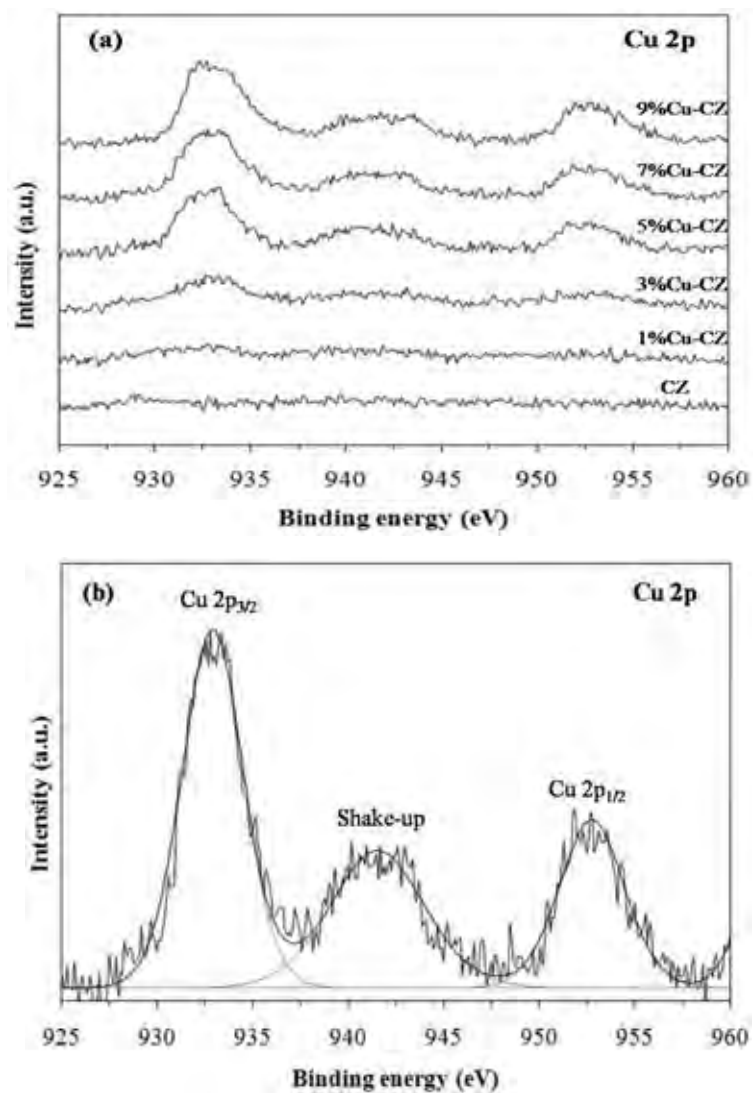


**Figure 5.5** (a) Cu 2p XPS spectra of CZ support and Cu-CZ catalysts and (b) The deconvoluted Cu 2p XPS spectrum of the 7%Cu-CZ catalyst.

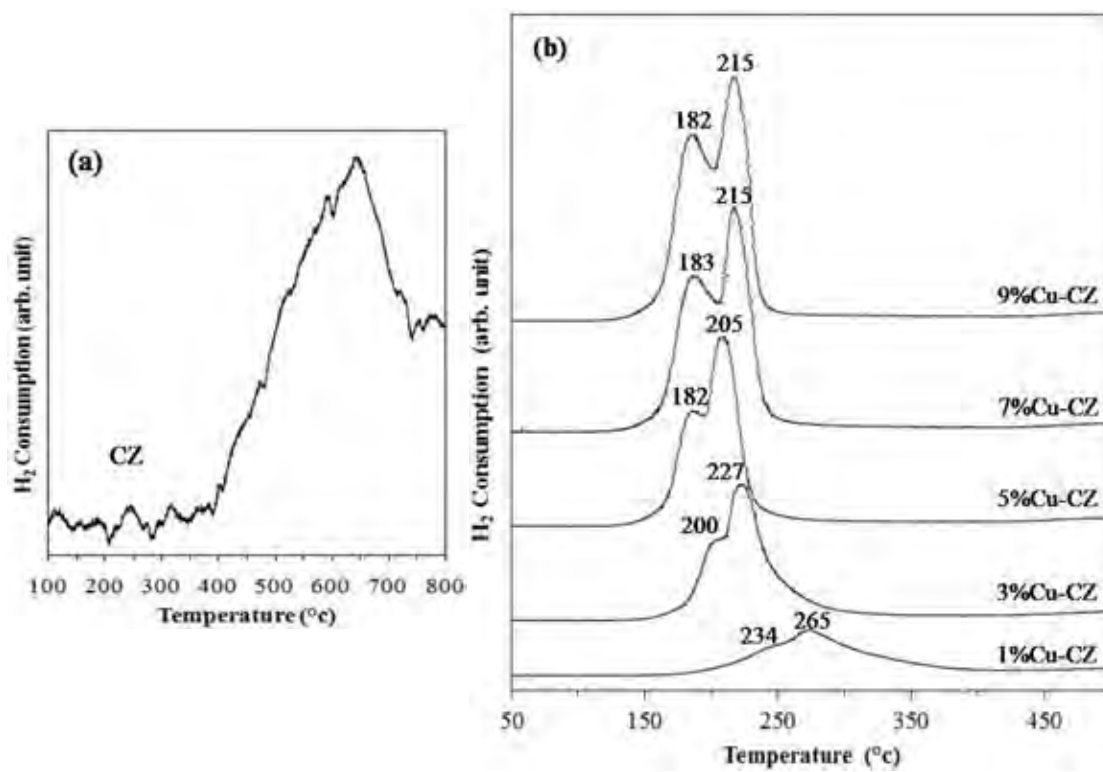


**Figure 5.6** (a) H<sub>2</sub>-TPR profiles of the CZ support (inset) and (b) Cu-CZ catalysts.

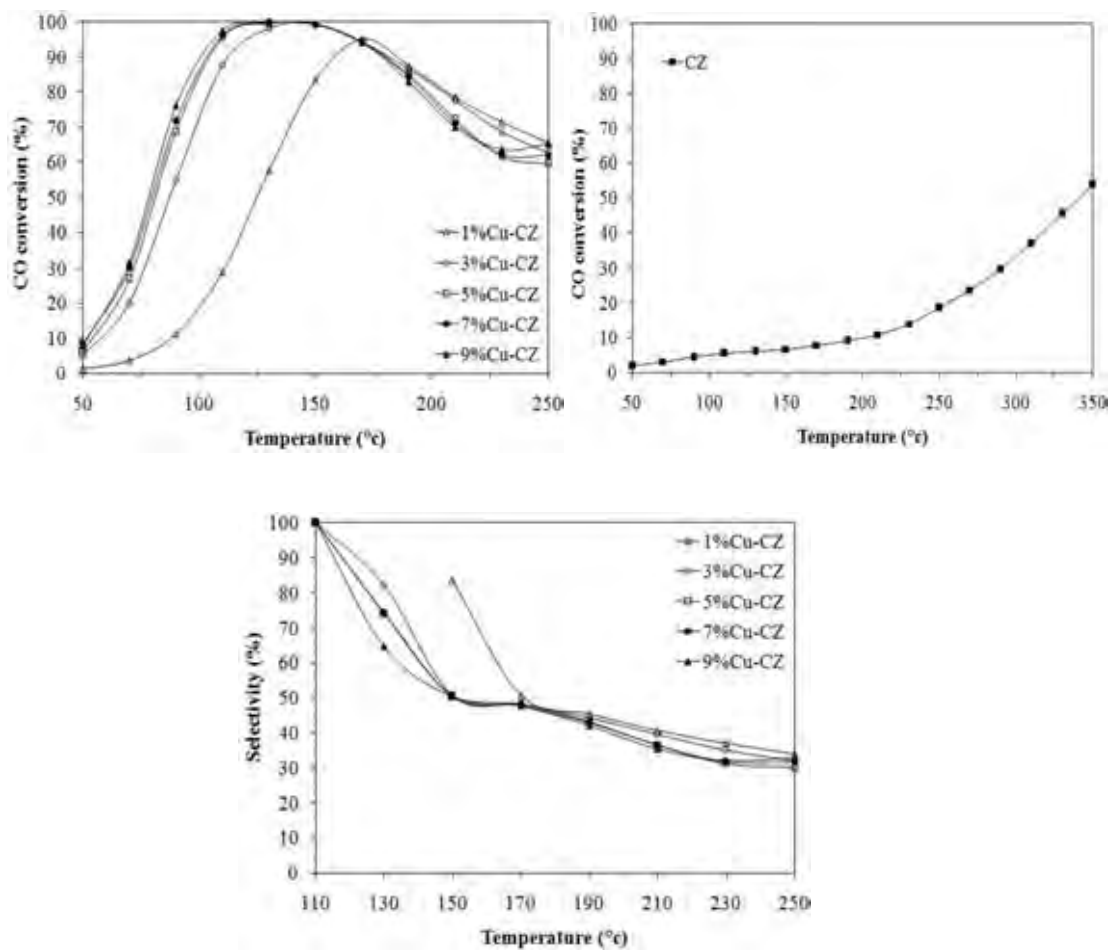


**Figure 5.7** CO conversion and selectivity as a function of temperature of the CZ support and Cu-CZ catalysts, Gas compositions: 1 vol.% CO, 1 vol.% O<sub>2</sub>, 40 vol.% H<sub>2</sub> and He as balance.

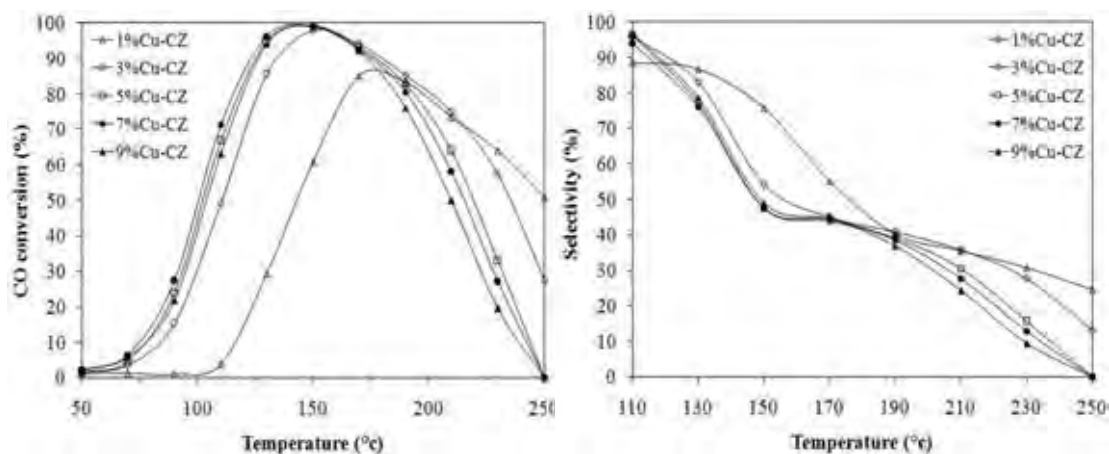


**Figure 5.8** CO conversion and selectivity as a function of temperature of the CZ support and Cu-CZ catalysts, Gas compositions: 1 vol % CO, 1 vol.% O<sub>2</sub>, 10 vol.% CO<sub>2</sub>, 40 vol.% H<sub>2</sub> and He as balance.

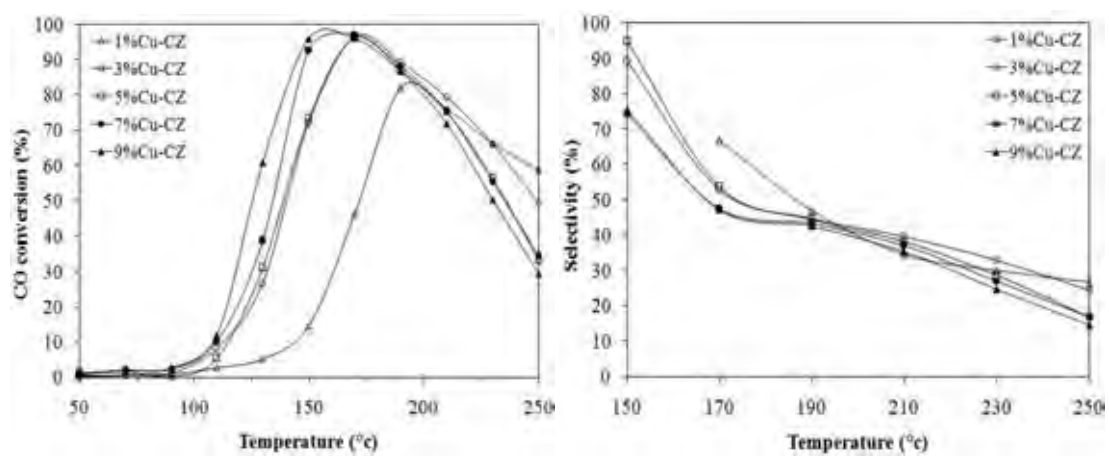


**Figure 5.9** CO conversion and selectivity as a function of temperature for the CZ support and Cu-CZ catalysts, Gas compositions: 1 vol.% CO, 1 vol.% O<sub>2</sub>, 10 vol.% CO<sub>2</sub>, 10 vol.% H<sub>2</sub>O, 40 vol.% H<sub>2</sub> and He as balance.

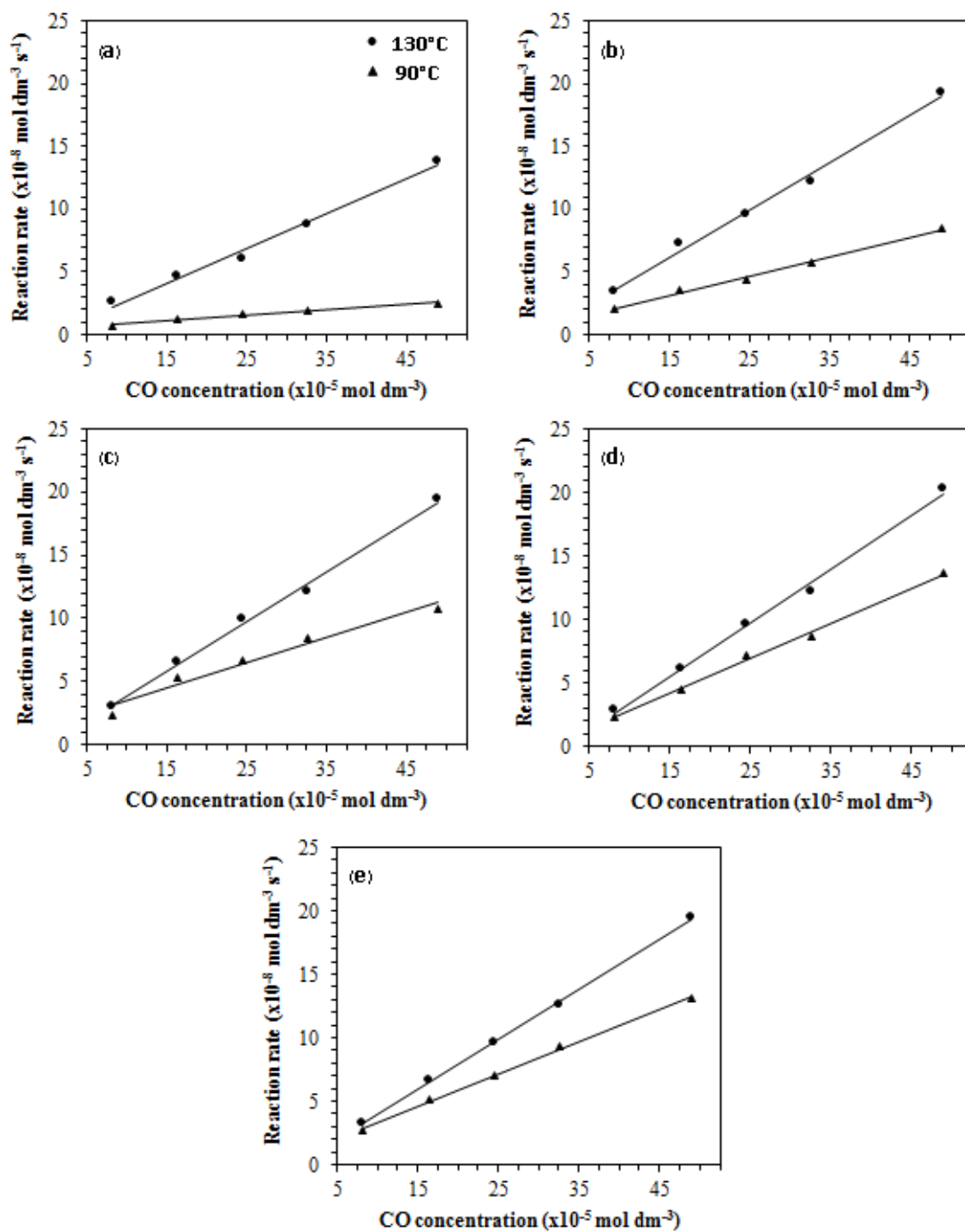


**Figure 5.10** Reaction rates at various CO concentrations of (a) 1, (b) 3, (c) 5, (d) 7, and (e) 9%Cu-CZ at the reaction temperatures of 90° and 130 °C.

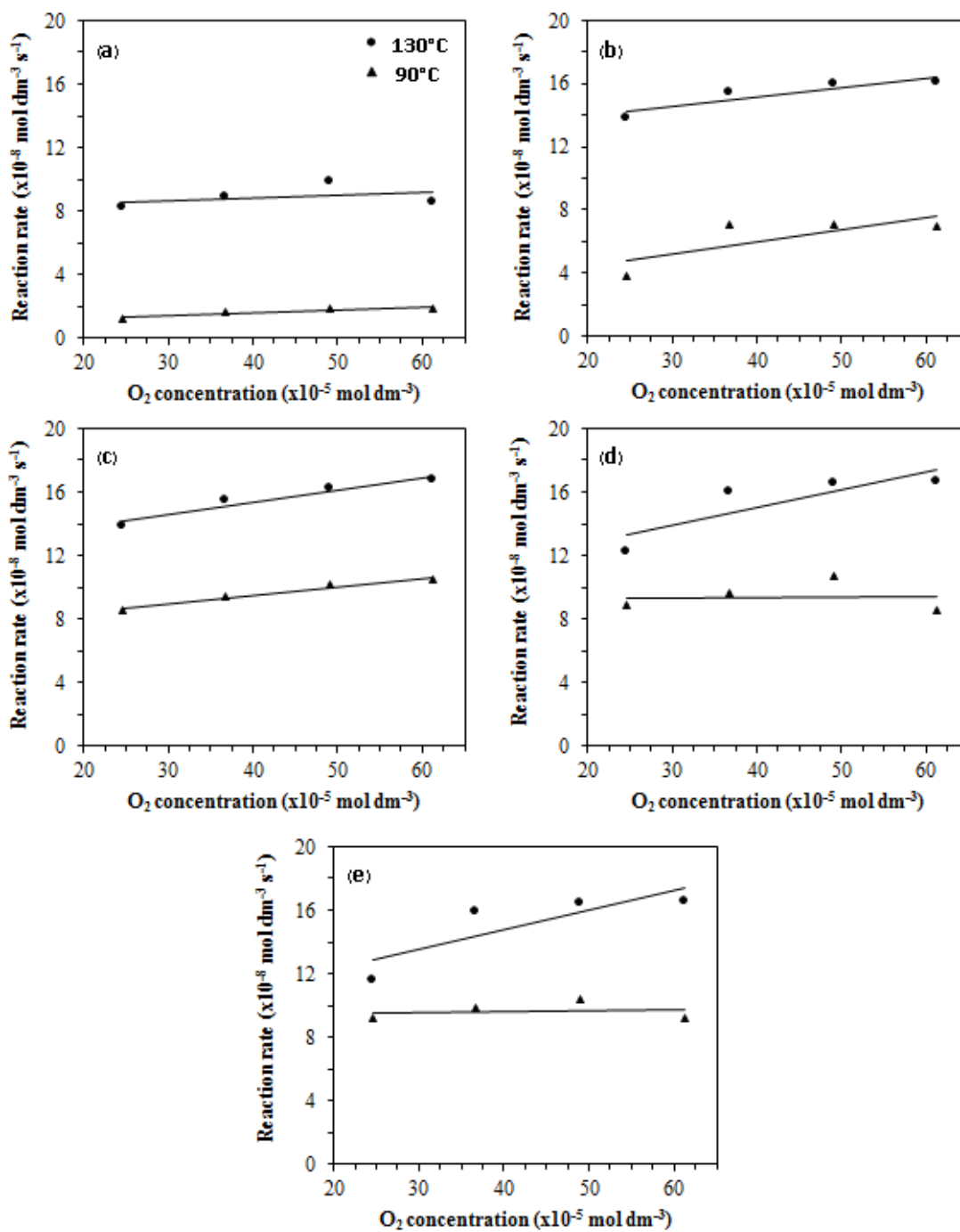


**Figure 5.11** Reaction rates at various  $\text{O}_2$  concentrations of (a) 1, (b) 3, (c) 5, (d) 7, and (e) 9%Cu-CZ at the reaction temperatures of 90° and 130 °C.

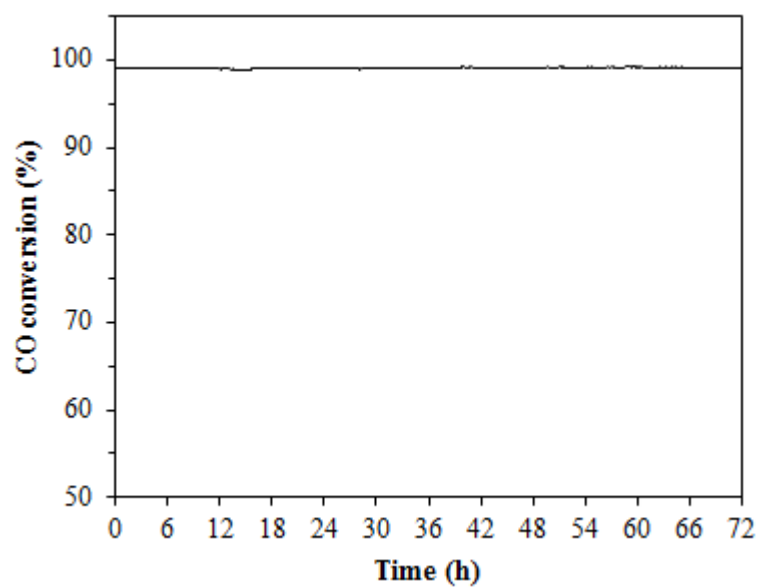


**Figure 5.12** CO conversion is continuously monitored over a 72 hr period as a measure of performance stability of the 9%Cu-CZ for catalysis of the CO-PROX reaction.



**CHAPTER VI**  
**ACHIEVEMENT OF HYDROGEN PRODUCTION FROM AUTOTHERMAL**  
**STEAM REFORMING OF METHANOL OVER Cu-LOADED**  
**MESOPOROUS CeO<sub>2</sub> AND Cu-LOADED MESOPOROUS CeO<sub>2</sub>-ZrO<sub>2</sub>**  
**CATALYSTS**

**6.1 Abstract**

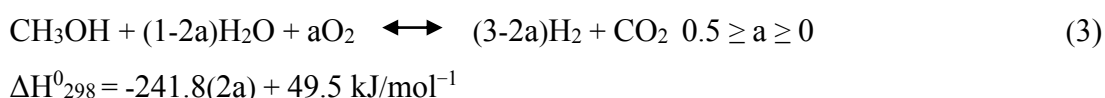
Hydrogen production by oxidative steam reforming of methanol (OSRM) or autothermal steam reforming of methanol (ASRM) was investigated over Cu-loaded mesoporous CeO<sub>2</sub> and Cu-loaded mesoporous CeO<sub>2</sub>-ZrO<sub>2</sub> catalysts, synthesized via a nanocasting process using MCM-48 as a hard template, followed by a deposition-precipitation technique. Various Cu contents were loaded on the mesoporous CeO<sub>2</sub> and CeO<sub>2</sub>-ZrO<sub>2</sub> supports. The fresh and spent catalysts were characterized by N<sub>2</sub> adsorption-desorption, X-ray diffraction, temperature-programmed oxidation, and X-ray photoelectron spectroscopy. The ASRM results showed that 9 wt% Cu loading onto mesoporous CeO<sub>2</sub> and CeO<sub>2</sub>-ZrO<sub>2</sub> provided the best catalytic performance with 100% methanol conversion and 60% H<sub>2</sub> yield at 350° and 300 °C, respectively. Furthermore, the time-on-stream stability testing of the 9 wt% Cu loading catalyst was at 168 h, and the CO selectivity of these two catalysts indicated that the addition of ZrO<sub>2</sub> into the catalyst reduced the CO selectivity during the ASRM process.

**(Keywords:** H<sub>2</sub> production; Autothermal steam reforming of methanol; Mesoporous CeO<sub>2</sub>; Mesoporous CeO<sub>2</sub>-ZrO<sub>2</sub>; Cu-CeO<sub>2</sub>; Cu-CeO<sub>2</sub>-ZrO<sub>2</sub>)

## 6.2 Introduction

Nowadays, fuel cells are considered to be environmentally friendly and high efficiency systems to produce electricity as clean energy for powering vehicles (Cacciola *et al.*, 2001). Among various types of fuel cells, polymer electrolyte fuel-cells (PEMFC) are the most viable candidates for mobile applications (Cleghorn *et al.*, 1997; Song, 2002; Wang *et al.*, 2003; Gregoriev *et al.*, 2006; Hotza *et al.*, 2008). On-board hydrogen ( $H_2$ ) is an essential fuel for PEMFC to generate energy for vehicles. However, on-board  $H_2$  storage in high pressure tanks is still not commercially available for vehicles due to safety, costs of storage, and handling of  $H_2$ . Consequently, on-board  $H_2$  production from liquid fuels as an effective option is widely investigated (Agrell *et al.*, 2003). Methanol has been identified as a prominent liquid fuel to produce  $H_2$  because it has a low boiling point, a high hydrogen to carbon ratio, and no strong C–C bonds (Huang *et al.*, 2009). Thus, it is easily reformed at a relatively low temperature using either steam or oxygen. Moreover, this reforming process reduces chances of coke formation during the reaction (Agrell *et al.*, 2003). Hydrogen can be produced from methanol by several different catalytic processes: (i) partial oxidation, (ii) steam reforming, and (iii) autothermal steam reforming. Partial oxidation of methanol (POM, Eq. (1)) is an exothermic reaction with a high reaction rate, however, the important drawback of POM is the formation of hot spots, resulting in sintering and decreasing of catalyst activity (Alejo *et al.*, 1997; Velu *et al.*, 2001; Papavasiliou *et al.*, 2004). Steam reforming of methanol (SRM, Eq. (2)) is an endothermic reaction which provides high  $H_2$  concentration. Unfortunately, SRM processes involve slow heat transfer in the catalytic bed, causing slow response start-up (Alejo *et al.*, 1997; Papavasiliou *et al.*, 2004). A third process which is an attractive and promising way for  $H_2$  production is autothermal steam reforming of methanol (ASRM, Eq. (3)), also known as oxidative reforming of methanol (OSRM). The ASRM process is a combination of POM and SRM (Patel and Pant, 2007), in which methanol and steam are supplied simultaneously with oxygen to the reactor system. The overall ASRM reaction is thermal-neutral or only moderately exothermic because the exothermic oxidation of POM supplies energy for the endothermic reforming of SRM (Brown, 2001; Reitz *et al.*, 2001). More importantly, the ASRM process generates low carbon

monoxide yield and high H<sub>2</sub> concentration with a high reaction rate (Pérez-Hernández *et al.*, 2007).



Copper-based catalysts are commonly employed for ASRM (Huang and Wang, 1986; Huang and Chren, 1988). Velu *et al.* (2000) reported highly selective hydrogen production via ASRM over CuZnAl(Zr)-oxide catalysts derived from hydroxycarbonate precursors containing hydrotalcite/aurichalcite phase. Shan *et al.* (2004) prepared Ce<sub>0.9</sub>Cu<sub>0.1</sub>O<sub>Y</sub> catalysts by complexation–combustion methods for ASRM and found 85% methanol conversion with 90% H<sub>2</sub> yield was obtained at 240 °C. Turco *et al.* (2007) studied ASRM reaction over Cu/ZnO/Al<sub>2</sub>O<sub>3</sub> catalysts derived from layered double hydroxide (LDH) precursors and concluded that the catalytic performance for ASRM depends on the composition of the catalysts. Murcia-Mascaros *et al.* (2001) synthesized CuZnAl catalysts for ASRM derived from hydrotalcite-like precursors, reporting methanol conversion of 73% with 67% H<sub>2</sub> selectivity and no CO selectivity. They also found Cu<sub>2</sub>O species on the active catalyst surface during the ASRM reaction. Pérez-Hernández *et al.* (2007) reported that catalysts with 2 and 6 wt% of Cu supported on CeO<sub>2</sub> exhibit high activity for H<sub>2</sub> production via ASRM with almost 100% methanol conversion for both catalysts. The presence of CeO<sub>2</sub> as a support material in Cu-based catalysts can promote the catalytic performance for SRM and ASRM reactions due to its redox cycle between Ce<sup>4+</sup> and Ce<sup>3+</sup>, leading to high oxygen storage capacity with reversible addition and removal of oxygen in its fluorite structure, and which results in the presence of highly active oxygen (Shan *et al.*, 2004; Patel and Pant, 2006; Srisiriwat *et al.*, 2009). It is also known that the incorporation of zirconia (ZrO<sub>2</sub>) into CeO<sub>2</sub> effectively improves oxygen storage capacity of CeO<sub>2</sub>, redox activity, thermal stability, and metal dispersion causing better catalytic performance (Roh *et al.*, 2004; Srisiriwat *et al.*, 2009). Furthermore, a mesoporous support structure with high surface area and uniform pores has facilitated good properties for various metals or catalytic active species, favorably influencing the

performance of the catalytic system (Ceika, 2003; Calles *et al.*, 2009; Eswaramoorthi and Dalai, 2009). Although, many researchers have studied on ASRM reaction over Cu-based catalysts, up-to-date, there were no reports indicating the use of both high surface area mesoporous CeO<sub>2</sub> and CeO<sub>2</sub>-ZrO<sub>2</sub> support prepared via nanocasting process with Cu catalyst for ASRM reaction. In this work, the catalytic performance and stability for the ASRM reaction were thus investigated for high surface area Cu-loaded mesoporous CeO<sub>2</sub> and Cu-loaded mesoporous CeO<sub>2</sub>-ZrO<sub>2</sub> catalysts synthesized via a nanocasting technique, followed by the deposition-precipitation (DP) method. The effects of operating variables, viz. % Cu content, reaction temperature, H<sub>2</sub>O/CH<sub>3</sub>OH molar ratios, and reaction time, were studied. Moreover, the characteristics of the catalysts after ASRM reaction were characterized using various analytical techniques.

## 6.3 Experimental

### 6.3.1 Chemicals

Fumed silica (SiO<sub>2</sub>, 99.8%, Nippon Aerosil, Japan), triethanolamine (TEA, QRĕc chemical, Thailand), ethylene glycol (EG, 99%, J.T. Baker, USA), HP grade nitrogen (N<sub>2</sub>, 99.98% purity, Thai Industrial Gases Public Company Limited (TIG), Thailand), acetonitrile (CH<sub>3</sub>CN, 99.9%, Labscan, Thailand), cetyltrimethylammonium bromide (CTAB, 96.0%, Fluka, Germany), cerium(III) nitrate hexahydrate (Ce(NO<sub>3</sub>)<sub>3</sub>.6H<sub>2</sub>O, 99%, Sigma-Aldrich, Germany), zirconium oxide chloride octahydrate (ZrOCl<sub>2</sub>.8H<sub>2</sub>O, 99.9%, Merck, Germany), copper(II) nitrate trihydrate (Cu(NO<sub>3</sub>)<sub>2</sub>.3H<sub>2</sub>O, 99.5%, Merck, Germany), ethanol (CH<sub>3</sub>CH<sub>2</sub>OH, 99.9%, Labscan, Thailand), sodium hydroxide (NaOH, 99%, Labscan, Thailand), sodium carbonate (Na<sub>2</sub>CO<sub>3</sub>, 99.8%, Ajax, Thailand), and methanol (CH<sub>3</sub>OH, 99.9%, Labscan, Thailand) were used without further purification.

### 6.3.2 Catalyst Preparation

Following Wongkasemjit's synthetic method (Phiriyawirut *et al.*, 2003) to prepare silatrane, a mixture consisting of 0.1 mol fumed silica, 0.125 mol TEA, and 100 ml EG was refluxed at 200 °C under nitrogen atmosphere for 12 h in an

oil bath. The excess EG was then removed under vacuum at 110 °C to obtain a crude brown solid. The product was washed with acetonitrile, followed by vacuum-drying to obtain white silatrane for use as a silica source for MCM-48 preparation. The synthesis of MCM-48 followed Longloilert's synthetic method (Longloilert *et al.*, 2011), using a molar composition of SiO<sub>2</sub>:CTAB:NaOH:H<sub>2</sub>O = 1:0.3:0.5:62. CTAB as surfactant was dissolved in aqueous solution containing 2 M NaOH. The mixture was continuously stirred at 50 °C until the solution was homogeneously dissolved, after which silatrane was added to the mixture with constant stirring at 50 °C for 1 h. Then, the mixture was transferred to a Teflon-lined stainless steel autoclave and treated at 140 °C for 16 h. The obtained solid product was collected by filtration, dried, and calcined at 550 °C for 6 h to remove all organic components.

Mesoporous CeO<sub>2</sub> and CeO<sub>2</sub>-ZrO<sub>2</sub> supports were synthesized via the nanocasting method by using MCM-48 as template (Jampa *et al.*, 2017). For preparation of mesoporous CeO<sub>2</sub>, 50 wt% of Ce(NO<sub>3</sub>)<sub>3</sub>.6H<sub>2</sub>O as a precursor was mixed with MCM-48 in 5 ml of ethanol and continuously stirred for 30 mins. Ce(NO<sub>3</sub>)<sub>3</sub>.6H<sub>2</sub>O and ZrOCl<sub>2</sub>.8H<sub>2</sub>O in a molar ratio of Ce:Zr = 0.75:0.25, used as precursors to synthesize mesoporous CeO<sub>2</sub>-ZrO<sub>2</sub>, were dissolved in 5 ml of ethanol and then MCM-48 was directly added to the mixture, with constant stirring for 4 h. Afterward, ethanol was removed by evaporation in an oven at 100 °C. The obtained solid product was calcined at 550 °C for 6 h. The template was removed by stirring 3 times with 2 M NaOH at 50 °C. The resulting product was washed with deionized water until neutral and dried at 80 °C overnight.

Cu loaded mesoporous CeO<sub>2</sub> (Cu-C) and Cu loaded mesoporous CeO<sub>2</sub>-ZrO<sub>2</sub> supports (Cu-CZ) were prepared by the deposition-precipitation (DP) technique, initially, Cu(NO<sub>3</sub>)<sub>2</sub>.3H<sub>2</sub>O (Cu loadings of 1, 3, 5, 7, 9, and 12% by wt.) was dissolved in aqueous solution [30]. Mesoporous support was then added to the aqueous solution of Cu(NO<sub>3</sub>)<sub>2</sub>.3H<sub>2</sub>O under constant stirring at room temperature for 1 h. Na<sub>2</sub>CO<sub>3</sub> solution was added dropwise to the mixture until its pH ≈ 7 in order to precipitate the Cu ions. Next, the mixture was heated to 80°C and then aged for another hour. The resulting solid was filtered, washed with warm distilled water and dried at 80°C

overnight. Eventually, the product was calcined in air at 500 °C for 6 h to obtain Cu-C and Cu-CZ catalysts.

### 6.3.3 Catalyst Characterization

The specific surface area of catalysts was determined by the Brunauer-Emmett-Teller (BET) method by N<sub>2</sub> adsorption-desorption at -196 °C using a Quantachrome Autosorb-1. Wide angle x-ray diffraction (WAXD) patterns of catalysts were obtained by a Rigaku Smartlab<sup>®</sup> diffractometer with a scanning speed of 1°min<sup>-1</sup> and CuK $\alpha$  radiation ( $\lambda$ = 1.5406 Å) in a range of  $2\theta = 20$ –80°. The crystallite size of the catalysts was also calculated by applying the Debye–Scherrer equation. X-ray photoelectron spectra of catalysts were collected with a XPS Kratos AXIS Ultra DLD spectrometer using monochromatic AlK $\alpha$  X-ray radiation (15 kV) at a pressure lower than  $5 \times 10^{-7}$  Torr. All the binding energy (BE) values were calibrated using C1s peak fixed at 284.6 eV. The chemical composition and oxidation states at the catalyst surface were obtained. Temperature-programmed oxidation (TPO) was used to measure the amount of carbon formation on the catalysts. About 60 mg of sample was contained in a quartz tube reactor. The sample was oxidized by 5.27% O<sub>2</sub>/He (v/v) at a heating rate of 10 °C/min with a gas flow rate of 30 ml/min.

### 6.3.4 Catalytic Activity

The catalytic activity measurement for oxidative steam reforming of methanol was performed in a fixed-bed reactor. 100 mg of catalyst was contained in the reactor and fixed in the middle of the reactor by quartz wool. The catalytic test was carried out over a temperature range from 200 to 400 °C at atmospheric pressure. The catalyst temperature was controlled by a thermocouple directly contacting with the reactor. The mixture of distilled water and methanol was pumped consistently by a syringe pump at a rate of 1.5 ml/h to a vaporizer set at 160 °C to generate a vapor mixture of methanol and steam. The mixture vapor was mixed with He carrier gas (45 ml/min) and oxygen (5 ml/min) before being fed into the catalytic reactor. The outlet stream passed through condenser cooled by ice bath to condense some liquid. The effluent gases from the reactor (e.g. H<sub>2</sub>, CO<sub>2</sub> and CO) were analyzed by a Hewlett

Packard 5890 series II gas chromatograph equipped with a thermal conductivity detector (TCD) and carbosphere (80/100 mesh) column (10 ft x 1/8 inch). The effect of % Cu loading from 1 to 12 %wt. on the ASRM reaction was studied in this experiment. The H<sub>2</sub>O/CH<sub>3</sub>OH molar ratios were varied from 1/1 to 3/1. Moreover, the stability of the catalysts was tested for 168 h.

## 6.4 Results and Discussion

### 6.4.1 Textural and Structural Properties

The BET specific surface areas of all fresh and spent catalysts, measured by N<sub>2</sub> adsorption at -196 °C, are listed in Table 6.1. Mesoporous CeO<sub>2</sub> and mesoporous CeO<sub>2</sub>-ZrO<sub>2</sub> supports each showed large specific surface areas around 260 m<sup>2</sup>g<sup>-1</sup>, and still retained some order from the MCM-48 template (Jampa *et al.*, 2017). The addition of Cu content onto both mesoporous supports causes a decrease in the specific surface area of the catalysts due to the presence of small CuO crystallites in the pores of the mesoporous supports, obstructing the adsorption of N<sub>2</sub> during the BET experiment (Araujo *et al.*, 2012). Interestingly, a slight decrease of specific surface area of the catalysts did show no effect on the catalytic activity. Furthermore, the specific surface areas of all catalysts after ASRM process decreased, as compared to the fresh catalysts, because of the phenomenon of the metal sintering or agglomeration from high reaction temperature and deposition of carbonaceous species, such as amorphous carbon and carbonate species (Avgouropoulos and Ioannides, 2006; Djinovic *et al.*, 2010).

The XRD patterns of all fresh and spent catalysts observed in the range of 20° and 80° are illustrated in Figure 6.1. All fresh Cu-C and Cu-CZ catalysts showed the characteristic diffraction peaks at 28.51°, 33.12°, 47.78°, 56.75°, 69.61°, 76.94° and at 28.77°, 33.28°, 47.98°, 56.84°, 69.98°, 77.28°, as shown in Figure 6.1A and 6.1B, respectively. These peaks which correspond to {1 1 1}, {2 0 0}, {2 2 0}, {3 1 1}, {4 0 0}, and {3 3 1} planes, respectively, indicated the fluorite-type cubic crystal structure of the CeO<sub>2</sub> phase (Reddy *et al.*, 2005; Zhou *et al.*, 2005). The diffraction peaks of all fresh Cu-CZ catalysts appeared at slightly higher 2θ than those of all fresh

Cu-C catalysts due to the incorporation of the smaller  $Zr^{4+}$  cations (0.084 nm) to  $Ce^{4+}$  cations (0.097 nm) (Rao and Sahu, 2001; Reddy *et al.*, 2005). Perez-Hernandez *et al.* (2011) also showed XRD patterns of both Ni/CeO<sub>2</sub> and Ni/CeO<sub>2</sub>-ZrO<sub>2</sub>, indicating that the diffraction peaks of the catalysts were shifted to the higher  $2\theta$  when adding the amount of ZrO<sub>2</sub>. Figures 6.1C and 6.1D presenting the XRD patterns of Cu-C and Cu-CZ catalysts after ASRM reaction showed that the diffraction peaks of all catalysts still appeared at the same  $2\theta$  position as fresh catalysts from which we can postulate that Cu-C and Cu-CZ catalysts still retain fluorite-type cubic crystal structure of the CeO<sub>2</sub> phase after the ASRM reaction. Interestingly, all fresh and spent catalysts, except 12%Cu-C and 12%Cu-CZ, exhibited no diffraction peaks from CuO crystallites possibly due to a high dispersion of CuO, or the formation of an interfacial solid solution between CuO and support (Delimaris and Ioannides, 2009), or that the CuO crystallites were very small (Shan *et al.*, 2003), resulting in a good catalytic performance for ASRM reaction due to no agglomeration of CuO. However, fresh and spent catalysts of 12%Cu-C and 12%Cu-CZ presented very small diffraction peaks of Cu species, as the result of agglomeration of Cu species.

Both crystallite sizes of ceria and unit cell parameters of fresh and spent catalysts are summarized in Table 6.2. The crystallite sizes of ceria of fresh and spent catalysts are calculated from the diffraction peak broadening at  $\{1\ 1\ 1\}$  plane by using Scherrer's equation. At 1, 3, 5, 7, 9, and 12 wt% Cu contents of the fresh Cu-C and Cu-CZ catalysts, the crystallite sizes of ceria are very similar while those of ceria in the spent catalysts slightly increase after ASRM reaction due to the occurrence of catalyst aggregation, as mentioned previously. Moreover, the unit cell parameters of the fresh and the spent catalysts evaluated from the diffraction peak at  $\{1\ 1\ 1\}$  plane using Bragg's equation also indicate no significant differences, consistent with the fact that negligible change is seen in crystallite sizes of ceria after ASRM reaction.

## 6.4.2 Evaluation of Catalytic Performance for ASRM Reaction

### 6.4.2.1 *Effect of Reaction Temperature*

The temperature dependence of catalytic activity for ASRM over Cu-C and Cu-CZ catalysts at various % Cu contents is illustrated in Figure 6.2. For all catalysts, the major produced gases are H<sub>2</sub>, CO<sub>2</sub>, and CO. The Cu-C catalysts



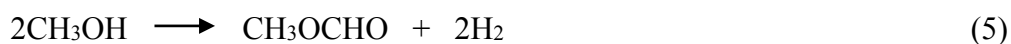
with 5, 7, 9 and 12 wt% Cu loadings provide high methanol conversion more than 80% at the beginning of reaction temperature while the 9%Cu-CZ catalyst achieves more than 90% methanol conversion at 200 °C. From Figure 6.2A and 6.2B, it can be clearly seen that the ASRM reaction is favored by increase of the reaction temperature. The %H<sub>2</sub> yield, as shown in Figure 6.2C and 6.2D, corresponds to methanol conversion in a temperature range from 200° to 400 °C, giving a maximum % H<sub>2</sub> yield of 60%. Figures 2E and 2F exhibit the selectivity of ASRM reaction toward H<sub>2</sub> and CO. It is found that the 9%Cu-C and the 9%Cu-CZ give H<sub>2</sub> selectivity around 60% over the whole range of reaction temperatures. In term of CO selectivity, it can be seen that CO production from ASRM reaction over 9%Cu-C and 9%Cu-CZ catalysts is quite low and H<sub>2</sub> and CO<sub>2</sub> are the primary products. However, CO formation increases with increasing temperature, as shown in Figure 6.2E and 6.2F, because CO is generated at high temperature by the reverse water-gas shift reaction (RWGS, Eq. (4)) (Breen and Ross, 1999).



#### 6.4.2.2 Effect of %Cu Content

Various Cu loadings also have an effect on catalyst behavior for the ASRM reaction, as presented in Figure 6.2A and 6.2B. The methanol conversion increases with increasing the Cu content up to 9 wt% and then decreases upon increasing the Cu content to 12 wt% because of the agglomeration of Cu species at 12 wt% Cu content which is confirmed by XRD results in Figure 6.1, causing the decrease of active sites on catalyst. Both 9%Cu-C and 9%Cu-CZ provide the highest methanol conversion and H<sub>2</sub> yield, as compared to the other catalysts. Sa *et al.* (2010) explained that high catalytic performance of Cu-based catalysts was a function of Cu dispersion, surface area, and small particle sizes. Moreover, Wang *et al.* (2005) reported that the catalytic activity for ASRM was improved by the appearance of a catalyst-support interaction, specifically the formation of interfacial active centers between CuO and the oxygen vacancy sites of CeO<sub>2</sub>.

During the ASRM reaction involving POM, Eq. (1) and SRM, Eq. (2) reactions, it is also found that methanol can interact with the -OH groups of CeO<sub>2</sub> and CeO<sub>2</sub>-ZrO<sub>2</sub> supports, having oxygen vacancy sites, to generate methoxide and water molecules (Velu *et al.*, 2000). The adsorbed methoxide species are dehydrogenated into formaldehyde and hydrogen. Then, formaldehyde is hydrolyzed to form methanol and formic acid, which subsequently decomposes into H<sub>2</sub> and CO<sub>2</sub>. Thus, the important role of CuO is to adsorb H<sub>2</sub> generated on the surface of the support and subsequent release desorbed H<sub>2</sub> into the system (Velu *et al.*, 2000). Breen *et al.* (1999) suggested the sequence of the reactions, as presented in Eq. (5), (6), and (7), over Cu-based catalysts:



#### 6.4.2.3 Effect of H<sub>2</sub>O/CH<sub>3</sub>OH Molar Ratio

The influence of H<sub>2</sub>O/CH<sub>3</sub>OH (W/M) molar ratios of 1/1, 2/1 and 3/1 on the catalytic performance for the ASRM reaction over 9%Cu-C and 9%Cu-CZ catalysts is shown in Figure 6.3. This study was carried out over a temperature range from 200 to 400°C using a constant feed of O<sub>2</sub> at 5 ml/min. It can be seen from Figure 6.3 that the catalytic performance in terms of methanol conversion and H<sub>2</sub> yield at all H<sub>2</sub>O/CH<sub>3</sub>OH molar ratios increases weakly with increasing reaction temperature. In addition, the catalytic activity is also enhanced with increase of the H<sub>2</sub>O/CH<sub>3</sub>OH molar ratio from 1/1 to 2/1 and 1/1 to 3/1 because the increase of steam level can importantly promote the SRM reaction which is an endothermic component of the ASRM reaction (Velu *et al.*, 2001; Pojanavaraphan *et al.*, 2012). At a H<sub>2</sub>O/CH<sub>3</sub>OH molar ratio of 2/1, 9%Cu-C and 9%Cu-CZ catalysts exhibit the highest catalytic performance over the whole range of reaction temperatures when compared to H<sub>2</sub>O/CH<sub>3</sub>OH molar ratios of 1/1 and 3/1. The decrease of catalytic activity after increasing the H<sub>2</sub>O/CH<sub>3</sub>OH molar ratio to 3/1 can be explained by the formation of carbonate, formate and hydroxyl species, which are formed during the ASRM reaction at high levels of steam. These species can block and deactivate the catalytic sites,

causing a reduction in catalytic performance (Datel and Haruta, 2001; Pojanavaraphan *et al.*, 2015).

#### 6.4.2.4 Stability of Catalysts

The stabilities of both 9%Cu-C and 9%Cu-CZ catalysts were studied during the ASRM reaction over a period of 168 h, at reaction temperatures of 350° and 300 °C, respectively, using a H<sub>2</sub>O/CH<sub>3</sub>OH molar ratio of 2/1 and a constant O<sub>2</sub> feed at 5 ml/min. The time dependence of the catalytic efficiency is illustrated in Figure 6.4, showing that the methanol conversion and the H<sub>2</sub> yield of both catalysts (Figure 6.4A and 6.4B) gradually decreased from around 95 to 75% and around 55 to 35%, respectively. As a result, we infer that coke formation and agglomeration of the catalysts during the ASRM reaction interrupts the active sites of the catalyst surfaces, causing the reduction of the catalyst performance (Patel and Pant, 2006; Pojanavaraphan *et al.*, 2014). Interestingly, the 9%Cu-CZ catalyst exhibits lower CO selectivity than that of the 9%Cu-C catalyst. This phenomenon can be explained on the basis that the incorporation of ZrO<sub>2</sub> into the catalyst support can enhance H<sub>2</sub> production but with lower CO selectivity (Velu *et al.*, 2000; Perez-Hernandez *et al.*, 2008). The previous studies reported that the addition of ZrO<sub>2</sub> into CeO<sub>2</sub> improved not only the redox property and thermal stability but also oxygen storage capacity, resulting in a better performance in CO oxidation reaction which caused a low CO level during ASRM reaction (Biswas and Kunzru, 2008; Srisiriwat *et al.*, 2009). Furthermore, it can be observed that the increase in CO selectivity of the 9%Cu-C shows an initial steep rise to a plateau and later a second steep rise to a second plateau. Purnama *et al.* (2004) reported that the level of CO formation in methanol–steam reforming over copper-based catalysts can be influenced by particle size of catalyst. The lower levels of CO can be achieved by using a very small particle size, where intraparticle diffusion limitation disappears. So, the obvious increase in CO selectivity of the spent 9%Cu-C can be explained by agglomeration of catalyst during ASRM reaction, causing the formation of much larger Cu particle size about 19.2103 nm, calculating Scherrer's equation.

To confirm the agglomeration of the 9%Cu-C and 9%Cu-CZ catalysts after the ASRM stability tests, XRD patterns of each catalyst were obtained

and are shown in Figure 6.5. The spent 9%Cu-C and 9%Cu-CZ catalysts exhibit characteristic diffraction peaks at the same positions as for the fresh catalysts, corresponding to the fluorite-type cubic crystal structure of the CeO<sub>2</sub> phase. Nevertheless, the crystallite sizes of ceria in the spent catalysts after 168 h ASRM operation, as shown in Table 6.2, evidently increase and diffraction peaks of Cu species, such as CuO, Cu<sub>2</sub>O, and metallic Cu are clearly present, as a result of aggregation and/or sintering of catalysts during the ASRM reaction. During ASRM reaction, Cu<sup>2+</sup> could be reduced to Cu<sup>1+</sup> and Cu<sup>0</sup>, and Cu<sup>1+</sup> and Cu<sup>0</sup> could also be oxidized to Cu<sup>2+</sup> by synergistic function between Cu<sup>2+</sup>/Cu<sup>+</sup> and Ce<sup>4+</sup>/Ce<sup>3+</sup> (Shan *et al.*, 2004). There are many studies confirming that both Cu<sup>2+</sup> and its reduced form can show good activity for ASRM. Perez-Hernandez *et al.* (2007) studied catalytic performance of Cu/CeO<sub>2</sub> catalyst at various Cu contents for ASRM reaction. Their prepared catalysts were reduced with a H<sub>2</sub> (5%)/He stream at 330 °C for 1 h before an activity test. They found that at higher temperatures the 6Cu/CeO<sub>2</sub> catalyst had the best performance towards H<sub>2</sub>. It was proved that the reduced form of copper was also active for ASRM reaction. Udani *et al.* (2009) studied steam reforming (SRM) and oxidative steam reforming of methanol (OSRM or ASRM) reactions over CuO-CeO<sub>2</sub> catalysts synthesized by the coprecipitation method. Without reducing the CuO-CeO<sub>2</sub> catalysts before activity testing, they found that 70 wt% of CuO CeO<sub>2</sub> catalyst exhibited the highest activity in the temperature range of 160-300 °C for both SRM and ASRM. It can be indicated that CuO is an important, active form for ASRM reaction.

In addition, the significant decrease in the BET specific surface area of the spent 9%Cu-C and 9%Cu-CZ catalysts from 206 to 64 m<sup>2</sup>g<sup>-1</sup> and 165 to 78 m<sup>2</sup>g<sup>-1</sup>, respectively, is evidence that supports the aggregation of the spent catalysts during ASRM stability tests.

To evaluate the formation of coke or other carbonaceous on the spent catalysts during stability tests TPO measurements were performed. The TPO profiles of the spent 9%Cu-C and 9%Cu-CZ catalysts after the stability testing for 168 h are shown in Figure 6.6. It can be seen that the spent 9%Cu-C catalyst presents oxidation peaks at 207° and 296 °C, whereas the oxidation peaks of the spent 9%Cu-CZ catalyst appear at 266° and 484 °C. Two distinct oxidation peaks indicate two

different types of coke or carbonaceous species which are deposited on the surface of the spent catalysts. The oxidation peaks at low temperatures of 207°, 266, and 296 °C are assigned to the oxidation of the poorly polymerized coke deposited on the catalyst particles while the other oxidation peak at a high temperature of 484 °C is assigned to highly polymerized coke deposited near the catalyst-support interface (Luengnaruemitchai and Kaengsilalai, 2008). In this work, the amounts of coke deposited on the spent 9%Cu-C and 9%Cu-CZ catalysts are 0.39 and 0.29 wt%, respectively, as shown in Table 6.3. Carbon monoxide formation during the reaction is another important source of coke formation (Faungnawakij *et al.*, 2006). The amount of coke on the spent 9%Cu-C is slightly higher than that on the spent 9%Cu-CZ because the 9%Cu-C catalyst shows higher CO selectivity during the ASRM reaction. From the TPO results, it is confirmed that the catalytic activities of both 9%Cu-C and 9%Cu-CZ catalysts are indeed inhibited by coke formation.

Moreover, TEM images were investigated to confirm coke formation on the spent catalysts. TEM images of the fresh and the spent 9%Cu-C and 9%Cu-CZ catalysts after the stability testing for 168 h are shown in Figure 6.7. The fresh 9%Cu-C and 9%Cu-CZ catalysts show the long-range three-dimensional order structure whereas the spent 9%Cu-C and 9%Cu-CZ catalysts exhibit much less order structure due to the coke formation after stability testing on catalysts. The TEM images of both spent catalysts obviously indicate a large amount of agglomerated carbon, causing the decrease of catalytic activity.

Finally, the XPS technique was used to establish the oxidation states of Cu species located on the catalyst surface. Figure 6.8 shows XPS spectra of fresh and spent 9%Cu-C and 9%Cu-CZ catalysts. All catalysts exhibit a prominent peak of Cu 2p<sub>3/2</sub> at a binding energy in the range of 932.2-933.1 eV which is characteristic of reduced Cu species (Cu<sub>2</sub>O or Cu), and a Cu 2p<sub>1/2</sub> peak at around 952.8 eV. In addition, shake-up peaks of both fresh and spent catalysts at 937.4-947.9 eV indicate the presence of Cu<sup>2+</sup> species (CuO) on the catalyst surface (Kundakovic and Flytzani-Stephanopoulos, 1998; Zhang *et al.*, 2014; Jeong *et al.*, 2015). From the XPS result, it can be confirmed that both 9%Cu-C and 9%Cu-CZ catalysts contain various Cu species, consistent with the XRD results presented in Figure 6.5.

## 6.5 Conclusions

In this work, Cu loaded mesoporous CeO<sub>2</sub> and Cu loaded mesoporous CeO<sub>2</sub>-ZrO<sub>2</sub> catalysts with high surface area, successfully prepared via nanocasting and deposition-precipitation techniques using MCM-48 as a hard template, were investigated for H<sub>2</sub> production by autothermal steam reforming of methanol (ASRM). The XRD patterns confirm high dispersion of Cu species on the mesoporous CeO<sub>2</sub> and CeO<sub>2</sub>-ZrO<sub>2</sub> supports. Both catalysts have large BET specific surface areas of 259 and 256 m<sup>2</sup>g<sup>-1</sup>, respectively. Generally, higher Cu contents in catalysts can increase catalytic activity of the ASRM reaction. However, excess Cu content loaded on the supports, 12%Cu-C and 12%Cu-CZ, can cause the agglomeration of Cu species, leading to a significant decrease in catalyst surface area and active sites, and a decrease in catalytic performance. Among all synthesized catalysts, 9%Cu-C and 9%Cu-CZ catalysts exhibit the best catalytic behavior. Methanol conversion of 100% and H<sub>2</sub> yield of 60% are achieved at 350 °C for 9%Cu-C and at 300 °C for 9%Cu-CZ catalysts in the presence of O<sub>2</sub> at 5 ml/min with H<sub>2</sub>O/CH<sub>3</sub>OH molar ratios of 2/1. Furthermore, 9%Cu-C and 9%Cu-CZ catalysts generate H<sub>2</sub> yields of around 34% and 36%, respectively, after stability testing for 168 h with low CO selectivity. The introduction of ZrO<sub>2</sub> into the catalyst support in 9%Cu-CZ enhances the catalytic activity albeit with very low CO selectivity compared to 9%Cu-C. Promisingly, the high performance ASRM reaction over 9%Cu-C and 9%Cu-CZ catalysts can be utilized for on-board hydrogen production for polymer electrolyte fuel-cells (PEMFC) to generate energy for vehicles.

## 6.6 Acknowledgements

This research is financially supported by the Grant for International Research Integration: Chula Research Scholar, Ratchadaphiseksompote Endowment Fund, Chulalongkorn University, Thailand, Development and Promotion of Science and Technology Talents Project.

## 6.7 References

- Agrell, J., Boutonnet, M., and Fierro, J.L.G. (2003) Production of hydrogen from methanol over binary Cu/ZnO catalysts Part II. Catalytic activity and reaction pathways. Applied Catalysis A, 253, 213-223.
- Alejo, L., Lago, R., Pefia, M.A., and Fierro, J.L.G. (1997) Partial oxidation of methanol to produce hydrogen over Cu-Zn-based catalysts. Applied Catalysis A, 162, 281-297.
- Araujo, V.D., Bellido, J.D.A., Bernardi, M.I.B., Assaf, J.M., and Assaf, E.M. (2012) CuO-CeO<sub>2</sub> catalysts synthesized in one-step: Characterization and PROX performance. International Journal of Hydrogen Energy, 37, 5498-5507.
- Avgouropoulos, G. and Ioannides, T. (2006) Effect of synthesis parameters on catalytic properties of CuO-CeO<sub>2</sub>. Applied Catalysis B, 67, 1-11.
- Biswas, P. and Kunzru, D. (2008) Oxidative steam reforming of ethanol over Ni/CeO<sub>2</sub>-ZrO<sub>2</sub> catalyst. Chemical Engineering Journal, 136, 41-49.
- Breen, J.P. and Ross, J.R.H. (1999) Methanol reforming for fuel-cell applications: development of zirconia-containing Cu-Zn-Al catalysts. Catalysis Today, 51, 521-533.
- Brown, L.F. (2001) A comparative study of fuels for on-board hydrogen production for fuel-cell-powered automobiles. International Journal of Hydrogen Energy, 26, 381-397.
- Cacciola, G., Antonucci, V., and Freni, S. (2001) Technology up date and new strategies on fuel cells. Journal of Power Sources, 100, 67-79.
- Calles, J.A., Carrero, A., and Vizcaíno, A.J. (2009) Ce and La modification of mesoporous Cu-Ni/SBA-15 catalysts for hydrogen production through ethanol steam reforming. Microporous Mesoporous Materials, 119, 200-207.
- Cejka, J. (2003) Organized mesoporous alumina: synthesis, structure and potential in catalysis. Applied Catalysis A, 254, 327-338.
- Cleghorn, S.J.C., Ren, X., Springer, T.E., Wilson, M.S., Zawodzinski, C., Zawodzinski, T.A., and Gottesfeld, S. (1997) PEM fuel cells for transportation and stationary power generation applications. International Journal of Hydrogen Energy, 22, 1137-1144.

- Date1, M. and Haruta, M. (2001) Moisture effect on CO oxidation over Au/TiO<sub>2</sub> catalyst. Journal of Catalysis, 201, 221-224.
- Delimaris, D. and Ioannides, T. (2009) VOC oxidation over CuO-CeO<sub>2</sub> catalysts prepared by a combustion method. Applied Catalysis B, 89, 295-302.
- Djinovic, P., Batista, J., Cehic, B., and Pintar, A. (2010) Utilization of high specific surface area CuO-CeO<sub>2</sub> catalysts for high temperature processes of hydrogen production: Steam re-forming of ethanol and methane dry re-forming. Journal of Physical Chemistry A, 114, 3939-3949.
- Eswaramoorthi, I. and Dalai, A.K. (2009) A comparative study on the performance of mesoporous SBA-15 supported Pd-Zn catalysts in partial oxidation and steam reforming of methanol for hydrogen production. International Journal of Hydrogen Energy, 34, 2580-2590.
- Faungnawakij, K., Kikuchi, R., and Eguchi, K. (2006) Thermodynamic evaluation of methanol steam reforming for hydrogen production. Journal of Power Sources, 161, 87-94.
- Grigoriev, S.A., Poremsky, V.I., and Fateev, V.N. (2006) Pure hydrogen production by PEM electrolysis for hydrogen energy. International Journal of Hydrogen Energy, 31, 171-175.
- Hotza, D. and Diniz da Costa, J.C. (2008) Fuel cells development and hydrogen production from renewable resources in Brazil. International Journal of Hydrogen Energy, 33, 4915-4935.
- Huang, G., Liaw, B.J., Jhang, C.J., and Chen, Y.Z. (2009) Steam reforming of methanol over CuO/ZnO/CeO<sub>2</sub>/ZrO<sub>2</sub>/Al<sub>2</sub>O<sub>3</sub> catalysts. Applied Catalysis A, 358, 7-12.
- Huang, T.J. and Chren, S.L. (1988) Kinetics of partial oxidation of methanol over a copper-zinc catalyst. Applied Catalysis, 40, 43-52.
- Huang, T.J. and Wang, S.W. (1986) Hydrogen production via partial oxidation of methanol over copper-zinc catalysts. Applied Catalysis, 24, 287-297.
- Jampa, S., Wangkawee, K., Tantisriyanurak, S., Changpradit, J., Jamieson, A.M., Chaisuwan, T., Luengnaruemitchai, A., and Wongkasemjit, S. (2017) High performance and stability of copper loading on mesoporous ceria catalyst for



- preferential oxidation of CO in presence of excess of hydrogen. International Journal of Hydrogen Energy, 42, 5537-5548.
- Jeong, D.W., Jang, W.J., Na, H.S., Shim, J.O., Jha, A., and Roh, H.S. (2015) Comparative study on cubic and tetragonal Cu-CeO<sub>2</sub>-ZrO<sub>2</sub> catalysts for water gas shift reaction. Journal of Industrial and Engineering Chemistry, 27, 35-39.
- Kundakovic, L. and Flytzani-Stephanopoulos, M. (1998) Reduction characteristics of copper oxide in cerium and zirconium oxide systems. Applied Catalysis A, 171, 13-29.
- Longloilert, R., Chaisuwan, T., Luengnaruemitchai, A., and Wongkasemjit, S. (2011) Synthesis of MCM-48 from silatrane via sol-gel process. Journal of Sol-Gel Science and Technology, 58, 427-435.
- Luengnaruemitchai, A. and Kaengsilalai, A. (2008) Activity of different zeolite-supported Ni catalysts for methane reforming with carbon dioxide. Chemical Engineering Journal, 144, 96-102.
- Murcia-Mascaros, S., Navarro, R.M., Gomez-Sainero, L., Costantino, U., Nocchetti, M., and Fierro, J.L.G. (2001) Oxidative methanol reforming reactions on CuZnAl catalysts derived from hydrotalcite-like precursors. Journal of Catalysis, 198, 338-347.
- Papavasiliou, J., Avgouropoulos, G., and Ioannides, T. (2004) Production of hydrogen via combined steam reforming of methanol over CuO-CeO<sub>2</sub> catalysts. Catalysis Communications, 5, 231-235.
- Patel, S. and Pant, K.K. (2006) Activity and stability enhancement of copper–alumina catalysts using cerium and zinc promoters for the selective production of hydrogen via steam reforming of methanol. Journal of Power Sources, 159, 139-143.
- Patel, S. and Pant, K.K. (2007) Selective production of hydrogen via oxidative steam reforming of methanol using Cu-Zn-Ce-Al oxide catalysts. Chemical Engineering Science, 62, 5436-5443.
- Perez-Hernandez, R., Galicia, G.M., Anaya, D.M., Palacios, J., Angeles-Chavez, C., and Arenas-Alatorre, J. (2008) Synthesis and characterization of bimetallic

- Cu-Ni/ZrO<sub>2</sub> nanocatalysts: H<sub>2</sub> production by oxidative steam reforming of methanol. International Journal of Hydrogen Energy, 33, 4569-4576.
- Perez-Hernandez, R., Gutiérrez-Martínez, A., and Gutiérrez-Wing, C.E. (2007) Effect of Cu loading on CeO<sub>2</sub> for hydrogen production by oxidative steam reforming of methanol. International Journal of Hydrogen Energy, 32, 2888-2894.
- Perez-Hernandez, R., Gutierrez-Martinez, A., Palacios, J., Vega-Hernandez, M., and Rodriguez-Lugo, V. (2011) Hydrogen production by oxidative steam reforming of methanol over Ni/CeO<sub>2</sub>ZrO<sub>2</sub> catalysts. International Journal of Hydrogen Energy, 36, 6601-6608.
- Phiriyawirut, P., Magaraphan, R., Jamieson, A.M., and Wongkasemjit, S. (2003) Morphology study of MFI zeolite synthesized directly from silatrane and alumatrane via the sol-gel process and microwave heating. Microporous Mesoporous Materials, 64, 83-93.
- Pojanavaraphan, C., Luengnaruemitchai, A., and Gulari, E. (2012) Hydrogen production by oxidative steam reforming of methanol over Au/CeO<sub>2</sub> catalysts. Chemical Engineering Journal, 192, 105-113.
- Pojanavaraphan, C., Nakaranuwattana, W., Luengnaruemitchai, A., and Gulari, E. (2014) Effect of support composition and metal loading on Au/Ce<sub>1-x</sub>Zr<sub>x</sub>O<sub>2</sub> catalysts for the oxidative steam reforming of methanol. Chemical Engineering Journal, 240, 99-108.
- Pojanavaraphan, C., Satitthai, U., Luengnaruemitchai, A., and Gulari, E. (2015) Activity and stability of Au/CeO<sub>2</sub>-Fe<sub>2</sub>O<sub>3</sub> catalysts for the hydrogen production via oxidative steam reforming of methanol. Journal of Industrial and Engineering Chemistry, 22, 41-52.
- Purnama, H., Ressler, T., Jentoft, R.E., Soerijanto, H., Schlögl, R., and Schomäcker, R. (2004) CO formation/selectivity for steam reforming of methanol with a commercial CuO/ZnO/Al<sub>2</sub>O<sub>3</sub> catalyst. Applied Catalysis A, 259, 83-94.
- Rao, G. and Sahu, H. (2001) XRD and UV-Vis diffuse reflectance analysis of CeO<sub>2</sub>-ZrO<sub>2</sub> solid solutions synthesized by combustion method. Proceedings of the Indian Academy of Sciences, 113, 651-658.

- Reddy, B.M., Khan, A., and Lakshmanan, P. (2005) Structural characterization of nanosized CeO<sub>2</sub>-SiO<sub>2</sub>, CeO<sub>2</sub>-TiO<sub>2</sub>, and CeO<sub>2</sub>-ZrO<sub>2</sub> catalysts by XRD, Raman, and HREM techniques. Journal of Physical Chemistry B, 109, 3355-3363.
- Reitz, T.L., Lee, P.L., Czaplewski, K.F., Lang, J.C., Popp, K.E., and Kung, H.H. (2001) Time-Resolved XANES investigation of CuO/ZnO in the oxidative methanol reforming reaction. Journal of Catalysis, 199, 193-201.
- Roh, H.S., Potdar, H.S., and Jun, K.W. (2004) Carbon dioxide reforming of methane over co-precipitated Ni-CeO<sub>2</sub>, Ni-ZrO<sub>2</sub> and Ni-Ce-ZrO<sub>2</sub> catalysts. Catalysis Today, 93, 39-44.
- Sa, S., Silva, H., Brandao, L., Sousa, J.M., and Mendes, A. (2010) Catalysts for methanol steam reforming-A review. Applied Catalysis B, 99, 43-57.
- Shan, W., Feng, Z., Li, Z., Zhang, J., Shen, W., and Li, C. (2004) Oxidative steam reforming of methanol on Ce<sub>0.9</sub>Cu<sub>0.1</sub>O<sub>y</sub> catalysts prepared by deposition-precipitation, coprecipitation, and complexation-combustion methods. Journal of Catalysis, 228, 206-217.
- Shan, W., Shen, W., and Li, C. (2003) Structural characteristics and redox behaviors of Ce<sub>1-x</sub>Cu<sub>x</sub>O<sub>y</sub> solid solutions. Chemistry of Materials, 15, 4761-4767.
- Song, C. (2002) Fuel processing for low-temperature and high-temperature fuel cells Challenges, and opportunities for sustainable development in the 21st century. Catalysis Today, 77, 17-49.
- Srisiriwat, N., Therdthianwong, S., and Therdthianwong, A. (2009) Oxidative steam reforming of ethanol over Ni/Al<sub>2</sub>O<sub>3</sub> catalysts promoted by CeO<sub>2</sub>, ZrO<sub>2</sub> and CeO<sub>2</sub>-ZrO<sub>2</sub>. International Journal of Hydrogen Energy, 34, 2224-2234.
- Turco, M., Bagnasco, G., Cammarano, C., Senese, P., Costantino, U., and Sisani, M. (2007) Cu/ZnO/Al<sub>2</sub>O<sub>3</sub> catalysts for oxidative steam reforming of methanol: The role of Cu and the dispersing oxide matrix. Applied Catalysis B, 77, 46-57.
- Udani, P.P.C., Gunawardana, P.V.D.S., Lee, H.C., and Kim, D.H. (2009) Steam reforming and oxidative steam reforming of methanol over CuO-CeO<sub>2</sub> catalysts. International Journal of Hydrogen Energy, 34, 7648-7655.

- Velu, S., Suzuki, K., Kapoor, M.P., Ohashi, F., and Osaki, T. (2001) Selective production of hydrogen for fuel cells via oxidative steam reforming of methanol over CuZnAl(Zr)-oxide catalysts. Applied Catalysis A, 213, 47-63.
- Velu, S., Suzuki, K., Okazaki, M., Kapoor, M.P., Osaki, T., and Ohashi, F. (2000) Oxidative steam reforming of methanol over CuZnAl(Zr)-oxide catalysts for the selective production of hydrogen for fuel cells: Catalyst characterization and performance evaluation. Journal of Catalysis, 194, 373-384.
- Wang, J.B., Li, C.H., and Huang, T.J. (2005) Study of partial oxidative steam reforming of methanol over Cu-ZnO/samaria-doped ceria catalyst. Catalysis Letters, 103, 239-247.
- Wang, L., Husar, A., Zhou, T., and Liu, H. (2003) A parametric study of PEM fuel cell performances. International Journal of Hydrogen Energy, 28, 1263-1272.
- Zhang, Q., Xu, L., Ning, P., Gu, J., and Guan, Q. (2014) Surface characterization studies of CuO-CeO<sub>2</sub>-ZrO<sub>2</sub> catalysts for selective catalytic reduction of NO with NH<sub>3</sub>. Applied Surface Science, 317, 955-961.
- Zhou, K., Wang, X., Sun, X., Peng, Q., and Li, Y. (2005) Enhanced catalytic activity of ceria nanorods from well-defined reactive crystal planes. Journal of Catalysis, 229, 206-212.

**Table 6.1** BET specific surface areas of all fresh and spent catalysts

Sample composition	Sample abbreviation	ASRM condition (w:m)	BET specific surface area $S_{\text{BET}}$ ( $\text{m}^2\text{g}^{-1}$ )	
			Fresh	Spent
1 wt.%Cu-CeO <sub>2</sub>	1%Cu-C	2:1	226	180
3 wt.%Cu-CeO <sub>2</sub>	3%Cu-C	2:1	218	178
5 wt.%Cu-CeO <sub>2</sub>	5%Cu-C	2:1	214	152
7 wt.%Cu-CeO <sub>2</sub>	7%Cu-C	2:1	219	151
9 wt.%Cu-CeO <sub>2</sub>	9%Cu-C	2:1	206	146
12 wt.%Cu-CeO <sub>2</sub>	12%Cu-C	2:1	204	140
9 wt.%Cu-CeO <sub>2</sub>	9%Cu-C	2:1 (stability)	206	64
1 wt.%Cu-Ce <sub>0.75</sub> Zr <sub>0.25</sub> O <sub>2</sub>	1%Cu-CZ	2:1	204	123
3 wt.%Cu-Ce <sub>0.75</sub> Zr <sub>0.25</sub> O <sub>2</sub>	3%Cu-CZ	2:1	203	128
5 wt.%Cu-Ce <sub>0.75</sub> Zr <sub>0.25</sub> O <sub>2</sub>	5%Cu-CZ	2:1	188	126
7 wt.%Cu-Ce <sub>0.75</sub> Zr <sub>0.25</sub> O <sub>2</sub>	7%Cu-CZ	2:1	179	130
9 wt.%Cu-Ce <sub>0.75</sub> Zr <sub>0.25</sub> O <sub>2</sub>	9%Cu-CZ	2:1	165	107
12 wt.%Cu-Ce <sub>0.75</sub> Zr <sub>0.25</sub> O <sub>2</sub>	12%Cu-CZ	2:1	151	103
9 wt.%Cu-Ce <sub>0.75</sub> Zr <sub>0.25</sub> O <sub>2</sub>	9%Cu-CZ	2:1 (stability)	165	78

**Table 6.2** Structural parameters of all fresh and spent catalysts from XRD

Catalysts	ASRM condition (w:m)	Crystallite size of ceria <sup>a</sup> (nm)		Unit cell parameter <sup>b</sup> (nm)	
		Fresh	Spent	Fresh	Spent
1%Cu-C	2:1	3.8139	4.4814	5.4176	5.4105
3%Cu-C	2:1	3.8875	4.0299	5.4172	5.3997
5%Cu-C	2:1	3.8978	4.1603	5.4148	5.3955
7%Cu-C	2:1	3.8639	3.9989	5.3969	5.3991
9%Cu-C	2:1	3.8598	4.0797	5.4069	5.3906
12%Cu-C	2:1	3.8233	4.0412	5.3829	5.3977
9%Cu-C	2:1 (stability)	3.8598	6.6532	5.4069	5.3945
1%Cu-CZ	2:1	3.6446	4.3277	5.3760	5.3853
3%Cu-CZ	2:1	3.6200	4.0028	5.3707	5.3644
5%Cu-CZ	2:1	3.5713	3.8972	5.3714	5.3665
7%Cu-CZ	2:1	3.6572	3.6168	5.3688	5.3557
9%Cu-CZ	2:1	3.6918	3.8294	5.3844	5.3504
12%Cu-CZ	2:1	3.5465	3.7602	5.3678	5.3645
9%Cu-CZ	2:1 (stability)	3.6918	6.3800	5.3844	5.6914

<sup>a</sup> Average crystallite size of ceria calculated from XRD data at (1 1 1) plane using Scherrer's equation

<sup>b</sup> Unit cell parameter of catalysts calculated from XRD data at (1 1 1) plane using Bragg's equation

**Table 6.3** TPO results of catalysts

Sample	Oxidation temperature (°C)	Used O <sub>2</sub> for oxidation (μmol/g)	Amount of copper (mg)	Amount of coke (mg)	% of coke (%wt)
9%Cu-C	243	8.28	1.52	-	-
9%Cu-C after stability testing	207, 296	455.47	1.52	3.94	0.39
9%Cu-CZ	237	14.26	1.82	-	-
9%Cu-CZ after stability testing	266, 484	396.23	1.82	4.76	0.29

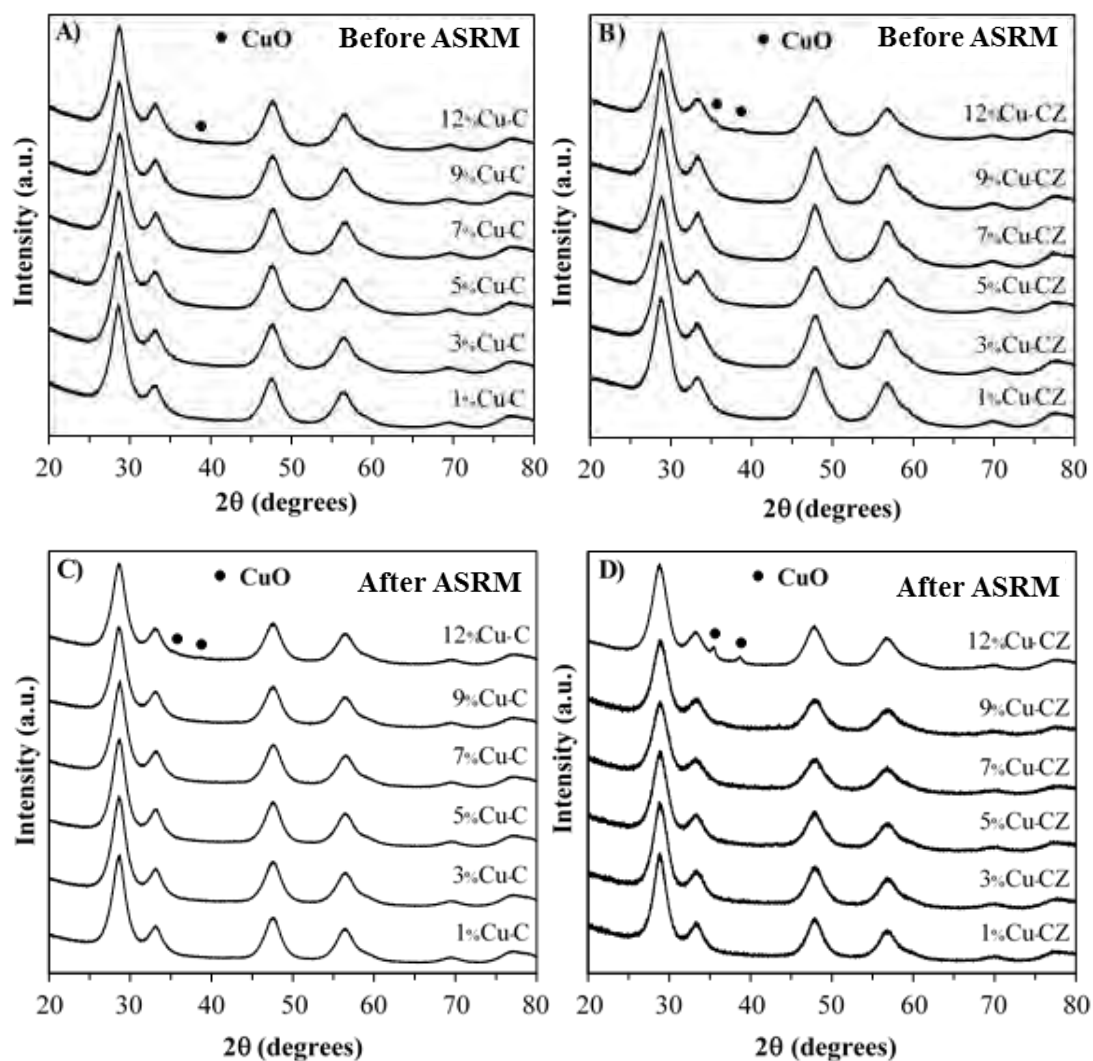


**Figure 6.1** Wide angle XRD patterns of (A) fresh Cu-C catalysts; (B) fresh Cu-CZ catalysts; (C) spent Cu-C catalysts and (D) spent Cu-CZ catalysts at various Cu contents.



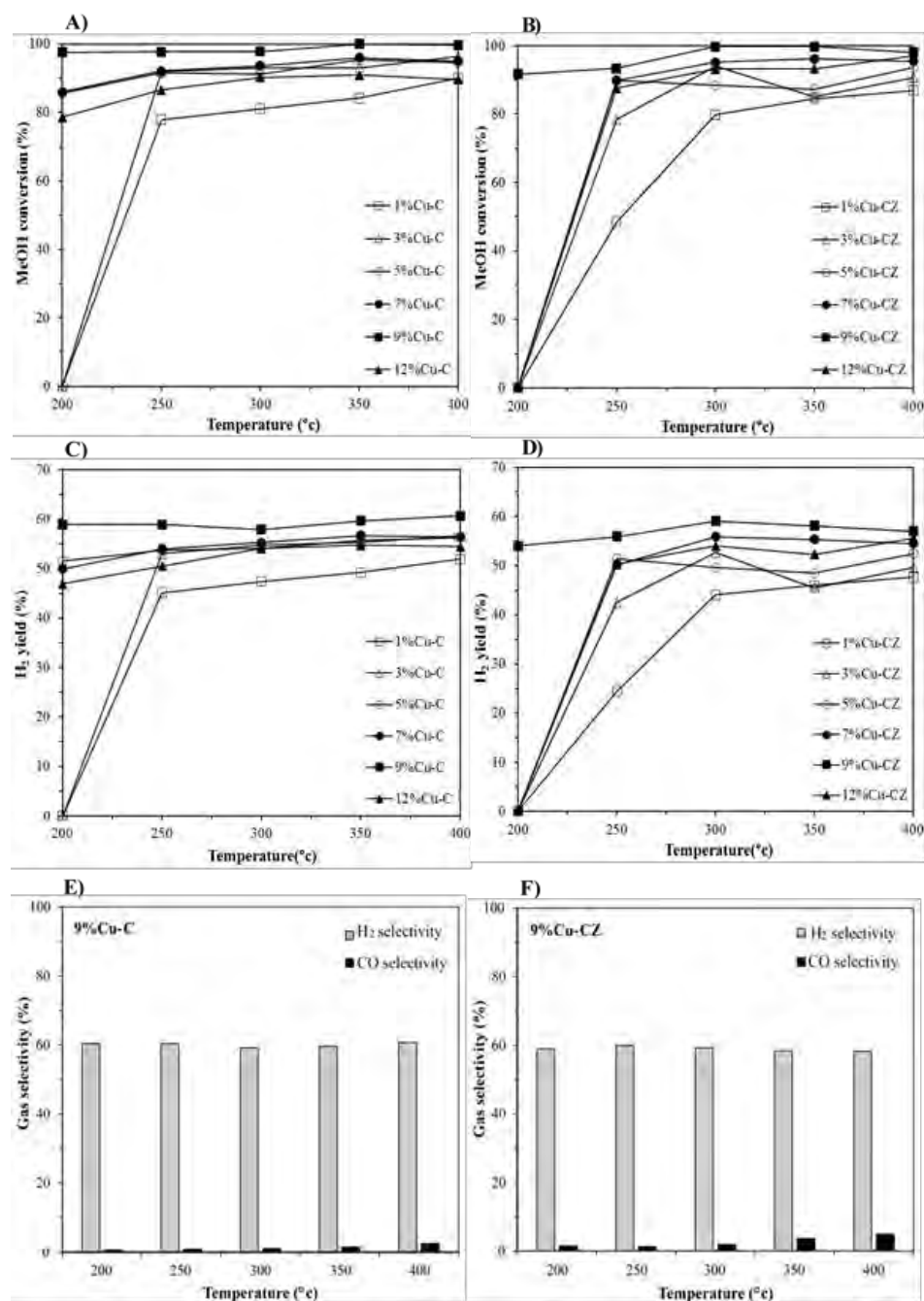


**Figure 6.2** (A) The methanol conversion of Cu-C catalysts; (B) The methanol conversion of Cu-CZ catalysts; (C) The H<sub>2</sub> yield of Cu-C catalysts; (D) The H<sub>2</sub> yield of Cu-CZ catalysts; (E) The gas selectivity of 9%Cu-C catalyst; (F) The gas selectivity of 9%Cu-CZ catalyst. (Reaction condition: H<sub>2</sub>O/CH<sub>3</sub>OH=2/1, O<sub>2</sub> 5 ml/min)

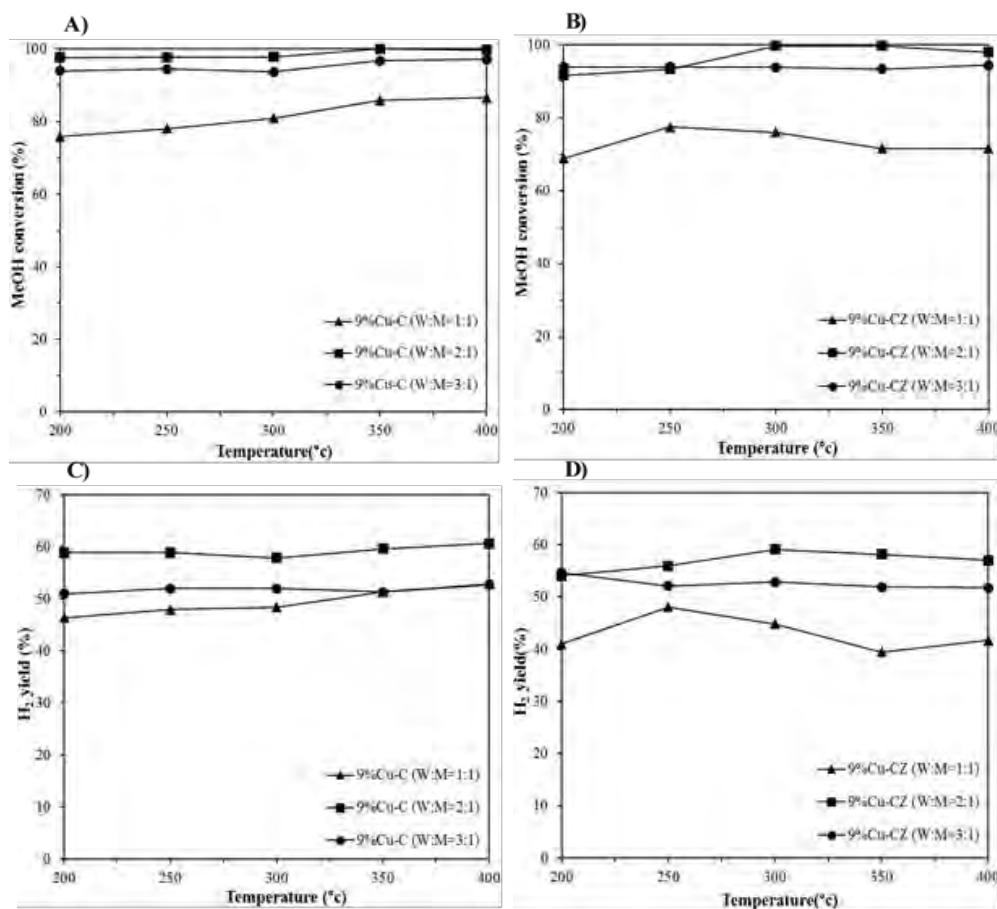


**Figure 6.3** The effect of H<sub>2</sub>O/CH<sub>3</sub>OH (W/M) molar ratio on catalytic performance (A) The methanol conversion of 9%Cu-C catalyst; (B) The methanol conversion of 9%Cu-CZ catalyst; (C) The H<sub>2</sub> yield of 9%Cu-C catalyst; (D) The H<sub>2</sub> yield of 9%Cu-CZ catalyst. (Reaction condition: O<sub>2</sub> 5 ml/min)

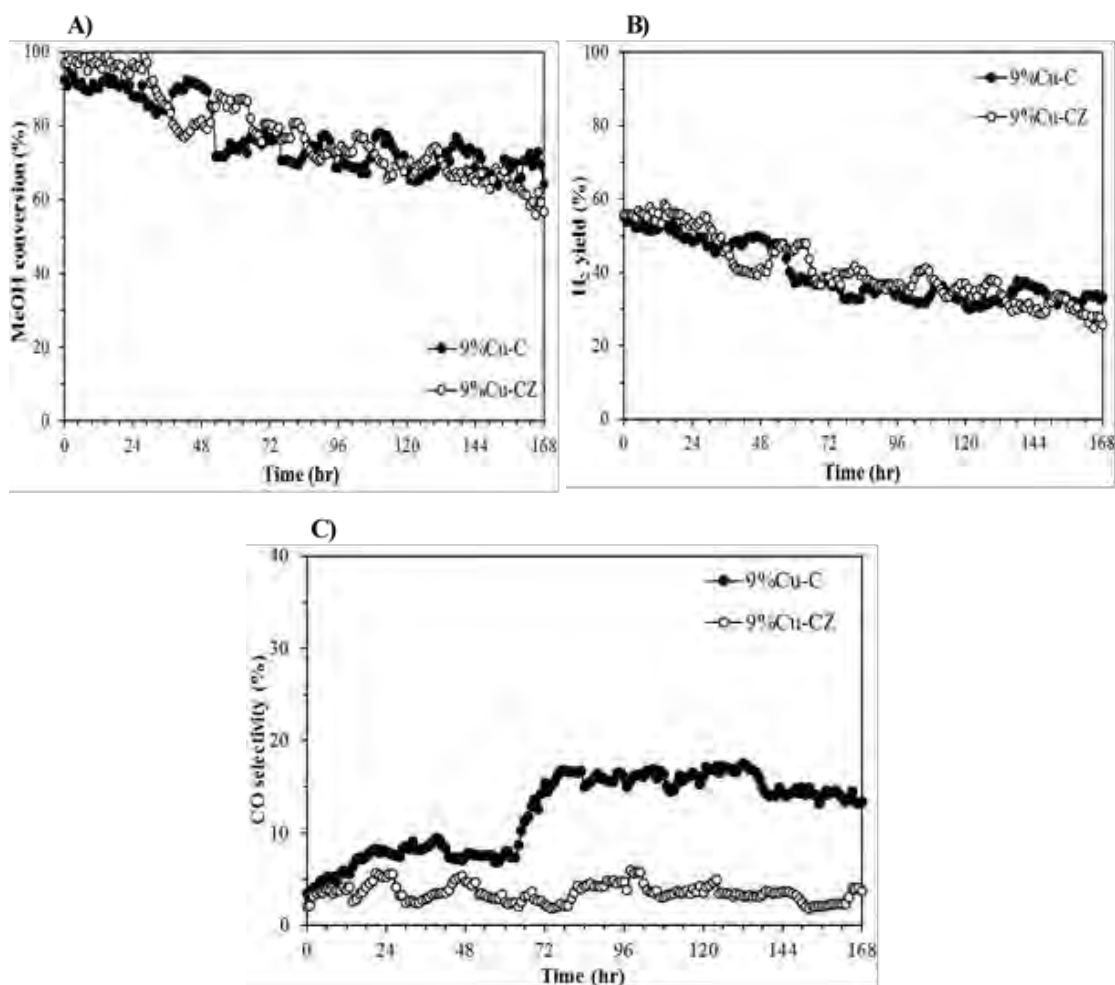


**Figure 6.4** Stability testing of 9%Cu-C and 9%Cu-CZ catalysts (A) The methanol conversion; (B) The H<sub>2</sub> yield; and (C) The CO selectivity. (Reaction conditions: H<sub>2</sub>O/CH<sub>3</sub>OH=2/1; O<sub>2</sub> 5 ml/min; reaction temperature at 350 °C for 9%Cu-C and 300°C for 9%Cu-CZ; and time-on-stream per catalyst 168 h)

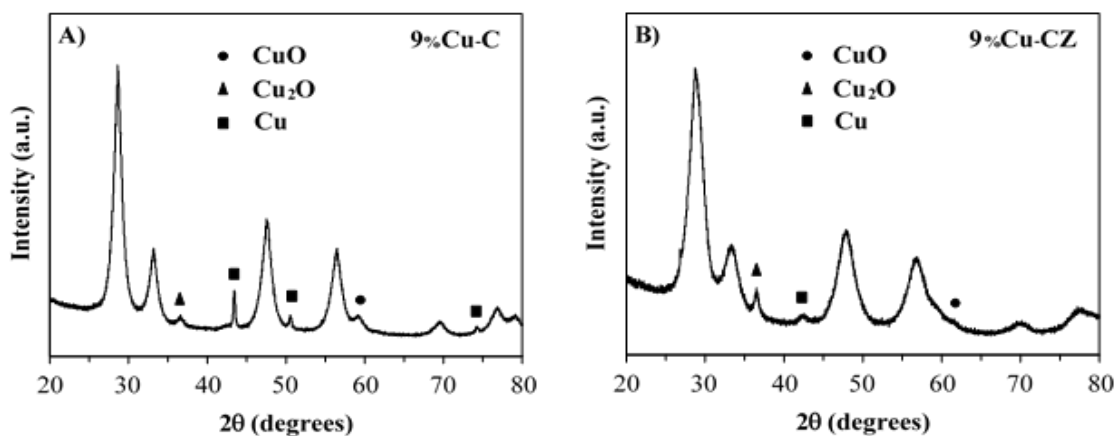


**Figure 6.5** Wide angle XRD patterns of (A) spent 9%Cu-C catalyst; (B) spent 9%Cu-CZ catalyst after stability testing for 168 h.

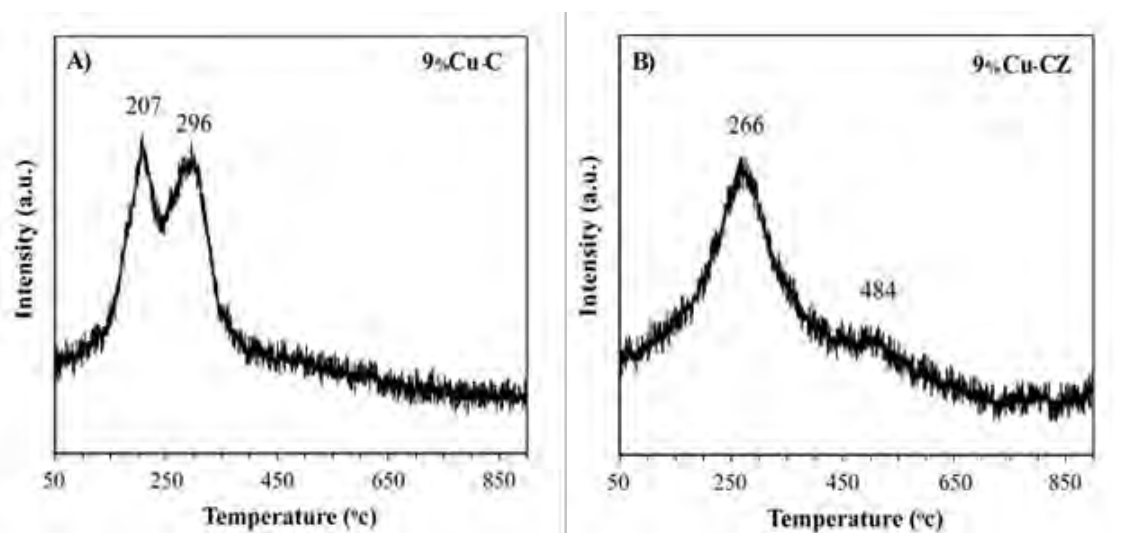


**Figure 6.6** TPO profiles of (A) spent 9%Cu-C catalyst; (B) spent 9%Cu-CZ catalyst after stability testing for 168 h.

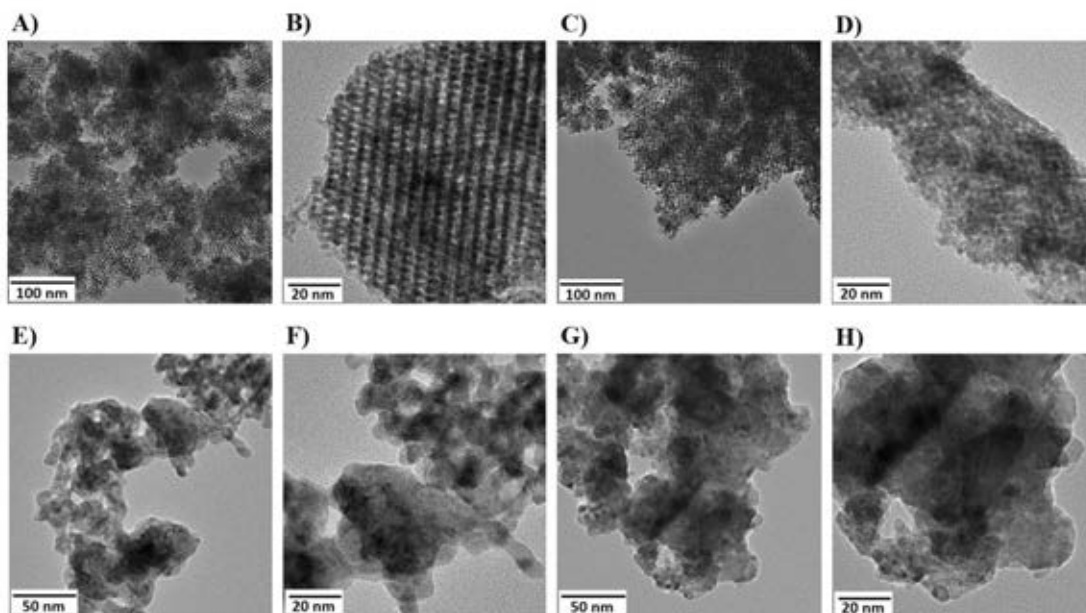


**Figure 6.7** TEM images of (A) and (B) fresh 9%Cu-C catalyst, (C) and (D) fresh 9%Cu-CZ catalyst, (E) and (F) spent 9%Cu-C catalyst, and (G) and (H) spent 9%Cu-CZ catalyst after stability testing for 168 h.

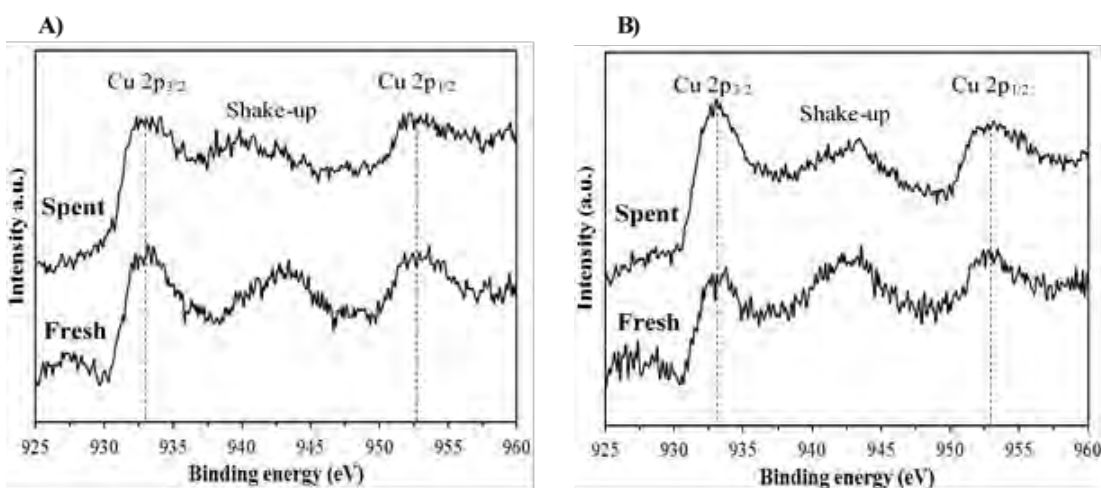


**Figure 6.8** (A) Cu 2p XPS spectra of fresh 9%Cu-C catalyst and spent 9%Cu-C catalyst after stability testing for 168 h; and (B) Cu 2p XPS spectra of fresh 9%Cu-CZ catalyst and spent 9%Cu-CZ catalyst after stability testing for 168 h.

**CHAPTER VII**  
**HIGH POTENTIAL OF MESOPOROUS CERIA/CERIA-ZIRCONIA**  
**SYNTHESIZED VIA NANOCASTING PATHWAY FOR CATALYTIC**  
**APPLICATIONS**

**7.1 Abstract**

Presently, nanocasting process, an alternative synthesis pathway, has been widely employed to synthesize ordered nonsiliceous mesoporous materials. In this work, mesoporous CeO<sub>2</sub> (C) and mesoporous CeO<sub>2</sub>-ZrO<sub>2</sub> (CZ), were successfully prepared via nanocasting method using MCM-48 as a hard template. Both C and CZ supports provided ordered structure with high specific surface area. Copper (Cu) loaded onto C and CZ supports by deposition-precipitation (DP) method exhibited high dispersion of Cu species. The structures and properties of both catalysts play a crucial role to interesting catalytic applications, such as preferential oxidation of CO (CO-PROX) and oxidative steam reforming of methanol (OSRM). The Cu-C and Cu-CZ catalysts showed good potential for CO-PROX reaction with 100% CO conversion at 110° and 130 °C, respectively, and also exhibited excellent catalytic performance for OSRM reaction with 100% methanol conversion at 350° and 300 °C, respectively.

**(Keywords:** Mesoporous ceria/ceria-zirconia, Catalytic applications)

## 7.2 Introduction

Porous materials, divided into three classes; microporous ( $< 2$  nm), mesoporous (2-50 nm) and macroporous ( $> 50$  nm) materials (Sing *et al.*, 1985), have been extensively studied for several applications, especially ordered mesoporous materials. Due to their extremely large surface area within a relatively small volume, mesoporous materials show promising potential to use as adsorbents, catalysts, catalyst supports, chemical sensors and molecular separation (Ciesla *et al.*, 1999; Wan *et al.*, 2007). An alternative synthesis pathway, nanocasting process, has been developed to obtain ordered nonsiliceous mesoporous materials that are difficult to synthesize by conventional processes (Yang *et al.*, 2005). The nanocasting process involves in three main steps: i) formation of the template; ii) the casting step with precursors and iii) removal of the template (Lu and Schuth, 2006). This method can occur in a limited nanospace of template and the sintering of precursors is restricted in the limited nanopores, resulting in the achieved materials having high surface area and special nanostructure (Tang *et al.*, 2015). The hard templates for nanocasting process show important potential over the soft template because the hard templates provide well-ordered structure of frameworks, generating high surface areas and ordered structure of replica (Deeprasertkul *et al.*, 2014). Cubic MCM-48 as mesoporous material, indexed in the space group of  $Ia3d$ , is a good candidate using as hard template in nanocasting process on account of its three-dimensional pore structure and interconnected channels, reducing diffusion limitations and avoiding pore blockage of reactants (Monnier *et al.*, 1993).

Ceria ( $\text{CeO}_2$ ), a fluorite-type oxide, is the most important rare-earth oxide for the oxidation reactions because of its redox cycle between  $\text{Ce}^{4+}$  and  $\text{Ce}^{3+}$  and high oxygen storage capacity (OSC) (Shan *et al.*, 2003; Madier *et al.*, 1999). Furthermore, the introduction of zirconia ( $\text{ZrO}_2$ ) to C is an alternative way to improve thermal resistance, redox property, and oxygen storage and release capacity of pure C (Trovarelli *et al.*, 2001). Therefore, both C and CZ are the excellent supports for many metal catalysts. In this study, mesoporous C and mesoporous CZ supports were prepared via nanocasting process using MCM-48 as hard template. Cu catalyst was loaded onto supports by the deposition-precipitation (DP) method. The catalytic

performance of Cu loaded onto the mesoporous C and CZ supports )Cu-C and Cu-CZ( was evaluated by preferential oxidation of CO )CO-PROX( and oxidative steam reforming of methanol )OSRM(.

### 7.3 Experimental

#### 7.3.1 Preparation of Mesoporous CeO<sub>2</sub> and CeO<sub>2</sub>-ZrO<sub>2</sub>

Mesoporous C and CZ supports were prepared via nanocasting process using MCM-48 as hard template. In case of mesoporous C preparation, 50 wt% of Ce(NO<sub>3</sub>)<sub>3</sub>.6H<sub>2</sub>O as a precursor and 50 wt% of MCM-48 were mixed in 5 ml of ethanol and continuously stirred for 30 min. For preparation of mesoporous CZ, Ce(NO<sub>3</sub>)<sub>3</sub>.6H<sub>2</sub>O and ZrOCl<sub>2</sub>.8H<sub>2</sub>O in a molar ratio of Ce:Zr = 0.75:0.25 were dissolved in 5 ml of ethanol and then MCM-48 was directly added to the mixture, with constant stirring for 4 h. Then, ethanol was removed by evaporation in an oven at 100 °C. The dried powder was calcined at 550 °C for 6 h. MCM-48 was removed by 2 M NaOH at 50 °C. The obtained product was washed with deionized water until neutral and dried overnight.

#### 7.3.2 Preparation of Cu Loaded Mesoporous CeO<sub>2</sub> and CeO<sub>2</sub>-ZrO<sub>2</sub>

Cu loaded mesoporous C and CZ were synthesized by the deposition-precipitation )DP( method. Mesoporous C and CZ were added to aqueous solution of Cu(NO<sub>3</sub>)<sub>2</sub>.3H<sub>2</sub>O and continuously stirred for 1 h at room temperature. Subsequently, the mixture was heated to 80 °C, and its pH adjusted to 7 by Na<sub>2</sub>CO<sub>3</sub> before aging for another hour. The obtained product was filtered, washed with warm distilled water, dried overnight, and eventually calcined in air at 500 °C for 6 h.

#### 7.3.3 Catalytic Activity Measurement

The synthesized catalysts were evaluated for the preferential oxidation of CO by packing 100 mg of catalyst into a U-tube between layers of glass wool. The reactant gas composition containing 1 vol.% CO, 1 vol.% O<sub>2</sub> and 40 vol.% H<sub>2</sub> balancing with He was fed into the CO-PROX reactor. The total flow rate of the mixed



gas was about  $50 \text{ ml min}^{-1}$ . The effluent gas stream was detected by an on-line gas chromatograph (Agilent Technologies 6890N) using a carbosphere column and a thermal conductivity detector (TCD).

The prepared catalysts were also evaluated for oxidative steam reforming of methanol. A 100 mg of catalyst was packed in the reactor and fixed by two layers of quartz wool. The mixture of methanol and distilled water was continuously pumped by a syringe pump to a vaporizer in order to generate a vapor mixture of methanol and steam. The mixture vapor was mixed with He carrier gas ( $45 \text{ ml/min}$ ) and oxygen ( $5 \text{ ml/min}$ ) before being fed into the catalytic reactor. The product gas stream from the reactor were analyzed by a Hewlett Packard 5890 series II gas chromatograph equipped with a thermal conductivity detector (TCD) and carbosphere column.

## 7.4 Results and Discussion

### 7.4.1 Characterization of Synthesized Catalysts

The mesoporous C and mesoporous CZ supports, preparing via nanocasting process using MCM-48 as template, show similar characteristic peaks at  $\{211\}$  and  $\{220\}$  to MCM-48. This result indicates that both mesoporous C and mesoporous CZ supports still maintain some order from the MCM-48 template.

The BET specific surface areas ( $S_{\text{BET}}$ ) and the average mesopore diameter ( $d_{\text{pore}}$ ) of mesoporous C and mesoporous CZ supports as well as Cu loaded mesoporous supports are summarized in Table 7.1. The prepared supports obviously show the high specific surface area with average pore diameters in the mesoporous range ( $2\text{-}50 \text{ nm}$ ) (Sing *et al.*, 1985). The addition of Cu onto supports causes the decrease of specific surface area of the catalysts because CuO can block the pores of supports and obstruct the  $\text{N}_2$  adsorption in the BET experiment.

The phase structure and crystallinity of both supports and Cu loaded mesoporous supports were confirmed by WAXD in a  $2\theta$  range of  $20^\circ$  and  $80^\circ$ , as shown in Figure 7.1. The main peaks of all samples appear at  $28.71^\circ$ ,  $33.31^\circ$ ,  $47.96^\circ$ ,  $56.95^\circ$ ,  $59.24^\circ$ ,  $70.00^\circ$  and  $76.93^\circ$  corresponding to  $\{1\ 1\ 1\}$ ,  $\{2\ 0\ 0\}$ ,  $\{2\ 2\ 0\}$ ,  $\{3\ 1\ 1\}$ ,  $\{2\ 2\ 2\}$ ,  $\{4\ 0\ 0\}$ , and  $\{3\ 3\ 1\}$  reflections, respectively, and representing the fluorite

cubic structure (Andrew *et al.*, 1990; Caputo *et al.*, 2008). Surprisingly, the addition of Cu into both C and CZ supports disappears the change of diffraction patterns and the intensity of peaks. Furthermore, there are no diffraction peaks of CuO phases at  $2\theta = 35.6^\circ$  and  $38.8^\circ$ . It can be mentioned that the DP method provides the high dispersion of Cu on C and CZ supports. The absence of the CuO diffraction peak can also confirm that CuO crystallites are very small (Shan *et al.*, 2003).

#### 7.4.2 Catalytic Activity for Preferential Oxidation of CO )CO-PROX(

The catalytic performance of Cu- C and Cu- CZ catalysts was investigated for CO-PROX reaction under an excess H<sub>2</sub> component in the temperature range of 50°–250 °C, as shown in Figure 7.2. At the first range of reaction temperature, CO conversion of both catalysts increase with increasing temperature, but the oxygen selectivity towards CO<sub>2</sub> decreases with temperature. Then, the Cu-C catalyst achieve 100% conversion at 110 °C while the Cu-CZ catalyst reached 100% conversion at 130 °C with the selectivity higher than 50%. Generally, CuO acts as catalyst which can adsorb CO molecules and it is reduced by CO to produce CO<sub>2</sub> molecules. CeO<sub>2</sub> and CeO<sub>2</sub>-based supports provides lattice oxygens for converting CO to CO<sub>2</sub> molecules. Oxygen competes with CO molecules in order to adsorb on the catalyst and oxygen vacancies are located at the Cu-CeO<sub>2</sub> interface (Royer *et al.*, 2011). Finally, oxygen can re-oxidize the surface metal atoms and repopulate oxygen vacancies on the C and CZ support (Mars *et al.*, 1954). The high activity and selectivity are the important evidence, indicating that the synthesized catalysts, ordered mesoporous material with high surface area, show good performance for CO-PROX reaction.

#### 7.4.3 Catalytic Activity for Oxidative Steam Reforming of Methanol )OSRM(

The catalytic activity of Cu- C and Cu- CZ catalysts was evaluated for oxidative steam reforming of methanol in a temperature range from 200° to 400 °C, as illustrated in Figure 7.3. The Cu-C catalyst exhibits high methanol conversion more than 80% at the beginning of reaction temperature while the Cu-CZ catalyst achieves more than 90% methanol conversion at 200 °C. This result shows that the OSRM reaction is favored by increase of the reaction temperature. The Cu- C catalyst shows

methanol conversion of 100% at 350 °C while the Cu-CZ catalyst achieve complete methanol conversion at 350 °C. The %H<sub>2</sub> yield of both catalysts corresponds to methanol conversion in a temperature range from 200° to 400 °C, providing a maximum % H<sub>2</sub> yield of 60%. Furthermore, CO production from OSRM reaction over Cu-C and Cu-CZ catalysts is quite low and H<sub>2</sub> and CO<sub>2</sub> are the primary products. Furthermore, it is found that CO formation increases with increasing temperature since CO molecules are generated at high temperature by the reverse water-gas shift reaction (Breen *et al.*, 1999).

## 7.5 Conclusions

In this study, mesoporous CeO<sub>2</sub> and mesoporous CeO<sub>2</sub>-ZrO<sub>2</sub> supports were successfully prepared via nanocasting process using MCM-48 as hard template. The C and CZ supports show an ordered mesoporous structure and a high surface area around 259 and 256 m<sup>2</sup>g<sup>-1</sup>. The deposition-precipitation technique was used to load Cu onto C and CZ supports. Wide angle XRD spectra can confirm that the loading of Cu onto C and CZ supports does not the change of diffraction patterns and the peak intensity of supports. Moreover, there are no diffraction peaks of CuO phases, indicating that DP method provides the high dispersion of Cu on C and CZ supports. The Cu-C and Cu-CZ catalysts exhibit excellent performance for CO-PROX reaction. The complete CO conversion of Cu-C and Cu-CZ catalysts appears at the reaction temperature of 110° and 130 °C, respectively. Furthermore, the OSRM results illustrate that Cu-C and Cu-CZ catalysts provide the best catalytic performance with 100% methanol conversion and 60% H<sub>2</sub> yield at 350° and 300 °C, respectively.

## 7.6 Acknowledgements

This study is financially supported by the Grant for International Research Integration: Chula Research Scholar, Ratchadaphiseksompotte Endowment Fund, Chulalongkorn University, Thailand, Development and Promotion of Science and Technology Talents Project.

## 7.7 References

- Andrews, D. (1990) Perspectives in modern chemical spectroscopy. Berlin: Springer-Verlag.
- Breen, J.P. and Ross, J.R.H. (1999) Methanol reforming for fuel-cell applications: development of zirconia-containing Cu-Zn-Al catalysts. Catalysis Today, 51, 521-533.
- Caputo, T., Lisi, L., Pirone, R., and Russo, G. (2008) On the role of redox properties of CuO/CeO<sub>2</sub> catalysts in the preferential oxidation of CO in H<sub>2</sub>-rich gases. Applied Catalysis A, 348, 42-53.
- Ciesla, U. and Schuth, F. (1999) Ordered mesoporous materials. Microporous and Mesoporous Materials, 27, 131-149.
- Deeprasertkul, C., Longloilert, R., Chaisuwan, T., and Wongkasemjit, S. (2014) Impressive low reduction temperature of synthesized mesoporous ceria via nanocasting. Materials Letters, 130, 218-222.
- Lu, A. and Schuth, F. (2006) Nanocasting: a versatile strategy for creating nanostructured porous materials. Advanced Materials, 18, 1793-1805.
- Madier, Y., Descorme, C., Le Govic, A.M., and Duprez, D. (1999) Oxygen mobility in CeO<sub>2</sub> and Ce<sub>x</sub>Zr<sub>(1-x)</sub>O<sub>2</sub> compounds: Study by CO transient oxidation and <sup>18</sup>O/<sup>16</sup>O isotopic exchange. Journal of Physical Chemistry B, 103, 10999-11006.
- Mars, P. and Krevelen, D.W. (1954) Oxidations carried out by means of vanadium oxide catalysts. Chemical Engineering Science, 3, 41-59.
- Monnier, A., Schuth, F., Huo, Q., Kumar, D., Margolese, D., Maxwell, R.S., Stucky, M., Krishnamurty, G.D., Petroff, P., Firouzi, A., and Janicke, M. (1993) Cooperative formation of inorganic-organic interfaces in the synthesis of silicate mesostructures. Science, 261, 1299-1303.
- Royer, S. and Duprez, D. (2011) Catalytic oxidation of carbon monoxide over transition metal oxides. ChemCatChem, 3, 24-65.
- Shan, W., Shen, W., and Li, C. (2003) Structural characteristics and redox behaviors of Ce<sub>1-x</sub>Cu<sub>x</sub>O<sub>y</sub> solid solutions. Chemistry of Materials, 15, 4761-4767.

- Sing, K.S.W., Everett, D.H., Haul, R.A.W., Moscou, L., Pierotti, R.A., Rouquerol, J., and Siemieniewska, T. (1985) Reporting physisorption data for gas/solid systems with special reference to the determination of surface area and porosity. Pure and Applied Chemistry, 57, 603-619.
- Tang, W., Wu, X., Li, S., Shan, X., Liu, G., and Chen, Y. (2015) Co-nanocasting synthesis of mesoporous Cu–Mn composite oxides and their promoted catalytic activities for gaseous benzene removal. Applied Catalysis B: Environmental, 162, 110-121.
- Trovarelli, A., Boaro, M., Rocchini, E., Leitenburg, C., and Dolcetti, G. (2001) Some recent developments in the characterization of ceria-based catalysts. Journal of Alloys and Compounds, 323, 584-591.
- Wan, Y. and Zhao, D. (2007) On the controllable soft-templating approach to mesoporous silicates. Chemical Reviews, 107, 2821-2860.
- Yang, H. and Zhao, D. (2005) Synthesis of replica mesostructures by the nanocasting strategy. Journal of Materials Chemistry, 15, 1217-1231.

**Table 7.1** N<sub>2</sub> physisorption data of the synthesized catalysts

Sample	Sample acronym	Specific surface area )m <sup>2</sup> g <sup>-1</sup> (	Mesopore diameter )nm(
CeO <sub>2</sub>	C	259	4.30
Cu-CeO <sub>2</sub>	Cu-C	206	4.63
CeO <sub>2</sub> -ZrO <sub>2</sub>	CZ	256	3.80
Cu-CeO <sub>2</sub> -ZrO <sub>2</sub>	Cu-CZ	165	3.61

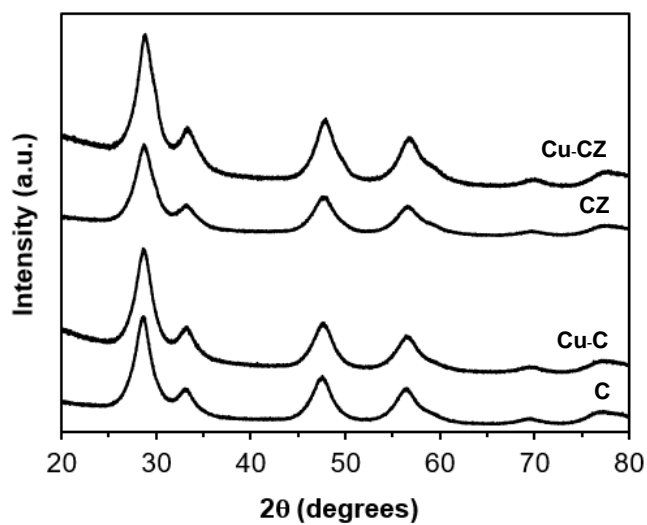


**Figure 7.1** Wide angle XRD patterns of mesoporous C, mesoporous CZ, Cu-C, and Cu-CZ.

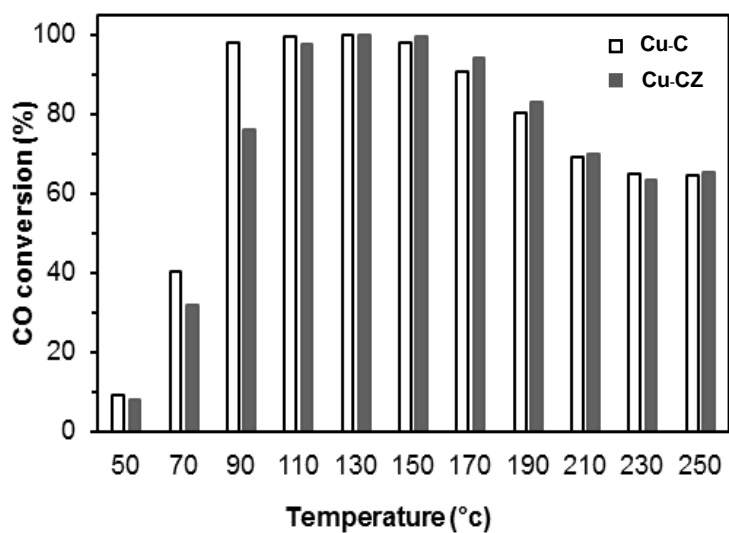


**Figure 7.2** CO conversion as a function of temperature of Cu-C and Cu-CZ catalysts.

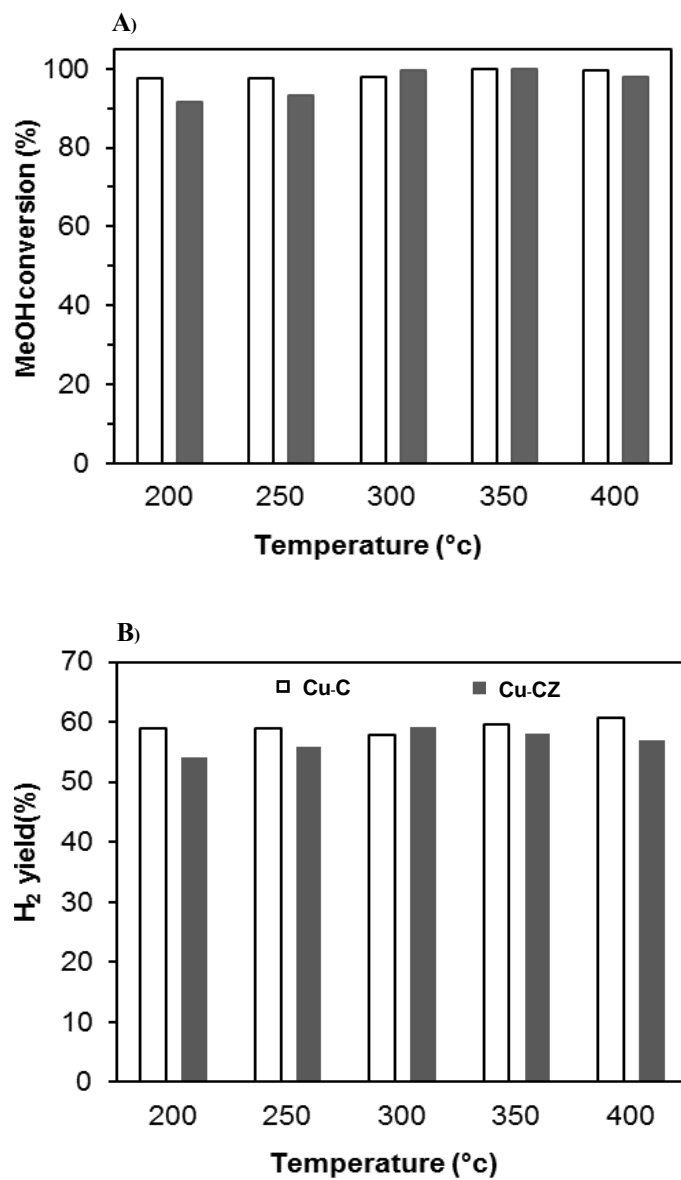


**Figure 7.3** A) Methanol conversion and B) H<sub>2</sub> yield of Cu-C and Cu-CZ catalysts.



## CHAPTER VIII

### CONCLUSIONS AND RECOMMENDATIONS

#### 8.1 Conclusions

The CuO loaded mesoporous CeO<sub>2</sub> and CuO loaded mesoporous CeO<sub>2</sub>-ZrO<sub>2</sub> catalyst were successfully synthesized via nanocasting and deposition-precipitation techniques, using MCM-48 as a hard template. Both CuO loaded mesoporous CeO<sub>2</sub> and CuO loaded mesoporous CeO<sub>2</sub>-ZrO<sub>2</sub> catalyst provided an ordered pore structure and a high surface area which was suitable to use in many catalytic applications. Moreover, all CuO loaded onto mesoporous CeO<sub>2</sub> and mesoporous CeO<sub>2</sub>-ZrO<sub>2</sub> supports exhibited a high dispersion of Cu species.

For CO-PROX reaction, among all synthesized CuO loaded mesoporous CeO<sub>2</sub> catalysts, 7Cu/CeO<sub>2</sub> presents 100% conversion at 110 °C and 87% selectivity toward CO<sub>2</sub> in excess H<sub>2</sub> and a feed free of CO<sub>2</sub> and H<sub>2</sub>O. In the presence of 10 % CO<sub>2</sub> or 10 % CO<sub>2</sub> with 10 % H<sub>2</sub>O, the catalytic activity of 7Cu/CeO<sub>2</sub> provides 100% CO conversion at higher temperatures (130° and 150 °C, respectively). Furthermore, all CuO loaded mesoporous CeO<sub>2</sub>-ZrO<sub>2</sub> catalysts showed maximum CO conversion in the range of 95-100% at lower temperatures and the selectivity was more than 50% at temperatures below 150°C. The activity of the Cu-CZ catalysts increases with increasing Cu content from 1 to 9 wt%. The presence of CO<sub>2</sub> or CO<sub>2</sub> plus H<sub>2</sub>O in the feed gas had an inhibiting effect on the CO-PROX performance. For ASRM application, among all synthesized catalysts, 9%Cu-C and 9%Cu-CZ catalysts exhibit the best catalytic behavior. Methanol conversion of 100% and H<sub>2</sub> yield of 60% are achieved at 350 °C for 9%Cu-C and at 300 °C for 9%Cu-CZ catalysts in the presence of O<sub>2</sub> at 5 ml/min with H<sub>2</sub>O/CH<sub>3</sub>OH molar ratios of 2/1. Furthermore, 9%Cu-C and 9%Cu-CZ catalysts generate H<sub>2</sub> yields of around 34% and 36%, respectively, after stability testing for 168 h with low CO selectivity. Promisingly, the high performance ASRM reaction over 9%Cu-C and 9%Cu-CZ catalysts can be

utilized for on-board hydrogen production for polymer electrolyte fuel-cells (PEMFC) to generate energy for vehicles.

## **8.2 Recommendations**

- 8.2.1 To use double-stage process for the preferential CO oxidation reaction.
- 8.2.2 To study other catalysts for loading onto mesoporous CeO<sub>2</sub> and mesoporous CeO<sub>2</sub>-ZrO<sub>2</sub> supports.
- 8.2.3 To use CuO loaded mesoporous CeO<sub>2</sub> and CuO loaded mesoporous CeO<sub>2</sub>-ZrO<sub>2</sub> catalyst for other catalytic applications.

## REFERENCES

- Agrell, J., Birgersson, H., and Boutonnet, M. (2002) Steam reforming of methanol over a Cu/ZnO/Al<sub>2</sub>O<sub>3</sub> catalyst: a kinetic analysis and strategies for suppression of CO formation. Journal of Power Sources, 106, 249-257.
- Ahmed, S. and Krumpelt, M. (2001) Hydrogen from hydrocarbon fuels for fuel cells. International Journal of Hydrogen Energy, 26, 291-301.
- Alejo, L., Lago, R., Pena, M.A., and Fierro, J.L.G. (1997) Partial oxidation of methanol to produce hydrogen over Cu-Zn-based catalysts. Applied Catalysis A: General, 162, 281-297.
- Alfredsson, V. and Anderson, W.M. (1996) Structure of MCM-48 revealed by transmission electron microscopy. Chemistry of Materials, 8, 1141-1146.
- Alvaro, R.C., Ana, A.D., Elisa, M., Aldo, T., Loretta, S., Maurizio, L., Antonio, J.L., and Enrique, R.C. (2011) CuO/CeO<sub>2</sub> supported on Zr doped SBA-15 as catalysts for preferential CO oxidation (CO-PROX). Journal of Power Sources, 196, 4382-4387.
- Araujo, V.D., Bellido, J.D.A., Bernardi, M.I.B., Assaf, J.M., and Assaf, E.M. (2012) CuO-CeO<sub>2</sub> catalysts synthesized in one-step: Characterization and PROX performance. International Journal of Hydrogen Energy, 37, 5498-5507.
- Armor, J.N. (1999) Review: The multiple roles for catalysis in the production of H<sub>2</sub>. Applied Catalysis A: General, 176, 159-176.
- Avgouropoulos, J. and Loannides, T. (2003) Selective CO oxidation over CuO-CeO<sub>2</sub> catalysts prepared via the urea-nitrate combustion method. Applied Catalysis A: General, 244, 155-167.
- Ayastuy, J.L., Gurbani, A., Gonzalez-Marcos, M.P., and Gutierrez-Ortiz, M.A. (2010) Effect of copper loading on copper-ceria catalysts performance in CO selective oxidation for fuel cell applications. International Journal of Hydrogen Energy, 35, 1232-1244.

- Bishop, S.R., Duncan, K.L., and Wachsman, E.D. (2009) Defect equilibria and chemical expansion in non-stoichiometric undoped and gadolinium-doped cerium oxide. Electrochimica Acta, 54, 1436-1443.
- Caputo, T., Lisi, L., Pirone, R., and Russo, G. (2008) On the role of redox properties of CuO/CeO<sub>2</sub> catalysts in the preferential oxidation of CO in H<sub>2</sub>-rich gases. Applied Catalysis A: General, 348, 42-53.
- Chang, C.-C., Chang, C.-T., Chiang, S.-J., Liaw, B.-J., and Chen, Y.-Z. (2010) Oxidative steam reforming of methanol over CuO/ZnO/CeO<sub>2</sub>/ ZrO<sub>2</sub>/Al<sub>2</sub>O<sub>3</sub> catalysts. International Journal of Hydrogen Energy, 35, 7675-7683.
- Deeprasertkul, C., Longloilert, R., Chaisuwan, T., and Wongkasemjit, S. (2014) Impressive low reduction temperature of synthesized mesoporous ceria via nanocasting. Materials Letters, 130, 218-222.
- Dow, W.P. and Huang, T.J. (1994) Effect of oxygen vacancy of yttria-stabilized zirconia support on carbon monoxide oxidation over copper catalyst. Journal of Catalysis, 147, 322-332.
- Edwards, P.P., Kuznetsov, V.L., and David, W.I.F. (2007) Hydrogen energy. Philosophical Transactions of the Royal Society A, 365, 1043-1056.
- Fechete, I., Wang, Y., and Vedrine, J.C. (2012) The past, present and future of heterogeneous catalysis. Catalysis Today, 189, 2-27.
- Fornasiero, P., Balducci, G., Monte, R.D., Kaspar, J., Sergio, V., Gubitosa, G., Ferrero, A., and Graziani, M. (1996) Modification of the redox behaviour of CeO<sub>2</sub> induced by structural doping with ZrO<sub>2</sub>. Journal of Catalysis, 164, 173-183.
- Fox, E.B., Velu, S., Engelhard, M.H., Chin, Y.H., Miller, J.T., Kropf, J., and Song, C.S. (2008) Characterization of CeO<sub>2</sub>-supported Cu–Pd bimetallic catalyst for the oxygen-assisted water-gas shift reaction. Journal of Catalysis, 260, 358-370.
- Galtayries, A., Sporken, R., Riga, J., Blanchard, G., and Caudano, R. (1998) XPS comparative study of ceria/zirconia mixed oxides: powders and thin film characterization. Journal of Electron Spectroscopy and Related Phenomena, 88, 951-956.

- Gamarra, D. and Martinez-Arias, A. (2009) Preferential oxidation of CO in rich H<sub>2</sub> over CuO/CeO<sub>2</sub>: *Operando*-DRIFTS analysis of deactivating effect of CO<sub>2</sub> and H<sub>2</sub>O. Journal of Catalysis, 263, 189-195.
- Gamarra, D., Munuera, G., Hungria, A.B., Fernandez-Garcia, M., Conesa, J.C., Midgley, P.A., Wang, X.Q., Hanson, J.C., Rodriguez, J.A., and Martinez-Arias, A. (2007) Structure-activity relationship in nanostructured copper-ceria-based preferential CO oxidation catalysts. The Journal of Physical Chemistry C, 111, 11026-11038.
- Gamboa-Rosales, N.K., Ayastuy, J.L., Gonzalez-Marcos, M.P., and Gutierrez-Ortiz, M.A. (2012) Oxygen-enhanced water gas shift over ceria-supported Au-Cu bimetallic catalysts prepared by wet impregnation and deposition-precipitation. International Journal of Hydrogen Energy, 37, 7005-7016.
- Goldstein, E.A. and Mitchell, R.E. (2011) Chemical kinetics of copper oxide reduction with carbon monoxide. Proceedings of the Combustion Institute, 33, 2803-2810.
- Graham, G.W., Weber, W.H., Peters, C.R., and Usman, R. (1991) Empirical method for determining CeO<sub>2</sub>-particle size in catalysts by raman spectroscopy. Journal of Catalysis, 130, 310-313.
- Gray, P.G. and Frost, J.C. (1998) Impact on clean energy in road transportation. Energy Fuels, 12, 1121-1129.
- Groen, J.C., Peffer, L.A.A., and Perez-Ramirez, J. (2003) Pore size determination in modified micro and mesoporous materials. Pitfalls and limitations in gas adsorption data analysis. Microporous and Mesoporous Materials, 60, 1-17.
- Haruta, M., Tsubota, S., Kobayashi, T., Kageyama, H., Genet, M.J., and Delmon, B. (1993) Low-temperature oxidation of CO over gold supported on TiO<sub>2</sub>, alpha-Fe<sub>2</sub>O<sub>3</sub> and Co<sub>3</sub>O<sub>4</sub>. Journal of Catalysis, 144, 175-192.
- Hoffmann, F., Cornelius, M., Morell, J., and Froba, M. (2006) Silica-Based Mesoporous Organic-Inorganic Hybrid Materials. Mesoporous Materials, 45, 3216-3251.
- Hong, S.J. and Virkar, A.V. (1995) Lattice parameters and densities of rare-earth oxide doped ceria electrolytes. Journal of the American Ceramic Society, 78:433-439.

- Houteit, A., Mahzoul, H., Ehrburger, P., Bernhardt, P., Legare, P., and Garin, F. (2006) Production of hydrogen by steam reforming of methanol over copper-based catalysts: The effect of cesium doping. Applied Catalysis A: General, 306, 22-28.
- Huang, G., Liaw, B.-J., Jhang, C.-J., and Chen, Y.-Z. (2009) Steam reforming of methanol over CuO/ZnO/CeO<sub>2</sub>/ZrO<sub>2</sub>/Al<sub>2</sub>O<sub>3</sub> catalysts. Applied Catalysis A: General, 358, 7-12.
- Jong, K.P. (2009) Synthesis of Solid Catalysts. Weinheim: WILEY-VCH Verlag GmbH & Co. KGaA.
- Kim, D.J. (1989) Lattice parameter, ionic conductivities, and solubility limits in fluorite structure MO<sub>2</sub> oxides (M=Hf<sup>4+</sup>, Zr<sup>4+</sup>, Ce<sup>4+</sup>, Th<sup>4+</sup>, U<sup>4+</sup>). Journal of the American Ceramic Society, 72, 1415-1421.
- Laguna, O.H., Centeno, M.A., Boutonnet, M., and Odriozola, J.A. (2011) Fe-doped ceria solids synthesized by the microemulsion method for CO oxidation reactions. Applied Catalysis B: Environmental, 106, 621-629.
- Laguna, O.H., Ngassa, E.M., Oraa, S., Alvarez, A., Dominguez, M.I., Romero-Sarria, F., Arzamendi, G., Gandia, L.M., Centeno, M.A. and Odriozola, J.A. (2012) Preferential oxidation of CO (CO-PROX) over CuO<sub>x</sub>/CeO<sub>2</sub> coated microchannel reactor. Catalysis Today, 180, 105-110.
- Liao, X., Chu, W., Dai, X., and Pitchon, V. (2013) Bimetallic Au–Cu supported on ceria for PROX reaction: Effects of Cu/Au atomic ratios and thermal pretreatments. Applied Catalysis B: Environmental, 142, 25-37.
- Liu, Y., Fu, Q., and Stephanopoulos, M.F. (2004) Preferential oxidation of CO in H<sub>2</sub> over CuO-CeO<sub>2</sub> catalysts. Catalysis Today, 93-95, 241-246.
- Longloilert, R., Chaisuwan, T., Luengnaruemitchai, A., and Wongkasemjit, S. (2011) Synthesis of MCM-48 from silatrane via sol-gel process. Journal of Sol-Gel Science and Technology, 58, 427-435.
- Lu, A.-H. and Schuth, F. (2005) Nanocasting pathways to create ordered mesoporous solids. Comptes Rendus Chimie, 8, 609-620.

- Lu, A.-H. and Schuth, F. (2006) Nanocasting: A Versatile Strategy for Creating Nanostructured Porous Materials. Advanced Materials, 18, 1793-1805.
- Luo, M.F., Zhong, Y.J., Yuan, X.X., and Zheng, X. (1997) TPR and TPD studies of CuO/CeO<sub>2</sub> catalysts for low temperature CO oxidation. Applied Catalysis A: General, 162, 121-131.
- Marino, F., Descorme, C., and Duprez, D. (2004) Noble metal catalysts for the preferential oxidation of carbon monoxide in the presence of hydrogen (PROX). Applied Catalysis B: Environmental, 54, 59-66.
- Marino, F., Descorme, C., and Duprez, D. (2005) Supported base metal catalysts for the preferential oxidation of carbon monoxide in the presence of excess hydrogen (PROX). Applied Catalysis B: Environmental, 58, 175-183.
- Martinez-Arias, A., Fernandez-Garcia, M., Galvez, O., Coronado, J.M., Anderson, J.A., Conesa, J.C., Soria, J., and Munuera, G. (2000) Comparative study on redox properties and catalytic behavior for CO oxidation of CuO/CeO<sub>2</sub> and CuO/ZrCeO<sub>4</sub> catalysts. Journal of Catalysis, 195, 207-216.
- Martinez-Arias, A., Gamarra, D., Fernandez-Garcia, M., Hornes, A., Bera, P., Koppány, Z.S., and Schay, Z. (2009) Redox-catalytic correlations in oxidised copper-ceria CO-PROX catalysts. Catalysis Today, 143, 211-217.
- McBride, J.R., Haas, K.C., Poindexter, B.D., and Weber, W.H. (1994) Raman and x-ray studies of Ce<sub>1-x</sub>RE<sub>x</sub>O<sub>2-y</sub>, where RE = La, Pr, Nd, Eu, Gd, and Tb. Journal of Applied Physics, 76, 2435-2441.
- Mishra, A. and Prasad, R. (2011) A review on preferential oxidation of carbon monoxide in hydrogen rich gases. Bulletin of Chemical Reaction Engineering & Catalysis, 6 (1), 1-14.
- Monnier, A., Schuth, F., Huo, Q., Kumar, D., Margolese, D., Maxwell, R.S., Stucky, M., Krishnamurty, G.D., Petroff, P., Firouzi, A., and Janicke, M. (1993) Cooperative Formation of Inorganic-Organic Interfaces in the Synthesis of Silicate Mesostructures. Science, 261, 1299-1303.

- Monyanon, S., Pongstabodee, S., and Luengnaruemitchai, A. (2006) Catalytic activity of Pt–Au/CeO<sub>2</sub> catalyst for the preferential oxidation of CO in H<sub>2</sub>-rich stream. Journal of Power Sources, 63, 547-554.
- Moretti, E., Storaro, L., Talon, A., Lenarda, M., Riello, P., Frattini, R., del Valle Martinez de Yuso, M., Jimenez-Lopez, A., Rodriguez-Castellon, E., Ternero, F., Caballero, A., and Holgado, J.P. (2011) Effect of thermal treatments on the catalytic behaviour in the CO preferential oxidation of a CuO–CeO<sub>2</sub>–ZrO<sub>2</sub> catalyst with a flower-like morphology. Applied Catalysis B: Environmental, 102, 627-637.
- Palermo, A., Williams, F.J., and Lambert, R.M. (2002) In situ control of the composition and performance of a bimetallic alloy catalyst: The selective hydrogenation of acetylene over Pt/Pb. Journal of Physical Chemistry B, 106, 10215-10219.
- Palo, D.R. (2007) Methanol steam reforming for hydrogen production. Chemical Reviews, 107, 3992-4021.
- Patel, S. and Pant, K.K. (2007) Selective production of hydrogen via oxidative steam reforming of methanol using Cu–Zn–Ce–Al oxide catalysts. Chemical Engineering Science, 62, 5436-5443.
- Pojanavaraphan, C., Nakaranuwattana, W., Luengnaruemitchai, A., and Gulari, E. (2014) Effect of support composition and metal loading on Au/Ce<sub>1-x</sub>Zr<sub>x</sub>O<sub>2</sub> catalysts for the oxidative steam reforming of methanol. Chemical Engineering Journal, 240, 99-108.
- Potemkin, D.I., Filatov, E.Yu., Zadesenets, A.V., Snytnikov, P.V. Shubin, Yu.V., and Sobyenin, V.A. (2012) Preferential CO oxidation over bimetallic Pt–Co catalysts prepared via double complex salt decomposition. Chemical Engineering Journal, 207-208, 683-689.
- Radovic, M., Dohcevic-Mitrovic, Z., Scepanovic, M., Grujic-Brojcin, M., Matovic, B., Boskovic, S., and Popovic, Z.V. (2007) Raman study of Ba-doped ceria nanopowders. Science of Sintering, 39, 281-286.
- Ramadhas, A.S., Jayaraj, S., and Muraleedharan, C. (2005) Biodiesel production from high FFA rubber seed oil. Fuel, 84, 335-340.



- Rango, R.G. and Mishra, B.G. (2003) Structural, redox and catalytic chemistry of ceria based materials. Bulletin of the Catalysis Society of India, 2, 122-134.
- Royer, S. and Duprez, D. (2011) Catalytic oxidation of carbon monoxide over transition metal oxides. ChemCatChem, 3, 24–65.
- Sa, S., Silva, H., Brandao, L., Sousa, J.M., and Mendes, A. (2010) Catalysts for methanol steam reforming—A review. Applied Catalysis B: Environmental, 99, 43-57.
- Shan, W., Feng, Z., Li, Z., Zhang, J., Shen, W., and Li, C. (2004) Oxidative steam reforming of methanol on Ce<sub>0.9</sub>Cu<sub>0.1</sub>O<sub>Y</sub> catalysts prepared by deposition–precipitation, coprecipitation, and complexation–combustion methods. Journal of Catalysis, 228, 206-217.
- Shannon, R.D. (1976) Revised effective ionic radii and systematic studies of interatomic distances in halides and chalcogenides. Acta Crystallographica Section A, 32, 751-767.
- Shen, W., Dong, X., Zhu, Y., Chen, H., and Shi, J. (2005) Mesoporous CeO<sub>2</sub> and CuO-loaded mesoporous CeO<sub>2</sub>: Synthesis, characterization, and CO catalytic oxidation property. Microporous Mesoporous Materials, 85, 157-162.
- Sing, K.S.W., Everett, D.H., Haul, R.A.W., Moscou, L., Pierotti, R.A., Rouquerol, J., and Siemieniewska, T. (1985) Reporting physisorption data for gas/ solid systems with special reference to the determination of surface area and porosity. International Union of Pure and Applied Chemistry, 57(4), 603-619.
- Souza, E.C.C., Brito, H.F., and Muccillo, E.N.S. (2010) Optical and electrical characterization of samaria-doped ceria. Journal of Alloys and Compounds, 491, 460-464.
- Taguchi, A. and Schuth, F. (2005) Ordered mesoporous materials in catalysis. Microporous and Mesoporous Materials, 77, 1-45.
- Trovarelli, A., Boaro, M., Rocchini, E., Leitenburg, C., and Dolcetti, G. (2001) Some recent developments in the characterization of ceria-based catalysts. Journal of Alloys and Compounds, 323-324, 584-591.

- Trovarelli, A., Leitenburg, C., Boaro, M., and Dolcetti, G. (1999) The utilization of ceria in industrial catalysis. Catalysis Today, 50, 353-367.
- Turco, M., Bagnasco, G., Cammarano, C., Senese, P., Costantino, U., and Sisani, M. (2007) Cu/ZnO/Al<sub>2</sub>O<sub>3</sub> catalysts for oxidative steam reforming of methanol: The role of Cu and the dispersing oxide matrix. Applied Catalysis B: Environmental, 77, 46-57.
- Twigg, M.V. and Spencer, M.S. (2003) Deactivation of copper metal catalysts for methanol decomposition, methanol steam reforming and methanol synthesis. Topics in Catalysis, 22, 191-203.
- Ubago-Pérez, R., Carrasco-Marín, F., and Moreno-Castilla, C. (2007) Methanol partial oxidation on carbon-supported Pt and Pd catalysts. Catalysis Today, 123, 158-163.
- Udani, P.P.C., Gunawardana, P.V.D.S., Lee, H.C., and Kim, D.H. (2009) Steam reforming and oxidative steam reforming of methanol over CuO–CeO<sub>2</sub> catalysts. International Journal of Hydrogen Energy, 34, 7648-7655.
- Van der Lee, M.K., Jos van Dillen, A., Bitter, J.H., and de Jong, K.P. (2005) Deposition precipitation for the preparation of carbon nanofiber supported nickel catalysis. Journal of the American Chemical Society, 127, 13573-13582.
- Velu, S., Suzuki, K., Kapoor, M.P., Ohashi, F., and Osaki, T. (2001) Selective production of hydrogen for fuel cells via oxidative steam reforming of methanol over CuZnAl(Zr)-oxide catalysts. Applied Catalysis A: General, 213, 47-63.
- Wang, X., Kang, Q., and Li, D. (2008) Low-temperature catalytic combustion of chlorobenzene over MnO<sub>x</sub>–CeO<sub>2</sub> mixed oxide catalysts. Catalysis Communications, 9, 2158-2162.
- Wei, Y.C., Liu, C.W., Chang, W.J., and Wang, K.W. (2011) Promotion of Pt–Ru/C catalysts driven by heat treated induced surface segregation for methanol oxidation reaction. Journal of Alloys and Compounds, 509, 535-541.
- Wild, P.J. and Verhaak, M.J.F.M. (2000) Catalytic production of hydrogen from methanol. Catalysis Today, 60, 3-10.

- Xiaodong, M., Xi, F., Xuan, H., Hongwen, G., Lu, L., Jie, G., Huiqin, C., and Ting, Z. (2012) Mesoporous CuO/CeO<sub>2</sub> bimetal oxides: One-pot synthesis, characterization and their application in catalytic destruction of 1,2-dichlorobenzene. Microporous Mesoporous Materials, 158, 214-218.
- Xiaoyuan, J., Guanglie, L., Renxian, Z., Jianxin, M., Yu, C., and Xiaoming, Z. (2001) Studies of pore structure, temperature-programmed reduction performance, and micro-structure of CuO/CeO<sub>2</sub> catalysts. Applied Surface Science, 173, 208-220.
- Zhang, Q., Xu, L., Ning, P., Gu, J., and Guan, Q. (2014) Surface characterization studies of CuO-CeO<sub>2</sub>-ZrO<sub>2</sub> catalysts for selective catalytic reduction of NO with NH<sub>3</sub>. Applied Surface Science, 317, 955-961.
- Zhang, Q., Zhang, K., Xu, D., Yang, G., Huang, H., Nie, F., Liu, C., and Yang, S. (2014) CuO nanostructures: Synthesis, characterization, growth mechanisms, fundamental properties, and applications. Progress in Materials Science, 60, 208-337.
- Zheng, Y., Zhu, X., Wang, H., Kongzhai, L., Wang, Y., and Wei Y. (2014) Characteristic of macroporous CeO<sub>2</sub>-ZrO<sub>2</sub> oxygen carrier for chemical-looping steam methane reforming. Journal of Rare Earths, 32, 842-848.
- Zhu, H., Qin, Z., Shan, W., Shen, W., and Wang, J. (2004) Pd/CeO<sub>2</sub>-TiO<sub>2</sub> catalyst for CO oxidation at low temperature: a TPR study with H<sub>2</sub> and CO as reducing agents. Journal of Catalysis, 225, 267-277.
- Zsoldos, Z., Gardin, F., Hilaire, L., and Guzzi, L. (1996) Genesis of cobalt oxide-induced surface structure in PtCo<sub>x</sub>/Al<sub>2</sub>O<sub>3</sub> catalysts. Journal of Molecular Catalysis A: Chemical, 111, 113-122.

## CURRICULUM VITAE



**Name:** Ms. Sureerat Jampa

**Date of Birth:** December 06, 1988

**Nationality:** Thai

### **University Education:**

2007-2011 Bachelor Degree of Chemistry, 1<sup>st</sup> Class Honors, Faculty of Science, Prince of Songkla University, Songkhla, Thailand

2011-2013 Master Degree of Polymer Science, Petroleum and Petrochemical College, Chulalongkorn University, Bangkok, Thailand

### **Thesis Topic:**

Catalytic Applications of CuO Loaded Mesoporous CeO<sub>2</sub> and CuO Loaded Mesoporous CeO<sub>2</sub>-ZrO<sub>2</sub> Catalyst

### **Thesis Advisors:**

Prof. Sujitra Wongkasemjit, Prof. Apanee Luengnaruemitchai, and Assoc. Prof. Thanyalak Chaisuwan

### **Scholarships:**

Development and Promotion of Science and Technology Talented Project (DPST)

### **Publications:**

1. Jampa, S., Wangkawe, K., Tantisriyanurak, S., Changpradit, J., Jamieson, A.M., Chaisuwan, T., Luengnaruemitchai, A., Wongkasemjit, S. (2017) High performance and stability of copper loading on mesoporous ceria catalyst for preferential oxidation of CO in presence of excess of hydrogen. International Journal of Hydrogen Energy, 42, 5537-5548.
2. Jampa, S., Jamieson, A.M., Chaisuwan, T., Luengnaruemitchai, A., Wongkasemjit, S. (2017) Achievement of hydrogen production from autothermal steam reforming of methanol over Cu-loaded mesoporous CeO<sub>2</sub> and Cu-loaded mesoporous CeO<sub>2</sub>-ZrO<sub>2</sub> catalysts. International Journal of Hydrogen Energy, 42, 15073-15084.

**Proceedings:**

1. Jampa, S., Luengnaruemitchai, A., Chaisuwan, T., Wongkasemjit, S. (2017, May 14-17) High potential of mesoporous ceria/ceria-zirconia synthesized via nanocasting pathway for catalytic applications. Proceedings of the TechConnect World 2017, Washington, D.C., U.S.A.
2. Wongvitvichot, W., Jampa, S., Luengnaruemitchai, A., Chaisuwan, T., Wongkasemjit, S. (2017, May 14-17) Catalytic activity of Cu-CeO<sub>2</sub>-ZrO<sub>2</sub> for biodiesel production. Proceedings of the TechConnect World 2017, Washington, D.C., U.S.A.

**Presentations:**

1. Jampa, S., Tokura, S., and Rujiravanit, R. (2013, June 18) Preparation of Silk Fibroin/Cellulose Whiskers Bionanocomposite Sponges for Immobilization of Yeast Cells Used in Continuous Ethanol Production. Poster presentation at The European Polymer Congress EPF 2013, Pisa, Italy.
2. Jampa, S., Luengnaruemitchai, A., Chaisuwan, T., Wongkasemjit, S. (2017, May 17) High potential of mesoporous ceria/ceria-zirconia synthesized via nanocasting pathway for catalytic applications. Oral presentation at the TechConnect World 2017, Washington, D.C., U.S.A.